Effect of Surfactant on Three-Phase Relative Permeability in Water-Alternating-Gas Flooding Experiment

A thesis submitted in partial fulfilment of the requirements for the Degree of Doctor of Philosophy in Chemical Engineering

BY

Perekaboere Ivy Sagbana

Student ID: 2827064

Supervised by

Dr Pedro Diaz

Dr John Orrin

School of Engineering, London South Bank University

April 2017

Declaration of Authorship

I, Perekaboere Ivy Sagbana, declare that this thesis and the work presented in it are my own and has been generated by me as the result of my own original research.

Signed: 

……

Date: …25/05/2017……

Dedication

I will like to dedicate this thesis to the almighty God and my` parents Mr and Mrs Sagbana, my siblings Kemo, Nina, Florence and Tamaraebi.

Acknowledgement

I will like to express my gratitude to the almighty God for his grace, mercy and guidance all through my PhD studies.

My gratitude also goes to my supervisor Dr Pedro Diaz, for his excellent supervision, great ideas, support and patience throughout my entire PhD. I learnt a great deal from him, which I'm sure, will assist me in further development of my technical and personal skills. In addition, I will like to thank all the staffs, lab technicians and colleagues in the university that have assisted me in this research. I really do appreciate the help, advice and encouragement all through my research.

I would also like to greatly appreciate my sponsors Niger Delta Development Commission, Nigeria for providing the funds for my research and Komboye Lambert for encouraging me to apply for scholarship and making sure I get the sponsorship.

Abstract

Three-phase flow occurs in petroleum reservoirs during tertiary enhanced oil recovery processes such as water-alternating-gas flooding (WAG). WAG process is used to improve the efficiency of gas flooding by controlling gas mobility. Water traps gas in the reservoir when injected alternatively in WAG. Continuous gas trapping causes a blocking effect that prevents the oil from being contacted by the water. Surfactants are introduced in WAG processes to decrease this water blocking effect and improve oil recovery. This technique of introducing surfactant in WAG processes is known as surfactant-alternating-gas flooding (SAG).

One of the important parameters to accurately model complex processes such as SAG is the relative permeability to each of the flowing fluids. However, relative permeability in SAG processes become extremely complicated due to different flow mechanisms and fluid interactions involved. Several researches in the open literature are based on three-phase relative permeability in WAG using three-phase empirical correlations for prediction. Few researchers have conducted experiments on SAG flooding, but their research focused on the aspect of oil recovery only.

The aim of this research project is to obtain a better understanding of surfactant interaction in three-phase flow. To do so, a surfactant formulation compatible with the oil and brine was selected by conducting aqueous stability test, surfactant phase behaviour and surfactant adsorption experiments. Water/oil interfacial tension was measured to determine the initial interfacial tension before surfactant injection. Surfactant/oil interfacial tension was calculated using Huh's correlation. This was followed by two and three-phase core flooding experiments.

The results showed that alcohol alkoxy sulphate and internal olefin surfactant blend is most suitable formulation compatible with the brine and oil by reducing water/oil interfacial tension from 22.7 mN/m to 1 x 10^{-3} mN/m and having very low adsorption of 0.00135 mg/g adsorption on the core sample.

Two-phase water/oil, gas/oil and gas/water experiments were conducted with and without surfactants to evaluate the effect of surfactants when only two fluids are present in the porous media. Sigmund and McCaffery correlation was used in Sendra software to history match experimental differential pressure and oil production data to obtain relative permeability curves. The results showed that in water/oil displacement

experiment, the presence of surfactant increases oil relative permeability but did not have any effect on water relative permeability. The cross point of the relative permeability curves moved further to the right indicating that surfactant increases the water wetness of the core sample causing oil to flow freely. Oil production increased in the presence of surfactant, this increase in oil production is because of the reduction in water/oil interfacial tension and decrease in pressure gradient during the experiment.

There was an increase in oil production and oil relative permeability also in gas/oil displacement experiment in the presence of surfactant when compared to gas/oil displacement experiment without surfactant. While in gas/water displacement experiment, a significant decrease in gas relative permeability occurred in the presence of surfactant when compared to gas/water displacement experiment with no surfactant.

To study surfactant effect on three-phase relative permeability, WAG and SAG core flooding experiments were conducted. The extension of JBN/Welge theory by Grader and O'Meara was applied to calculate three phase relative permeability. Eclipse reservoir simulation software was used to simulate surfactant WAG to predict surfactant effect on three-phase relative permeability using the three-phase correlations such as Stone 1, Stone 2, saturated weighted interpolation, linear interpolation and Stone exponent present in the software. Results from three-phase displacement experiments showed that the presence of surfactant does not have any effect on water relative permeability in three-phase flow. Oil relative permeability was affected by the presence of surfactant and gas. Oil relative permeability and recovery factor were higher in SAG when compared to WAG. In three-phase flow, gas relative permeability was lower in SAG compared to WAG. Gas breakthrough in the presence surfactant occurred at 0.48pore volume while in WAG breakthrough occurred at 0.34 pore volume. The decrease in gas relative permeability was because of foam creation with gas interaction with the surfactant. None of the three-phase relative permeability correlations could accurately predict the effect surfactant on three-phase relative permeability in WAG.

Table of Contents

List of figures

List of Tables

Nomenclature

Q (Volumetric flowrate)	cm^3/sec
A(Area)	cm^2
dP/dL (Pressure gradient)	atm/cm
N_c (Capillary number)	dimensionless
μ (Fluid viscosity)	cp
σ (Interfacial tension)	mN/m
θ (Rock porosity)	fraction
S^*_w (Normalised water saturation)	fraction
S_{wi} (Irreducible water saturation)	fraction
S_g (Gas saturation)	fraction
S_{gr} (Critical gas saturation)	fraction
S_o (Oil saturation)	fraction
Q (cumulative injection volume)	PV
P (Pressure)	atm
k (Absolute permeability)	Darcy
f (fractional flow)	fraction
L (length)	cm
krg (Gas relative permeability)	fraction
kro (Oil relative permeability)	fraction
krw (Water relative permeability)	fraction
ρ (Density)	g/cm^3
M (Molecular weight)	g/mol
R (Gas constant)	J / mol. K

T (Temperature)	kelvin
Z (Gas compressibility)	dimensionless
g- Gravity	m/s^2
D (Equatorial diameter)	m
H (Shape parameter)	dimensionless
d (Diameter)	m
S_j (Saturation of each phase)	fraction
S_j^0 (Initial saturation of a phase)	fraction
L_j (Pore volume produced)	mL
Q (Pore volume injected)	mL
C_o (Initial surfactant concentration)	vol%
C (Surfactant effluent concentration)	vol %
W_{sg} (Weight of sample)	grams

Chapter 1 Introduction

In the last few years, enhanced oil recovery (EOR) techniques have re-gained interest from the research and development phases to the oilfield implementation. This renewed interest has been furthered by the increase in demand for crude oil worldwide, the maturation of new oilfields, and few new-well discoveries (Aladasani & Bai, 2010). There has not been any sustainable economic replacement for crude oil presently, and this has been given as one of the reasons for continuous exploration and discovery of oil around the world. Other reasons for EOR recovery are access to some very prospective resource areas, and advances in technology (Lerch, 2010). By 2011, roughly 87million barrels of oil per day were produced in the world, which means that the oil industry must find twice the remaining oil just to meet the target to replace depleted reserves (Sheng, 2011).

Oil production from reservoirs is divided into three stages: primary, secondary, and tertiary (Alzayer et al, 2017). Figure 1-1 shows the three different oil recovery stages. Primary recovery is the initial production stage that occurs when using displacement energy naturally present in the reservoir to displace oil to the production wells. Primary recovery mechanisms include fluid and rock expansion, gas–cap drive, solution–gas drive, gravity drainage and natural water drive. Secondary recovery occurs because of the augmentation of the naturally occurring energy in the reservoir through injection of gas or water to displace oil to the production wells. Generally, water is injected into the aquifer, or gas is injected into the gas cap to maintain the reservoir pressure which has already been depleted due to primary recovery. Tertiary recovery refers to the injection of fluids into the reservoir such as water, gas, polymer and surfactants (Jelmert et al, 2010). The fluids injected may interact with the reservoir rock/oil creating conditions that are favourable to oil recovery. These interactions might be oil swelling, lowering of interfacial tension, oil viscosity reduction. Tertiary recovery mechanisms include polymer flooding, water-alternating-gas flooding (WAG), thermal recovery, gas flooding, microbial enhanced oil recovery, low salinity flooding and surfactant flooding (Green and Willhite, 1998).

One of the major EOR processes is WAG, this is commonly used in reservoirs containing light to medium crude oil. The mechanism of oil recovery with WAG is associated with improved microscopic and macroscopic sweep effieciency.

Experimental studies have shown that the increase in oil recovery and accelerated oil production in WAG is as a result of three-phase flow in the porous media (Skauge et al, 1999). Even with the advantages of WAG, the major setback is water blocking the oil from being contacted by the gas with continuos injection of alternating slugs of gas and water. As the water saturation increases, it prevents the gas from coming in contact with the oil (Zekri et al, 2011). This can decrease the efficiency of these processes. Surfactants can be used in WAG to reduce this blocking effect by creating a low interfacial tension between oil/water and reducing gas mobility by creating foam (Al-mossawy et al, 2011). These interactions with the reservoir fluids will affect three-phase mobility in the reservoir which results in improved oil recovery.

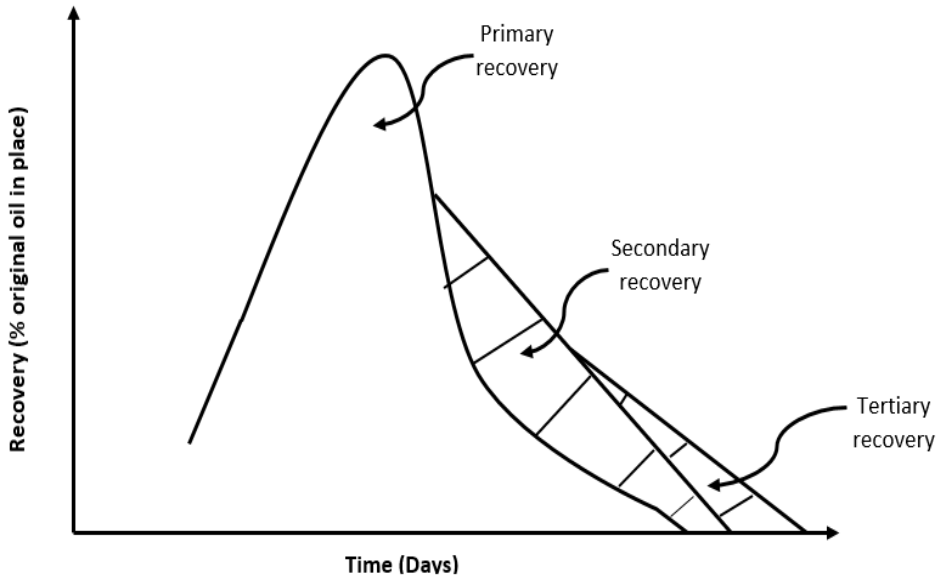

Figure 0-1: Oil recovery stages through time (Jelmert et al, 2000).

1.1 Statement of problem

There is a need to understand the underlying physics in three-phase flow when chemicals such as surfactant are used to improve the efficiency of WAG. Currently, only three-phase flow under WAG has been discussed in several researches. The improvement of oil recovery in WAG in the presence of surfactant is due to surfactant interaction with oil, water and gas. These interactions define the flow path (three-phase relative permeability) of the different phases in the porous media.

Different studies have been conducted on three-phase relative permeability in WAG flooding using two phase data water/oil and gas/ oil in empirical correlations to estimate three-phase relative permeability. Suramairy and Abdulrahman (2015); Spiteri and Juanes (2006); Zuo et al (2014) studied three-phase relative permeability in WAG using empirical models. They concluded that relative permeability for three-phase flow is much lower compared to two-phase flow and the different three-phase relative permeability models yield different results especially at low oil saturations which is the main point of interest when conducting WAG.

When a surfactant is introduced in WAG processes, the flow behaviour of the fluids (oil, water and gas) will be affected due to surfactant creating foam with gas and lowering water/oil interfacial tension. To predict oil recovery behaviour in surfactant enhanced water-alternating-gas flooding, three-phase flow in the presence of surfactant needs to be evaluated.

1.2 Contribution to knowledge

Most of the studies in the open literature on the presence of surfactant in WAG injection or surfactant-alternating-gas flooding (SAG) have focused on oil recovery. Salehi et al (2014) and Abdi et al (2014) studied surfactants in WAG flooding and then found out that oil recovery increased when surfactant is introduced to WAG. Although Cinar et al (2005) conducted research on three-phase relative permeability at low interfacial tension, the fluid systems used are not representative of reservoir fluids. There has not been any work done to describe three-phase relative permeability when surfactant is present in WAG. This research will investigate the effect of surfactant on the mobility of fluids in WAG. The study will include estimating three-phase relative permeability in WAG, evaluation of surfactant effect on three-phase flow and the investigation of different empirical correlations in determining surfactant effect on three-phase relative permeability. Other novel topics in this research will include the study of low concentration surfactant interaction with oil and hard brine. Surfactant formulation designs present in the open literature are with soft brine with only sodium chloride present. Also, to investigate the effect of surfactant on two-phase water/oil, gas/oil, and gas/water relative permeability.

This research will only focus on the surfactant effect on immiscible water-alternating-gas flooding thus the use of Nitrogen as the injection gas in this research. Nitrogen

gas is immiscible in oil. Only the three-phase correlations present in Eclipse software will be used to estimate three phase relative permeability.

1.3 Aim of research

Evaluate the effect of surfactant on three-phase relative permeability in WAG experiment and to investigate how the different three-phase relative permeability correlations will predict surfactant effect on three-phase relative permeability.

1.4 Research objectives

- To propose a surfactant formulation for Surfactant alternating gas flooding.
- To study the effect of surfactant on two-phase water/oil, gas/oil and gas/water relative permeability by conducting two-phase displacement experiments.
- Estimate three-phase relative permeability from water-alternating-gas flooding experiments.
- To investigate the effect of surfactants on three-phase relative permeability experimentally and numerically.

1.5 Description of chapters

Chapter 1 of this thesis presents the research objectives and aims, research problem and contribution to knowledge. Research publications for conference and journals are also included in chapter 1.

Chapter 2 contains a comprehensive review of background information on enhanced oil recovery processes, water-alternating-gas flooding, fundamentals and concepts of fluid flow in the porous media and description of two and three-phase experiments. A review of work done on three-phase relative permeability and surfactant-alternating-gas flooding will also be discussed. Chapter 2 will also present the different surfactant systems used for enhanced oil recovery, evaluation and characterisation of surfactants when designing a surfactant formulation for enhanced oil recovery, mechanism of surfactant enhanced oil recovery.

Chapter 3 showcases a detailed description of the methodology used in this research, a description of the experimental setup, materials, procedures, and software used for this research.

Chapter 4 presents the experimental results obtained from evaluating surfactant formulations, core flooding experiments to estimate two-phase relative permeability, and results from surfactant effect on two-phase water/oil, gas/oil, and gas/water relative permeability.

Chapter 5 will discuss the method used to estimate three-phase relative permeability and results obtained from experimental and simulated three-phase relative permeability from WAG and SAG. Comparisons will be made from the results obtained on the surfactant effect on three-phase relative permeability predictions using different correlations and from experiments in this chapter.

Chapter 6 will have the research conclusions and recommendations for future work and then the appendix will contain diagrams of equipment used in this research and publications for this research.

Chapter 2 Literature review

This chapter reviews the mechanisms involved in water-alternating-gas flooding, surfactant flooding and surfactant-alternating-gas flooding. A review of methods used in characterising surfactants used in enhanced oil recovery, experiments for obtaining two and three-phase relative permeability, correlations used in calculating two and three-phase relative permeability will also be discussed in this chapter.

2.1 Enhanced oil recovery (EOR) techniques

Enhanced oil recovery processes involve the injection of gases, chemicals or thermal energy into a reservoir to recover oil during the life of the reservoir. These processes can be classified into various categories such as chemical, miscible and immiscible gas injection (see Figure 2-1).

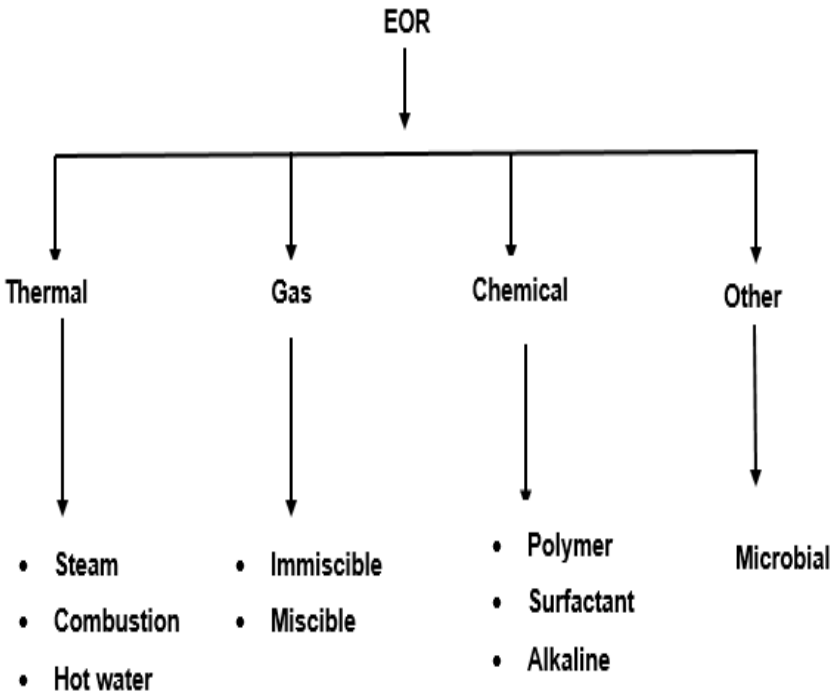

Figure 2-1: Classification of enhanced oil recovery processes (Doghaish, 2008).

2.1.1 Chemical flooding

This involves the recovery of residual oil by injecting chemicals into the reservoir after secondary recovery. Chemicals such as surfactants and polymers are injected into the reservoir to mobilise the trapped oil in the reservoir by altering the interfacial

tension and mobility between the displacing and displaced fluids respectively. Recovery efficiency depends on the capillary number which is a dimensionless property that describes the ratio of the viscous to capillary forces on two-phase relative permeability curves. By reduction of interfacial tension between oil and water using surfactants, the capillary number can be increased. Increase in capillary number generates a dominant viscous flow that allows the mobility of trapped oil (Mandal, 2015). This research will only focus on chemical enhanced oil recovery in three-phase flow.

2.2 Water-alternating-gas Injection (WAG)

There has been increasing interest in WAG enhanced oil recovery method because of the anticipated increase in recovery factor in WAG projects compared to water flooding (Foroonzafar and Aminshahidy, 2013; Aghdam et al, 2013). WAG is one of the improved oil recoveries that involve three-phase flow. The first WAG field experience was in Alberta, Canada in 1956 in a sandstone reservoir. Since then, many fields worldwide have adopted this technique both in offshore and onshore (Arogundade et al, 2013; Knappskog, 2012; Christensen et al, 2001).

WAG injection process offers better mobility control of gas compared to conventional gas flooding thus improves the volumetric sweep efficiency. This method was originally proposed to improve the sweep efficiency of gas injection by using water to control the mobility ratio, thus making WAG more effective than injecting only water or gas alone by utilising the advantages of both methods (gas and water) (Shahverdi et al, 2011a). Oil recovery by WAG injection has also been attributed to allowing the contact of upswept zones, especially in the recovery of attic or cellar oil by exploiting the segregation of gas to the top and water to the bottom (Christensen et al, 2001). Another advantage is the re-injection of produced gas which is favourable because of environmental issues and restrictions on gas flaring (Shahverdi et al, 2011a; Kulkarni and Rao, 2005). Figure 2-2 is a schematic of WAG process where a slug of gas is injected into the reservoir followed by water injection. Several cycles of water and gas can be injected into the reservoir.

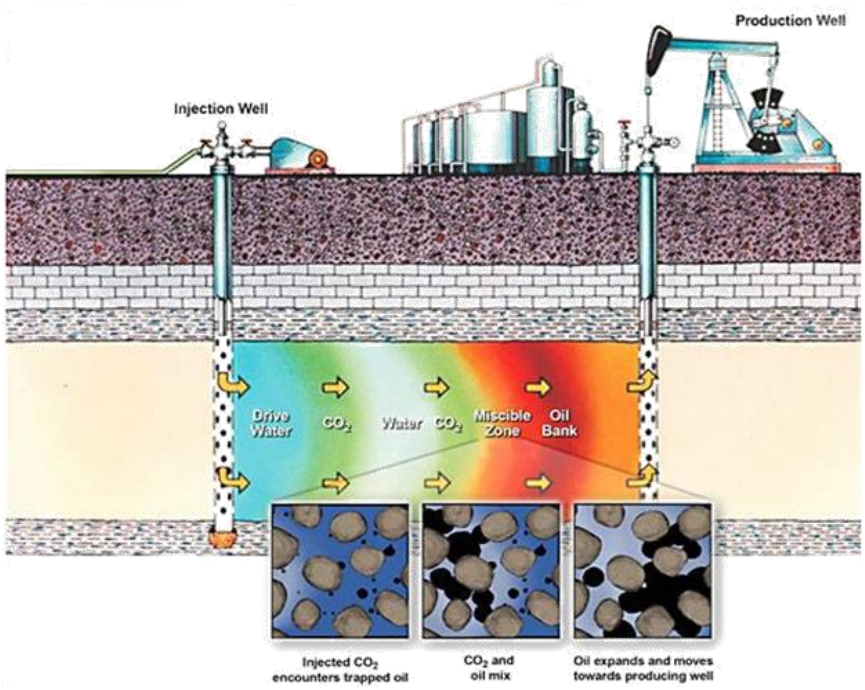

Figure 2-2: Schematic of water-alternating-gas (WAG) processes (Zahoo et al, 2011).

2.2.1 Classification of water-alternating-gas (WAG) processes

Many authors have suggested a comprehensive classification of WAG. These classifications include immiscible WAG, miscible WAG, hybrid WAG, simultaneous WAG and selective WAG (Christensen, 1998; Al-Mamari, 2007; Skauge, 2007).

Miscible WAG

Miscible WAG usually occurs when the reservoir bubble point pressure is well above the minimum miscibility pressure (MMP). The injected gas is miscible with the reservoir oil at first contact or miscibility happens with time as displacement continues under the prevailing conditions (Faroozanfar and Aminshahidy, 2013). Although gas miscibility provides an additional advantage of decreasing the viscosity of oil, which results in mobilisation of trapped oil during later production stages, the miscible front created has low volumetric sweep efficiency because of the low viscosity. Miscible WAG is predominantly found in onshore and has been performed on close well spacing (Skauge and Berg, 1997).

Immiscible WAG

During immiscible WAG process, the injected gas is not miscible with the reservoir oil and it displaces the oil still maintaining its gaseous phase. This technique occurs well below the minimum miscibility pressure (MMP) of the reservoir and a displacement front is created between the two phases (Zahoor, 2011). The main objective of conducting immiscible WAG is to form a good frontal stability and contact unswept zones. The application of this method has been in petroleum reservoirs were gravity stable gas injection cannot be applied due to reservoir heterogeneities and limited gas resources (Dalen et al, 1993; Christensen et al, 2001). This research will focus on immiscible WAG injection since the gas used is nitrogen and does not have miscibility with oil and the minimum miscibility pressure is not measured in this study.

Hybrid WAG

This involves the injection of a large slug of gas into the reservoir previously, and then followed by several small slugs of water and gas (Hustad, 2002). It has been anticipated that the hybrid WAG operation effectively would create an oil bank during single-slug injection and maintain higher oil production rates through improved mobility control during WAG injection (Lin and Poole, 1991).

Simultaneous WAG

In simultaneous water-alternating-gas flooding (SWAG), water and gas are injected at the same time. Both fluids are injected into the reservoir through a single injection well. When the water and gas are mixed at the surface and then injected into the reservoir, the injection technique is referred to as SWAG injection, but when the gas and water are pumped separately using a dual completion injector without mixing the two phases on the surface, the process is known as selective simultaneous water alternating gas (SSWAG). One essential element to the technical success of WAG process is the optimum utilisation of gas injection. WAG optimisation is widely recognised as a viable technique in controlling miscible processes. However, these processes guaranty mobility control in the high permeability zones where gas tends to choose a preferential channel and consequently, extends the oil recovery (Al-Ghanim et al, 2009).

2.2.2 Oil recovery mechanism by WAG injection in the oilfield

Displacement efficiency of WAG can be defined as the product of the microscopic and macroscopic efficiencies. The equation describing displacement efficiency is given in equation [1.1].

$$E=E_{micro} \cdot E_{macro} \quad [1.1]$$

Where E is total displacement efficiency (the volume of oil recovery by enhanced oil recovery divided by the amount of oil in place at the start of enhanced oil recovery). E_{micro} is microscopic displacement efficiency, which refers to the displacement of the oil at pore level, which means E_{micro} represents the effectiveness of the displacing fluid in mobilising the oil at those pores of the formation where the displacing fluid contacts the oil.

While E_{macro} is macroscopic (volumetric) displacement efficiency, which relates to the success of the displacing fluids in contacting the reservoir in a volumetric scale.

E_{macro} is a quantity of that explains how effectively the displacing fluid can sweep out the volume of a reservoir; both in areal and vertical scale, as well as how efficiently the displacing fluid moves the displaced oil toward production wells. WAG injection improves oil recovery by modifying both microscopic and macroscopic sweep efficiencies. However, the high gas mobility, with its low viscosity, causes gas fingering and early breakthrough of which reduces the macroscopic (areal and vertical) sweep efficiency (Thakur and Satter, 1998; Zekri et al, 2014). The injection of water in the presence of gas leads to trapping of gas. This can prevent gas fingering and reduce gas mobility (Touray, 2013).

When surfactant is introduced in WAG, the interaction of the surfactant and gas which creates foam will improve the macroscopic displacement efficiency by the foam ability to contact the oil bearing portion of the reservoir. The presence of surfactant reduces water/oil interfacial tension thus allowing the oil to flow freely through the pore throat of the porous media. This in turn improve microscopic displacement efficiency (Jamaloei and Kharrat, 2010).

2.3 Concept of relative permeability

Henry Darcy in 1856 carried out a research on the flow of water through horizontal sea beds by conducting series of experiments. He postulated that the rate of flow of water through a sand column can be expressed by equation [2.1].

$$Q = -KA\frac{dp}{dl} \quad [2.1]$$

Where

K is the coefficient of permeability

Q is the flowrate

A is the cross-sectional area of the sand column

$\frac{dp}{dl}$ is the pressure gradient (Ahmed, 2006).

Darcy's law provides a powerful and simple tool to reservoir engineers to describe, visualise and evaluate fluid flow in the porous media and factors that affect fluid flow (Satter et al, 2007). Although Darcy's experiments were confined to sand packs which were fully saturated with water, later investigators found out that Darcy's law is applicable to any fluid flow through a porous medium with some adjustments (Abaci and Edwards, 1992). One of the adjustments was that the constant K can be replaced by K/μ in which μ is the viscosity of the flowing fluid and K is a property of the porous medium which is known as permeability. By following this simple dimensional analysis, it can be shown that the permeability of a porous medium has the unit of squared length, and it was named Darcy to honour Henry Darcy.

The physical meaning of Darcy unit may be easily described by considering a single-phase fluid with a viscosity of 1cp (centipoise) and flow rate of 1 cm^3 / sec flowing through a porous medium with a cross-sectional area of 1 cm^2 under the pressure drop of 1 $atmcm^{-1}$. In this case, the porous material would have the permeability of 1 Darcy (Modaresghazani, 2015).

The permeability obtained from this equation is known as the absolute permeability, as only one phase of fluid is saturated in the rock. Usually, a reservoir rock has more than one fluid flowing simultaneously in the porous medium. The permeability of one fluid flowing in the presence of another is the effective permeability (Dake, 2001).

2.3.1 Relative permeability

Relative permeability is the ratio of the effective permeability to the absolute permeability of a porous media. The relative permeability of a fluid is strongly dependent on the wettability of the porous medium, as it controls the initial distribution of fluids and the further displacement of one fluid by another. The wetting phase

occupies the smaller pores while the non-wetting phase retains the larger pores. As a result of occupying the smaller pores, the relative permeability of the wetting phase will be lower compared to that of the non-wetting phase. This difference in permeability is because the wetting phase will be traveling through tighter paths that have poor connectivity as compared to the paths that will be followed by the non-wetting phase (Ahmed, 2006).

2.3.2 Factors affecting relative permeability

There are several factors that can affect the relative permeability of a porous medium. The relative permeability of fluids in the porous media has been shown in several research to depend on the following factors wettability, fluid saturation, and saturation history, gravitational, viscous and capillary forces (Donaldson et al, 1985).

Wettability effect on relative permeability

Wettability is defined as the ability of a fluid to adhere or spread on a solid surface in the presence of an immiscible fluid. The wettability of a reservoir rock controls the distribution of oil, water and gas flow in the pore spaces (Falode and Manuel, 2014). In a water-wet rock system containing brine and oil, the smaller pores will be occupied by water and major portions of the larger pores will be wetted by water. In areas with high oil saturations, the oil will rest on a film of water that is spread over the surface of the rock. If the rock is preferentially oil wet and saturated with water, the oil will imbibe the smaller pore spaces and displace water from the core when it is contacted by oil (Tiab et al, 2015). In general, the relative permeability of a non-wetting fluid is higher at a given saturation. A good example is in water flooding. The water relative permeability in an oil-wet system is higher than it would be if the porous medium was water-wet. At a low saturation of the non-wetting phase, the non-wetting phase will become trapped as globules that are discontinuous in the larger pores. These globules tend to block pore throats, lowering the wetting phase relative permeability. On the other hand, the non-wetting phase relative permeability is high because the non-wetting phase flows through the centres of the larger pores. At low wetting phase saturations, the non-wetting phase effective permeability will often approach the absolute permeability, showing that the wetting phase does not significantly restrict the flow of the non-wetting phase (Anderson, 1987).

Effect of fluid saturation and saturation history

Relative permeability is a function of fluid saturation which means that it is directly proportional to fluid saturations. As the fluid saturation increases so does the relative permeability of the particular fluid (Dandekar, 2013). The relative permeability of a particular fluid depends on whether the maximum saturation has been reached by flowing from lower to higher saturation values. This flow from one saturation to another can be referred to as hysteresis or saturation history. During fluid displacement processes, as the saturation of the wetting phase is moving from low to high values, the resulting relative permeability curve is defined as imbibition. The imbibition process implies an increase in wetting phase saturation.

A very good example of an imbibition process is water flooding process. An opposite scenario where the relative permeability of the wetting phase is attained by decreasing the saturation of the wetting phase is called the drainage relative permeability. For a strongly water-wet rock, the relative permeabilities of water drainage and imbibition are equal, but for the non-wetting phase, the relative permeability of drainage is greater than the relative permeability for imbibition. This is because hysteresis is believed to be related to the size distribution of the pore space. During water imbibition, as the water invades the oil-filled pores of different sizes and pushes the oil out, oil displacement will continue if there are still continuous escape paths available for oil. During drainage process, these continuous escape paths re-establish at higher oil saturations which causes the higher relative permeability to drainage process (Modaresghazani, 2015; Bennion et al, 1996).

Effect of viscous and capillary forces

Capillary number is a dimensionless number used to establish the relationship between the viscous and capillary forces in fluid flow. This relationship is necessary to study the effect of viscous and capillary forces on relative permeability. The viscous forces are defined by the flow velocity, flow path length and fluid viscosity while the capillary force is defined by the interfacial tension (Dandekar, 2013). This relationship is defined by equation [2.2].

$$N_c = \frac{\mu v}{\sigma \theta} \qquad [2.2]$$

Where

N_c - Capillary number

μ - Fluid viscosity

σ - Interfacial tension

θ - Rock porosity in fraction.

Bloom et al (1997) studied the effect of interfacial tension, flow velocity and capillary number on relative permeability. The effect of flow velocity was investigated by keeping the interfacial tension constant at 0.06 and 0.26 mN/m during a two-phase displacement experiment in a glass bead pack with a fluid system of hexane (non-wetting phase) and methanol (wetting phase). When flow velocity was increased from 14 to 49 m^3/day, the relative permeability of the non-wetting phase was slightly enhanced while there was no observed change in the wetting phase relative permeability.

Bloom et al (1997) also investigated the effect of interfacial tension on relative permeability by changing the interfacial tension between the fluids from to 0.29 to 0.01 mN/m at a flow velocity of 14 m^3/day. The result obtained from the experiments showed that there is a clear dependence of relative permeability on interfacial tension. The relative permeability to the non-wetting phase increased gradually when the interfacial tension was decreased by a factor of 30. At an interfacial tension of 0.01mN/m, the non-wetting phase relative permeability approaches to a value equal to the non-wetting phase saturation. The relative permeability of the wetting phase is not affected when the value of the interfacial tension was decreased to 0.06 mN/m.

2.4 Two-phase relative permeability

Two-phase flow refers to the process where only two fluids or phases are flowing simultaneously in a system (Ibrahim et al, 2001). An example is the water relative permeability which decreases sharply when there is a small reduction in water saturation. This is observed from the shape of the water relative permeability curve (Abaci and Edwards, 1992). Figure 2-3 shows relative permeability curves for the water/oil system. Where the wetting phase is water and the non-wetting phase is oil. The non-wetting phase begins to flow at a relatively low saturation known as the critical oil saturation S_{oc}. This low saturation of the non-wetting phase decreases the

relative permeability of the wetting phase, this is because the non-wetting phase occupies the larger pores and it is in the larger pores that flow occurs with less difficulty. The wetting phase relative permeability curve shows that the wetting phase will cease to flow at a relatively large saturation of the non-wetting phase and the saturation of the wetting phase will be at the connate water saturation S_{wi}. At lower saturation of the wetting phase, changing of the wetting phase saturation has only a small effect on the non-wetting phase relative permeability curve. This happens because, at low saturations, the wetting phase occupies the smallest pores and does not contribute to flow (Ahmed, 2006).

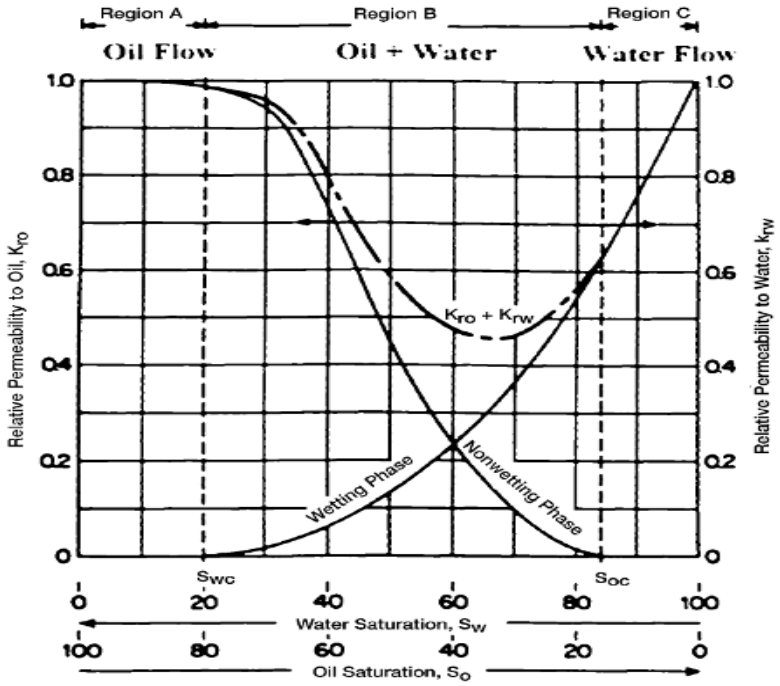

Figure 2-3: Two-phase relative permeability curves (Ahmed, 2006).

2.4.1 Estimating two-phase relative permeability

Several methods have been developed to estimate two-phase relative permeability and the commonly used method is the laboratory experiments. The widely used methods are steady state, unsteady state and centrifuge methods (Yuqi and Dacun, 2004).

Centrifuge method

The centrifuge method for measuring relative permeability evolved from capillary pressure measurement using the centrifuge. To measure the capillary pressure and relative permeability relationship, a rock sample is fixed on the cup on a centrifuge rotor. The rotor is kept spinning at a constant speed. As the rotor spins, fluid drains from the rock at an exponentially declining rate, eventually ceasing. By measuring the rate of fluid drainage at the centrifuge speed, the capillary pressure relationship can be determined. The data processing technique is equivalent to the history matching techniques used in reservoir management and numerical modelling of reservoirs. With this data processing technique, it is possible to determine the capillary pressure and the relative permeability at the same time (Christiansen and Howarth, 1995).

Saeedi and Pooladi-Darvish (2011) measured water/oil drainage relative permeability using the centrifuge. The results they obtained from the experiment had errors because of capillary end effects and they concluded that if a minimum rotational speed is not honoured, the problem of the capillary end effect will arise.

Two-phase steady state method

In the steady state method of measuring two-phase relative permeability, the equilibrated two-phase fluids are injected into a core sample until the measured overall saturation and overall pressure drop does not change with time (Akbarabadi and Piri, 2015; Bennion and Bachu, 2006; Al-Abri et al, 2012; Krevor et al, 2012; Farokhpoor et al, 2014).

The flow rates of the fluid phases, saturation, and the pressure drop are constant along the core when steady state has been achieved. Thus, in steady-state methods, the global measurements are equivalent to the local measurements and the relative permeability equation can be used directly.

Likely, there are some problems that can be encountered such as capillary end effects which can occur at the inlet and outlet of the core sample. These effects can be avoided by measuring saturations and pressure drops in the centre of the core (Gupta and Maloney, 2015). In each steady state, only two data points are obtained (the relative permeability of each phase). Due to this reason, the process must be repeated for each flux ratio to obtain a full relative permeability curve. This makes the steady state method very time consuming.

Attaining a steady state can take anytime from 20-40 hours depending on the permeability of the core sample used. Steady state is achieved very slowly at the endpoints, this makes the process very long (Reynolds and Krevor, 2015; Manceau et al, 2015; Al-Menhali et al, 2015). Figure 2-4 shows a steady state displacement experiment where the fluid proportions produced at the outlet are equal to the proportions injected at the inlet.

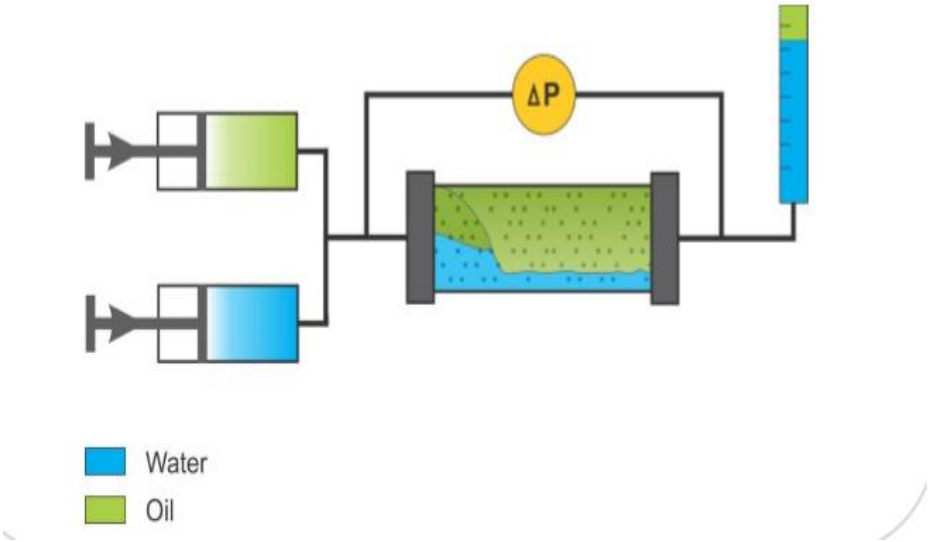

Figure 2-4: Schematic of steady state displacement experiment for water-oil system (Sendra user guide, 2011).

Two-phase unsteady state method

The unsteady state method of measuring two-phase relative permeability has been developed to speed up the measurement process, particularly when determining oil/brine relative permeabilities. The unsteady state method achieves the local saturations and phase flow rates from their measurements by solving the continuity equation along with Darcy-Buckingham equation either numerically or analytically. In the Johnson, Bossler, and Naumann (JBN) method one phase is injected into a core saturated with another phase and the overall pressure drop and effluent are measured versus time (Toth et al, 2002).

The unsteady state procedure is time dependent, this allows for many different saturations and relative permeabilities to be obtained from one displacement. Another method of measuring unsteady state two-phase relative permeability is the history matching method. The history matching method has become a more popular method

to obtain values from experimental measurements of effluent versus time, overall pressure drop and in some cases, in-situ saturation.

The method considers relative permeability models such as Corey, *LET*, Chierici, Sigmund and McCaffery, with prior fitting parameters and a capillary pressure curve (Hamouda et al, 2008). Figure 2-5 shows a schematic of unsteady state flow in displacement experiment. The unsteady state method will be used in this research to obtain two-phase relative permeability data. This is because the steady state method takes a very long time and steady state in the core sample may not be achieved.

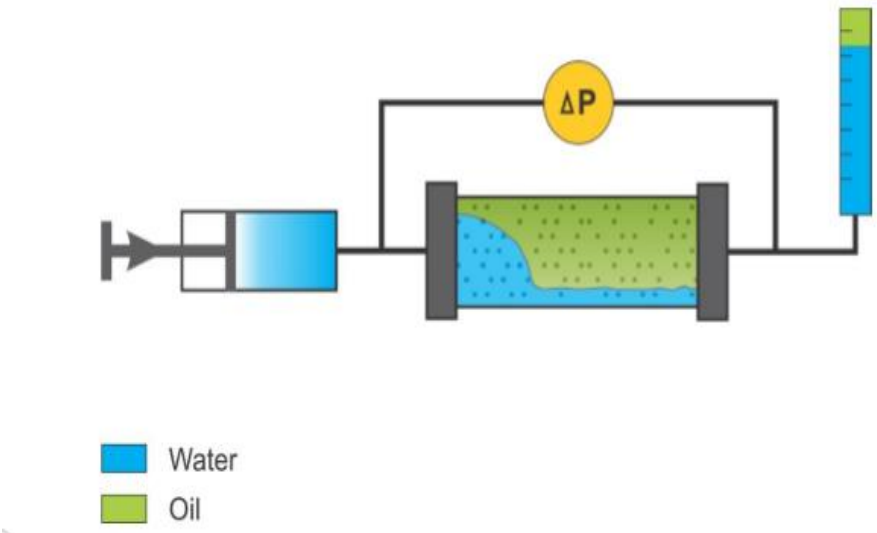

Figure 2-5: Schematic of unsteady state displacement experiment for water-oil system (Sendra user guide, 2011).

2.5 Two-phase relative permeability correlations

Assisted history matching techniques have been developed since the 1970s, to simultaneously estimate relative permeability and capillary pressure curves. Although the estimation accuracy was not satisfied at early stage due to limited measurement data were available for matching (Zhang, 2014). Subsequently, the estimation accuracy of the history matching technique has been significantly improved owing to the non-destructive measurement of 23 the in-situ saturation profiles by using X-ray, CT scanning, Gamma ray attenuation, and nuclear magnetic resonance (NMR) imaging (Watson et al, 1998).

Numerous studies have been conducted to estimate relative permeability and capillary pressure curves by history matching core flooding experiments (Kulkarni et

al, 1998). However, relative permeability and capillary pressure curves obtained from the small core samples may not be representative at the field-scale (Lohne and Virnovsky, 2006). Numerous efforts have also been made to estimate relative permeability and capillary pressure at the field-scale, focusing on two-phase relative permeability and capillary pressure curves (Kulkarni and Datta-Gupta, 2000).

History matching of core flooding data to obtain relative permeability curves have gained popularity in the oil and gas industry, it has become one of the main tools in reservoir engineering. In the last decade, many history matching techniques with core flooding experiments are presented in the literature (Loeve et al, 2011). Li et al (2010), Basburg and Karpyn (2008) have used the history matching of core flood experimental data to obtain two phase relative permeability curves in their study of fluid flow in the porous media. The history matching of experimental data in this work is done using Sendra software. Sendra simulator is a two-phase, 1-dimensional black oil simulator model that is based on Darcy's law and continuity equation (Sendra user guide, 2011; Abeysinghe et al, 2012). Sendra simulator uses the estimation mode in the software to history match experimental data and obtains two-phase relative permeability curves. There are several two-phase relative permeability correlations present in Sendra software. For all the correlations, the normalised water saturation is used.

$$S_w^* = \frac{S_w - S_{wi}}{1 - S_{wi} - S_{gr}} \qquad [2.3]$$

***LET* correlation**

Lomeland et al (2005) proposed a new 3 parameter versatile correlation to obtain a flexibility and proper curve for a wide saturation range. The three parameters used in describing this equation are L, E and T. The L parameter is used to describe the lower part of the relative permeability curve, the L-values can be compared to the appropriate Corey parameter. The upper part of the relative permeability curve is described by the parameter T in a way like that of the L parameter as it describes the lower part of the curve. The parameter E describes the slope of the curve.

In the *LET* correlation, a value of one is a neutral value, and the position of the slope is determined by the L and T parameters. By increasing the value of the E parameter, the slope is pushed towards the high end of the curve and decreasing the value of the E parameter pushes the slope towards the lower end of the curve. When using the

LET correlation, it has been indicated that the parameter L ≥1, E > 0 and T ≥ 0.5 (Lomeland et al, 2005). The *LET* correlations are given in equations [2.4] and [2.5]

$$K_{row} = K_{ro}^{x} \frac{(1-S_{wn})^{L_O^W}}{(1-S_{wn})^{L_0^W} + (E_o^w S_{wn})^{T_o^w}} \quad [2.4]$$

$$K_{rw} = K_{rw}^{x} \frac{S_{wn}^{L_w^o}}{S_{wn}^{L_0^W} + E_o^w (1-S_{wn})^{T_o^w}} \quad [2.5]$$

Burdine correlation

Burdine derived equations for calculating two-phase relative permeability from pore size distribution data using basic laws of fluid flow in the porous media.

$$K_{rw} = K_{rw}\ (S_w^*)^{2+3\lambda/\lambda} \quad [2.6]$$

$$\mathrm{K}_{ro} = K_{ro}^{0}\ (1-S_w^*)^2 * (1-(1-S_w^*)^{2+\lambda/\lambda}) \quad [2.7]$$

In the Burdine's equation, the subscript zero is the end point values while the subscript * is the normalised value for water saturation. λ is the pore size distribution index (Sendra user guide, 2011; Soroush et al, 2013).

Chierici correlation

Chierici proposed a relative permeability correlation by upscaling relative permeability curves of gas/oil drainage system and water/oil imbibition system (El-Sharawy, 2016).

$$K_{rw} = K_{rw}\ (S_{gr})e^{BR_w^{-m}} \quad [2.8]$$

$$K_{rg} = K_{rg}\ (S_{wi})e^{-AR_w^{L}} \quad [2.9]$$

Where A, B, L and M are all positive numbers, and R_w is used in place of the normalised water saturation.

Corey correlation

The Corey model is derived from the capillary pressure concept and this model is widely accepted to be accurate for a porous medium which is consolidated. Corey's model has also been suggested for unconsolidated sands using different empirical exponents (Honarpour et al, 1986).

$$K_{rw} = K_{rw}^{0} \, (S_w^*)^{nw} \quad [2.10]$$

$$K_{rg} = K_{rg}^{0} \, (1 - S_w^*)^{ng} \quad [2.11$$

ng and nw are Corey gas and water parameters. The curvature of the water and gas relative permeability curves is defined by these parameters.

Sigmund and McCaffery correlation

In 1972 Sigmund and McCaffery modified Corey's correlation. The constants nw and ng are similar to that of Corey's equation. The equation can be converted to Corey's correlation if the constants A and B are zero. A and B constants have very small values. They are used to linearize the relative permeability curves when the values of relative permeability approach zero (Soroush et al, 2013).

For this research, the Sigmund and McCaffery correlation will be used to history match experimental data to obtain two-phase relative permeability curves. This is due to the flexibility of the correlation in fitting experimental data. During simulation to match experimental core flood data for this research, Corey, LET, Cherici correlations could not accurately match the experimental data. Soroush et al (2013) in their study of estimating two phase relative permeability using two-phase relative permeability correlations in Sendra software, concluded that Sigmund and McCaffery correlation was the most suitable for history matching two phase relative permeability curves using Sendra software as it was the most flexible correlation to match experimental data.

$$K_{rw} = K_{rw}^{0} * \frac{(S_w^*)^{nw} + AS_w^*}{1 + A} \quad [2.12]$$

$$K_{rg} = K_{rg}^{0} * \frac{(1 - S_w^*)^{ng} + B(1 - S_w^*)}{1 + B} \quad [2.13]$$

Johnson, Bossler, and. Naumann (JBN) method

Another method of calculating two-phase relative permeability is the JBN technique. This theory was first developed by Buckley and Leverett (1942) and then later extended by Welge (1952) for calculating two-phase relative permeability under unsteady state conditions (Akhlaghinia, 2013). By combining Darcy's law with capillary pressure in differential form gives the following equation:

$$F_w = \frac{1 + \frac{K_O}{q_t \mu_o}(\frac{\partial p_c}{dx} - g.\Delta\rho sin\theta)}{1 + \frac{K_O \mu_w}{K_w \mu_o}} \quad [2.14]$$

Where

Δρ - Density difference between the displacing and displaced fluids,

q_t - Superficial velocity of the total outlet flow of the core

θ - Angle of core central axis with the horizontal direction.

F_w – Fractional flow of water

K_o – Oil relative permeability

K_w – Water relative permeability

For negligible capillary pressure and a core in horizontal position, Welge derived a simplified version of the equation which is

$$S_{w.avg} - S_w = F_{o2} Q_w \quad [2.15]$$

Where

Q_w _ Cumulative water in pore volume injected into the core.

$S_{w.avg}$ - Average water saturation

F_{o2} - Fractional flow of oil at the outlet face of the core.

In equation [2.15], $S_{w.avg}$ and Q_w can be obtained from experimental injection data by mass balance and then plotting a graph of Q_w against $S_{w.avg}$. The slope of this plot will be the fractional flow of oil at the outlet face of the core.

$$F_{o2} = \frac{q_o}{q_o + q_t} \quad [2.16]$$

Combining equation [16] with Darcy's law, a new equation for calculating the ratio of water and oil relative permeability can be obtained:

$$F_{O2} = \frac{1}{1 + \frac{\mu_o / K_{ro}}{\mu_w / K_{rw}}} \quad [2.17]$$

By calculating F_{o2} from equation [2.16], and having oil and water viscosities μ_o and μ_w, the relative permeability ratio K_{ro}/K_{rw} can be calculated from equation [2.17].

For gas/oil and gas/water systems, the similar equation can be expressed by changing the subscript.

The Welge equation was extended by Johnson to calculate individual relative permeability of each phase (Cao and Siddiqui, 2011). Then proposed method is known as the JBN method. The JBN method introduces the relative injectivity of the core sample denoted by I_r and the equations they came up with to calculate two-phase relative permeability are given in equations [2.18] and [2.19].

$$K_{ro} = \frac{F_{o2}}{d(\frac{1}{Q_w I_r})/d(\frac{1}{Q_w})} \quad [2.18]$$

$$K_{rw} = \frac{F_{w2}\mu_w}{F_{o2}\mu_o}\, k_{ro} \quad [2.19]$$

The JBN method, also states that relative injectivity Ir describes the way the intake capacity varies with cumulative injection $Q_{W.}$ The relative injectivity can then be considered as the ratio of intake capacity of the core sample at any instance during the injection process to the intake capacity of the system at the starting moment of the injection at which the only fluid flowing through the system is oil is flowing through the system. Thus, Ir can be determined through the following equation:

$$I_r = \frac{(\mu/\Delta p)\ at\ any\ stage\ of\ the\ flood}{(\mu/\Delta p) at\ the\ beginning\ of\ the\ flood} \quad [2.20]$$

2.6 Three-phase relative permeability

The existence of three-phase flow in most part of the reservoir especially during enhanced oil recovery has led to the interest in getting reliable three-phase relative permeability data (Cao and Siddiqui, 2011). Three-phase flow occurs when the water saturation is greater than the irreducible water saturation and there are oil and gas phases present as mobile phases.

Estimation of three-phase relative permeability for various oil recovery techniques such as WAG and water drive of reservoirs at pressure below bubble point is required to understand the pore-scale physics of these processes and how this leads to oil recovery (Juanes and Spiteri, 2004; Shahverdi et al, 2012a). Several efforts have been directed towards gaining a better understanding of three-phase relative

permeability. An accurate estimation of three-phase relative permeability remains a difficult task for the petroleum industry (Shahverdi, 2012). Although two-phase relative permeability data is easy to generate, it is not the same for three-phase relative permeability, this is because, for three-phase relative permeability, there are infinite displacement paths. Three-phase displacement involves the variation of two independent saturations whereas for two-phase relative permeability there are only two displacement paths (Siddiqui et al, 1996; Blunt, 2000).

2.6.1 Estimation of three-phase relative permeability

There are two methods of measuring three-phase relative permeability. These methods are, estimating three-phase relative permeability from displacement experiments or by empirical correlations using two-phase relative permeability data (Shahverdi, 2012).

2.6.2 Three-phase relative permeability from displacement experiments

The first experiment to measure three-phase relative permeability was done in 1941 by Leverett and Lewis (Dehghanpour et al, 2010). Three-phase relative permeability can be estimated experimentally by steady state and unsteady state method (Jiang and Tsuji, 2017). The steady state method involves the injection of fluids simultaneously into the core sample while in unsteady state method the fluids are injected alternatively into the core sample (Eleri et al, 1995).

Leverett and Lewis conducted steady state three-phase relative permeability measurements in a tightly packed sand core. The fluids used were brine, nitrogen, and kerosene representing water, gas and oil phases respectively to determine three-phase relative permeability. The study showed that water relative permeability depends only on water saturation (Dria et al, 1993).

Oak (1990) conducted steady state experiment to measure three-phase relative permeability on water-wet Berea sandstone. Oil, gas and water phase saturations were measured using x-ray absorption technique. Two different saturation histories were studied IID (Imbibition-Imbibition-Drainage) and DDI (Drainage-Drainage-Imbibition). The experimental results showed that the relative permeability of the three-phases versus the saturation depends on the saturation histories.

Weifeng et al (2012) measured three-phase relative permeability using the steady state method on oil-wet and water-wet sandstone cores. The effects of saturation history DDI (drainage, drainage, and imbibition) and IDD (imbibition, drainage, and drainage) were also investigated. They found out that three-phase relative permeability to water depends on water saturation and three-phase relative permeability to oil and gas depends on the saturations of all the fluids.

Grader and O'Meara (1988) measured three-phase relative permeability from series of steady state and unsteady displacement experiments. To analyse the unsteady state displacement data and obtain three-phase relative permeability they employed the extension of the JBN/Welge theory which is a simplified mathematical equation for expressing the outflow face saturation of a displacing fluid in a two-phase system. This equation was extended to a three-phase system. To monitor the saturation history, the material balance technique was adopted. The three-phase oil relative permeability for this three-phase displacement experiments functions of only the oil saturation. This implies that a single two-phase gas/oil displacement with irreducible water could be used to predict three-phase data for gas injection. They concluded that all three saturations are not functions of their individual saturations. This is contrary to the results obtained by oak et al (1990) in which water and gas relative permeabilities are functions of their own saturations.

Sarem and Aime (1966) studied three-phase relative permeability using the unsteady state method. They extended the Buckley-Leverett theory which is based on the material balance equation that relates the rate of change of displacing fluid saturation at a point in the fractional flow with respect to the distance at a particular time. This theory was extended into three-phase flow to express the saturation that is found at the outflow face in all three-phases in terms of the known parameters. In this expression, it has been assumed that the fractional flow and relative permeability of each phase are functions of the saturation of that phase. Other assumptions that have been made include the neglect of capillary and gravity effects. From their unsteady state experiment, it was shown that the relative permeability for three-phase flow, as in two-phase flow, is influenced by initial saturation conditions, this makes it necessary to attain a similar saturation history in laboratory core as exists in the field.

Siddiqui et al (1996) examined the Buckley-Leverett theory extension regarding three immiscible fluids by applying the X-ray computerized tomography. Three-phase

relative permeability measurement was conducted on a spherical glass bead porous media. The three fluids used were decane, benzyl alcohol, and distilled water. They concluded that the measurement of three-phase relative permeability using the extended version of the Buckley-Leverett theory was very reliable as it predicts a sound three-phase relative permeability.

Schneider and Owens (1970) investigated both steady and unsteady state relative permeability using sandstone and carbonate core samples. They discovered that in the water-wet sandstone, the oil relative permeability was insensitive in the presence of gas when there is an increase in gas saturation and depend only on its own saturation. While the non-wetting phase saturation in three-phase depends on the saturation history of the intermediate wetting phase, non-wetting phase and the saturation ratio of the intermediate wetting phase and the wetting phase. Oil relative permeability was insensitive in the presence of gas when there is an increase in gas saturation and depends only on its own saturation.

Saraf et al (1982) measured steady state and unsteady state two and three-phase relative permeabilities in water-wet Berea sandstone. It was found that steady state three-phase water and oil relative permeabilities were similar to the results of the unsteady state tests. The results showed that oil relative permeability is dependent on all three saturations and water relative permeability is a function of water saturation alone. Three-phase gas relative permeabilities of the steady state experiments were less sensitive to gas saturation history than those of the unsteady state experiments. They also observed that the steady state gas relative permeabilities were higher compared to the unsteady state values for decreasing gas saturation and were much lower for increasing gas saturation. They explained that these observations from the experiments are due to the different amounts of gas trapped during steady state and unsteady state flows. They believed that, since all three-phases compete for the same flow channels during steady state flow, the chance of fluid trapping and accessibility to flow channels in the steady state experiments would be lower than the unsteady state experiments.

Eleri et al (1995) measured three-phase relative permeability in water-wet Clashach core samples using the unsteady state method. They reported that the three-phase oil and gas relative permeabilities depend on more than one phase saturation,

hysteresis from increasing and decreasing saturations was most pronounced for the oil phase.

Cinar et al (2005) conducted an experimental investigation of the effect of interfacial tension variation three-phase relative permeability by using a quaternary liquid system. Their results indicated that the relative permeability of the wetting phase was not affected by the interfacial tension variation while the relative permeability of the other two-phase was clearly affected. As the interfacial tension decreases, oil and gas phases become more mobile at the same phase saturations.

Delshad et al (1996) presented experimental data for low interfacial tension three-phase relative permeabilities in Berea sandstone cores. They used a system of brine/surfactant/alcohol and oil mixture that included a microemulsion, excess oil and brine. The relative permeability measurements were conducted at steady state conditions with a constant capillary number of 10^{-2} between the other phases and the microemulsion. They concluded that at low interfacial tension, three-phase relative permeabilities are functions of their own saturations only.

Laboratory measurement of three-phase relative permeability is time consuming as it is very difficult to achieve steady state during three-phase experiment. This can take several days. For an easier and convenient method of establishing three-phase relative permeability, theoretical approaches have been developed which makes use of two-phase relative permeability to estimate three-phase relative permeability (Arogundade et al, 2013).

2.7 Three-phase relative permeability from empirical models

The alternate approach used in the petroleum industry to estimate three-phase relative permeability is by using two-phase relative permeability data obtained from the laboratory in the existing three-phase relative permeability correlations (Baker, 1988).

Three-phase relative permeabilities can be calculated from two-phase data using empirical correlations. These empirical models were basically developed for water-wet porous medium using the assumptions of the channel flow theory during three-phase flow (Stone, 1970; Hustad and Holt, 1992).

The channel flow theory states that at most only one fluid is mobile in any flow channel. The conclusion of the channel flow theory is that for a system that is water-wet, water (wetting phase) is located in the smallest pore spaces and gas (non-wetting phase) in the largest pore spaces. The intermediate phase spatially separates them. The theory also states that at equal water saturations, the microscopic fluid distribution at the water/oil interface will be uniform in a water/oil system and in a water/oil/gas system, if the direction of change of water saturation is the same in both.

The suggestion made is that water relative permeability in the three-phase system is a function of only the water saturation, irrespective of the relative saturations of oil and gas. This function is the same in the three-phase system as in the two-phase water/oil system. Also, the relative permeability to gas in the three-phase system is the same function of gas saturation as in the two-phase gas/oil system (Baker, 1988; Shahverdi, 2012).

Figure 2-6 presents a ternary diagram showing displacement path of water, oil and gas during WAG injection. Path 1 is the natural or manmade water flood, path two is gas flood into water or residual oil and path 3 is water flood into gas and residual oil. Three-phase relative permeabilities are usually plotted as isoperms in ternary diagrams. Each end of the ternary diagram is 100% saturation of the particular phase.

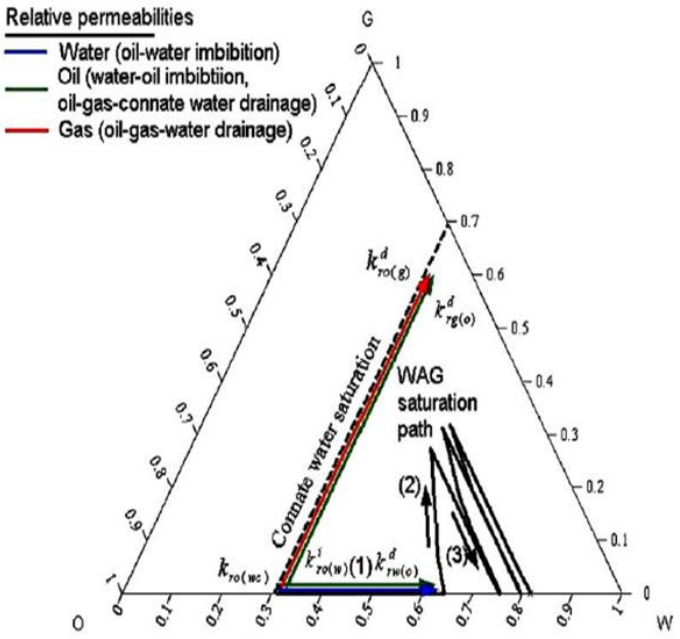

Figure 2-6: Saturation path in WAG displacement process (Spiteri and Juanes, 2006).

2.7.1 Corey three-phase correlation

In 1956, Corey proposed the first model for three-phase relative permeability. This model was established on the concept of making approximations on flow paths through a rock by the equivalent hydraulic radius and a bundle of capillary tubes. Tortuosity correction which was developed by Burdine was also included to account for path length differences of tubes of different sizes (Akhlaghinia, 2013).

Corey's model assumed that the relative permeabilities of the wetting and non-wetting phases are independent of the saturations of other phases. The intermediate wetting phase resides in the flow channels which have intermediate sizes and are between the flow channels occupied by the wetting phase (water) and the non-wetting phase (gas). The flow of the intermediate phase maybe interfered with by the wetting and non-wetting phases. The relative permeability of oil in Corey's model is proportional to the area of the pores occupied by the oil and to the relative saturation of the oil phase (Baker, 1988). The equation for Corey's three-phase relative permeability is expressed as:

$$K_{ro} = K_{ro}^{0} \frac{(S_o - S_{or})^{eo}}{(1 - S_{or} - S_{wr} - S_{gr})} \quad [2.21]$$

Where S_{or} is a f(S_g, S_w). Where there is absence of experimental data, the three-phase oil exponent can be estimated by:

$$e_o = be_{ow} + (1+b)_{eog} \quad [2.22]$$

The end-point relative permeability can also be attained:

$$K_{ro}^{0} = bK_{row}^{0} + (1-b)K_{rog}^{0} \quad [2.23]$$

Kianinejad et al (2016) examined the performance of Corey's correlation in predicting three-phase oil relative permeability against experimental data obtained from three-phase displacement experiment conducted along different saturation paths. They found out that Corey correlation fits their experimental data very well.

2.7.2 Land model

An improved model for imbibition relative permeability was developed by Land. The model takes into consideration the effect of initial saturations. Based on published experimental data, this model assumes that the maximum residual hydrocarbon saturation is constant, whether the hydrocarbon is oil or gas, and that the residual hydrocarbon is related to the initial hydrocarbon saturation.

$$\frac{1}{S_{hr}} - \frac{1}{S_{hi}^{*}} = \frac{1}{S_{hr}^{*}} - 1 = C \quad [2.24]$$

Land's model is represented as a set of integral equations giving the dependence of relative permeability on saturation history, saturation and the relation between capillary pressure and saturation. The relationship for the oil relative permeability is:

$$K_{ro} = \frac{S_{of}^{*2}}{\int_0^1 \frac{dS^{*}}{P_c^2}} \left[S_w^{*} \int_{S_{ob}^{*}}^{1-S_{gf}^{*}} \frac{dS^{*}}{P_c^2} - S_{hr(max)}^{*2} \int_{1-S_g^{*}}^{1-S_{gf}^{*}} \frac{dS^{*}}{(1-(1-S_{hr(max)}^{*})^2) P_c^2} \right] \quad [2.25]$$

Normalised saturation with respect to the effective pore space (1-S_{wc}) is denoted by the subscript *. The first integral in the numerator indicates the area of the pore space that is available to oil flow. The saturation ranges do not include oil trapped by water but the region that is trapped by oil is included. The second integral shows the

reduction in the region available for oil flow due to trapped gas. An analytical solution has been derived for three-phase relative permeability to oil using the saturation and capillary pressure relationship derived by Brookes and Corey using Burdine's tortuosity parameter $\lambda = 2$.

$$K_{ro} = S_{of}^{*2}\left[(1-S_{gf}^{*})^2 - \left(S_w^{*} + S_{ob}^{*}\right)^2 - \frac{2}{C^2}\left\{In\left[\frac{S_{hr(max)}^{*} + (1-S_{hrmax})S_{gf}^{*}}{S_{hr(max)}^{*}(1-S_{hr(max)}^{*}S_{gi}^{*}}\right]\right.\right.$$

$$\left.\left. + \frac{1}{S_{hr(max)}^{*} + (1-S_{hr(max)}^{*}S_{gf}^{*}} - \frac{1}{S_{hr(max)}^{*} - (1-S_{hr(max)}^{*})S_{gi}^{*}}\right]\right] \qquad [2.26]$$

Land's model predicts the relative permeability of the wetting phase at a given saturation caused by the trapping of the non–wetting phase. This is because it considers the fluid saturation history (Baker, 1988).

2.7.3 Stone 1 model

Stone proposed a probability model which uses two sets of two-phase data to predict relative permeability of the intermediate wetting phase (oil phase) in a three-phase system. Stone's model assumes that the flow of oil is restricted by the presence of water and gas and the effects of water and gas are independent.

The relative permeability to oil is regarded as a linear function of the normalised oil saturation S_o, which has been modified by the functions β_w and β_g. These functions depend on water and gas saturations respectively. Due to the assumptions that β_w and β_g are independent functions, they can be determined independently and to maintain consistency within the limits of two saturations oil/water or oil/gas, β_w is chosen to be proportional to the oil relative permeability in the presence of water at zero gas saturation. β_g is proportional to the relative permeability of oil at connate water saturation in the presence of gas.

In 1973, Stone modified his model by incorporating gas and water relative permeability in the calculation of three-phase relative permeability of oil to get better agreement with experimental results. Stone proposed a model for systems that are preferentially water-wet in which gas and water relative permeability depend only on water and gas saturations respectively (Stone H.L, 1970).

$$K_{ro} = K_{rowc}\, S_o^{*} F_w F_g \qquad [2.27]$$

Where $K_{ro(wc)}$ is relative permeability to oil at connate water saturation (S_{wc}) and K_{rog} is oil relative permeability to gas. S_o^*, S_w^*, S_g^* are normalised oil, water and gas saturations respectively. S_{om} is the minimum residual oil saturation during three-phase flow. F_w and F_g are functions of normalised water and gas saturations. Equations for normalised saturations are given in equations [2.28] – [2.32]:

$$S_o^* = \frac{S_o - S_{om}}{1 - S_{wc} - S_{om}} \qquad \text{Where } S_O > S_{om} \qquad [2.28]$$

$$S_w^* = \frac{S_w - S_{wc}}{1 - S_{wc} - S_{om}} \qquad \text{Where } S_w > S_{wc} \qquad [2.29]$$

$$S_g^* = \frac{S_g}{1 - S_{wc} - S_{om}} \qquad [2.30]$$

$$F_w = \frac{K_{row}}{K_{rocw}(1 - S_w^*)} \qquad [2.31]$$

$$F_g = \frac{K_{rog}}{K_{rocw}(1 - S_g^*)} \qquad [2.32]$$

The Stone 1 model also assumes that the three-phase relative permeability data are independent of viscosity. Thus, they are not so accurate at low concentrations (Saliu et al, 2014).

2.7.4 Stone 1 exponent

The Stone 1 model was modified by Hustad and Holt (1992) to address the inadequacy observed. The limitation of Stone 1 model is that if K_{row} and K_{rog} are not unity at connate water saturation and zero gas saturation, then a match in relative permeability cannot be achieved at the two-phase boundaries. An exponent term, n has been included to normalise the saturations equation by replacing the β term in Stone 1 model.

$$K_{ro} = \frac{K_{row}(S_w) K_{rog}(S_g)}{K_{rocw}} \beta^n \qquad [2.33]$$

$$\beta = \frac{S_o^*}{(1 - S_w^*) * (1 - S_g^*)} \qquad [2.34]$$

$$S_o^* = \frac{S_g - S_{om}}{1 - S_{wir} - S_{om} - S_{gc}} \qquad [2.35]$$

$$S_w^* = \frac{S_w - S_{wc}}{1 - S_{wir} - S_{om} - S_{gc}} \quad [2.36]$$

$$S_g^* = \frac{S_g - S_{gc}}{1 - S_{wir} - S_{om} - S_{gc}} \quad [2.37]$$

β is a variable that varies between zero and one for low and high oil saturations. Values of n greater than 1 causes the oil isoperms (three-phase relative permeability plot) to become more linear between the two-phase values (Saliu et al, 2014).

2.7.5 Stone 2 model

Stone proposed a second model which is a modification of the first model for estimating three-phase permeability. This model assumes that the total permeability which is the sum of the water, oil and gas relative permeabilities are products of the total water/oil relative permeability ($K_{row} + K_{rwo}$) measured at gas saturation equals to zero and the total gas/oil relative permeability ($K_{rog} + K_{rgo}$) measured at connate water saturation. Hence the gas relative permeability for the three-phase flow is assumed to be the same in two-phase flow and can be determined to form two-phase data (Blunt, 2000).

$$K_{ro}(S_w, S_g) = K_{row}^0 * \left[\frac{K_{row}(S_w)}{K_{row}^0} + K_{rw}(S_w)\right]\left[\frac{K_{rog}(S_g)}{K_{row}^0} + K_{rg}(S_g) - \left[K_{rw}(S_w) + K_{rg}(S_g)\right]\right] \quad [2.38]$$

Where K^0_{row} is the oil relative permeability at irreducible water saturation when there is a flow of oil and water and at the critical gas saturation in oil/gas flow. The Stone 2 model does not require an additional interpolation of the residual oil saturation like the Stone 1 model. Rather, the model predicts the residual oil saturation itself (Zuo et al, 2014; Juanes, 2004).

2.7.6 Saturated weighted interpolation

Baker proposed a three-phase relative permeability model also known as the saturated interpolation model for water, oil, and gas based on interpolation between two-phase relative permeability data in which the relative permeability of each phase is a function of two saturations. This model is used as default in Eclipse reservoir simulator (Pejic and Maini, 2000; Juane, 2003).

$$K_{ro} = \frac{(S_w - S_{wc})K_{row} + (S_g - S_{gr})K_{rog}}{(S_w - S_{wc}) + (S_g - S_{gr})} \quad [2.39]$$

S_{gr} and S_{wc} are the residual values of gas and water saturations. The weighing factors (S_g-S_{gr}) and (S_w - S_{wr}) in both the numerator and denominator must be non-negative values. The K_{row} value used is obtained from water/oil relative permeability data interpolated at the actual residual oil saturation. K_{rog} value is obtained from gas/oil experimental data measured at connate water saturation and interpolated at the actual gas saturation. Equations similar to the three-phase relative permeability can be written for gas and water relative permeability.

$$K_{rw} = \frac{(S_o - S_{or})K_{rwo} + (S_g - S_{gr})K_{rwg}}{(S_o - S_{or}) + (S_g - S_{gr})} \quad [2.40]$$

$$K_{rg} = \frac{(S_o - S_{or})K_{rgo} + (S_w - S_{wc})K_{rwg}}{(S_o - S_{or}) + (S_w - S_{wc})} \quad [2.41]$$

Baker's model assumes that the end points of the three-phase relative permeability isoperms coincide with the two-phase relative permeability data. Saturated weighting makes certain that as the saturation of one phase approaches zero or an irreducible saturation, the appropriate two-phase data will dominate (Baker, 1988; Blunt, 1999).

2.7.7 Linear interpolation model

Baker also proposed the linear interpolation model. In this model, it is assumed that straight lines between the corresponding equal relative permeabilities on the oil/gas and water/oil relative permeability curves determines the three-phase oil relative permeability at a given saturation between the two-phase permeability relative curves. At a given saturation, (water, oil, gas) straight lines pass through a specified saturation to intersect the oil relative permeability curves at equal permeabilities. This is a problem of non-linear programming, to find a straight line that can intersect the two other lines (the oil/water) and (oil/gas) curves at equal permeability values and simultaneously minimises the distance from the line to a point in a 3-dimensional saturation space. The advantage the interpolation model has over other models is that it does not assume that the wetting and non-wetting phase relative permeability is completely independent on the saturations of other phases. This makes it possible for the interpolation model to honour both sets of two-phase data for each phase. A good example is that Stone's models assume that in a water wet rock, the relative

permeability to water is a function of water saturation only. At fixed water saturation, the relative permeability to water is constant. This is very restricting as the assumption requires that water isoperms should be straight lines and coincide with lines of constant water saturation. Linear interpolation requires the isoperms to be straight lines but not parallel of constant saturations (Baker, 1995).

$$K_{ro}\left(S_w, S_g\right) = K_{row}\left(S_w^{ow}\right) = K_{rog}\left(S_g^{og}\right) \quad [2.42]$$

$$\frac{S_w - S_w^{ow}}{S_w - S_{wc}} = \frac{S_g - S_{sgc}}{S_g - S_g^{og}} \quad [2.43]$$

S_w^{ow} represents water saturation in the oil/water two-phase system while S_g^{og} represents gas saturation in a two-phase gas/oil system at connate water saturation. These equations represent an implicit formulation of oil relative permeability. For each pair of gas and water saturations in equations [2.42] and [2.43], iteration is necessary to solve the non-linear equation to obtain three-phase oil relative permeability (Zuo et al, 2014). Figure 2-7 shows a ternary diagram of three-phase oil relative permeability obtained from the linear interpolation model.

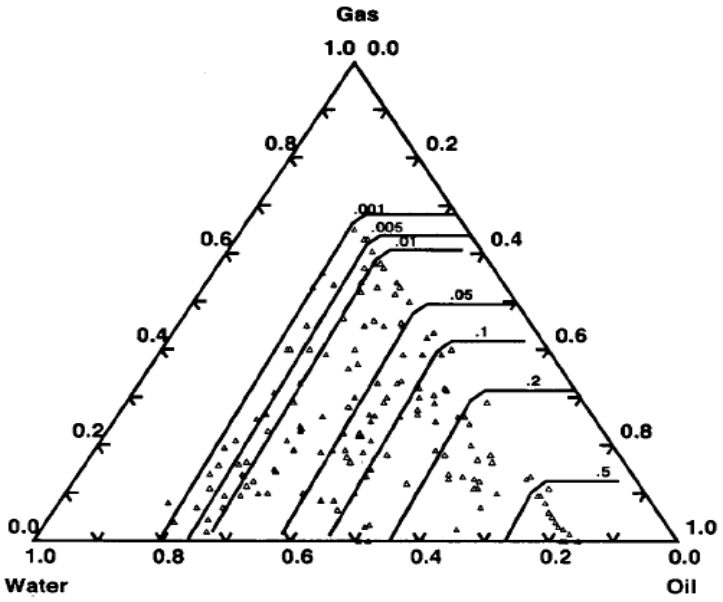

Figure 2-7: Ternary diagram showing three-phase relative permeability isoperms (Akhlaghinia, 2013).

2.8 Surfactants in enhanced oil recovery

Mobilising the residual oil saturation from the reservoir to the producing well is understood to occur when the water flood brine is replaced by a surfactant solution. The surfactant solution reduces the interfacial tension between the residual oil and the aqueous phase. Surfactants with good performance lower the interfacial tension to 10^{-3} mN/m from oil/water interfacial tension which is 30 mN/m (Flaaten et al, 2009). The very low interfacial tension nearly eliminates the capillary forces that trap the residual oil causing the oil to be mobilised (Levitt et al, 2006).

In gas injection enhanced oil recovery, the use of surfactant can also improve the sweep efficiency by creating foam when the gas interacts with the surfactant. This increases the viscosity of the gas preventing gas fingering (Farajzadeh et al, 2015). When using surfactants to lower interfacial tension or to improve the sweep efficiency of gas flooding, it must be considered that adsorption and chromatographic separation of the surfactant to the rock will happen therefore it is desired to develop a simple surfactant blend. It is also well known that surfactant systems are sensitive to both temperature and salinity in the reservoir, therefore a surfactant system that can resist these physical conditions are needed. For this approach, it is also crucial for the surfactant to form a three-phase system when injected into the reservoir where it is desired to form a microemulsion phase with the oil and brine (Barnes et al, 2010; Skauge and Fotland, 1990).

Surfactants also known as surface active agents are organic compounds that are composed of hydrocarbon chain (hydrophobic group tail) and a polar hydrophilic group head. They are soluble in both water and organic solvents. Surfactants have various uses in the oil industry and one of its usefulness is in enhanced oil recovery. Surfactants can adsorb to oil and water interface and alter surface properties such as interfacial tension which can lead to mobilisation of trapped oil in petroleum reservoirs (Sandersen, 2011). Figure 2-8 shows the structure of a surfactant molecule where they contain a non-polar part (hydrocarbon tail) and polar part in water.

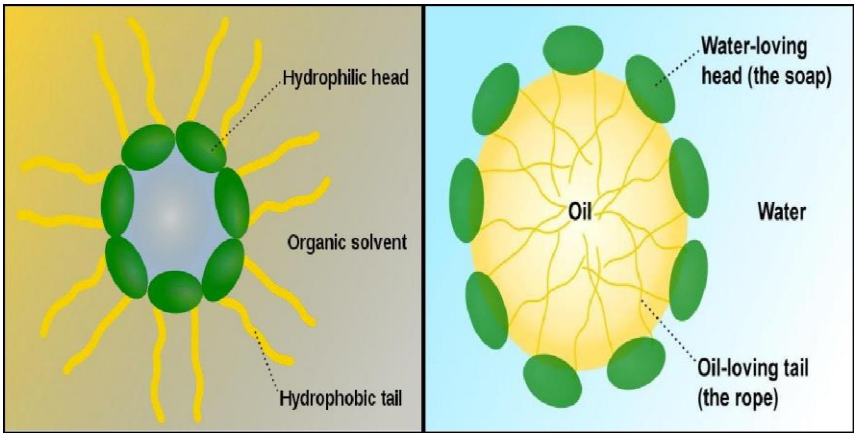

Figure 2-8: Micelle structure of surfactant (Emolfty, 2012).

2.8.1 Classification of surfactants

Surfactants are generally classified according to the ionic nature of their head groups; they are anionic, cationic, and non-ionic (Shramm, 2000).

Anionic surfactants

These surfactants have negative charge ions and are commonly used for enhanced oil recovery because of a range of properties such as lowering interfacial tension. They are relatively stable and can create self-assembled structures. They exhibit relatively low adsorption on sandstone reservoir rock and they can be manufactured economically. Anionic surfactants dissociate in water to form an amphiphilic anion (negative charge) and a cation (positive charge). Examples of anionic surfactants are sulphates and sulfonates (Farn, 2008).

Cationic surfactants

Cationic surfactants have positively charged head group and dissociates in water forming amphiphilic cation and anion. Cationic surfactants are adsorbed by sandstone rocks and for this reason; they are not used in sandstone reservoirs but are widely used to change the wettability of carbonate rocks from oil-wet to water-wet (Farn, 2008).

Non-ionic surfactants

Non-ionic surfactants are known not to have a charged head group. They have also been identified for use in enhanced oil recovery but mostly as a co-surfactant to

promote the surfactant process. They have a non-disassociating hydrophilic group that does not ionize in aqueous solution. Examples of non-ionic surfactants are alcohols, phenols, amides and ester (Sandersen, 2012).

Zwitterionic or amphoteric surfactants

Betaine and sulfo-betaine are good examples of amphoteric surfactants and they both exhibit anionic and cationic dissociation.

2.9 Mechanism of enhanced oil recovery by surfactants

The efficiency of any enhanced oil recovery displacement process can be increased by improving mobility ratio (M)**,** via increasing viscosity of displacing fluid and increasing the capillary number (Nc) by reducing interfacial tension (Romero-Zeron, 2012).

2.9.1 Improving mobility ratio

Mobility (M) of a fluid can be defined as the ratio of the effective permeability (K_i) of a fluid to the viscosity of the fluid (μ_i).

$$M = \frac{K_i}{\mu_i} \qquad [2.44]$$

Hence mobility ratio is defined as the mobility of the displacing fluid divided by the mobility of the fluid displaced.

$$M = \frac{K_{rw}}{\mu_w} / \frac{K_{ro}}{\mu_o} \qquad [2.45]$$

$$M = \frac{K_{rg}}{\mu_g} / \frac{K_{ro}}{\mu_o} \qquad [2.46]$$

Where K_{rw}, K_{rg}, and K_{ro} are relative permeabilities of water, gas and oil respectively. Then μ_w, μ_g and μ_o are water, gas and oil viscosities. Displacement of fluid from the reservoir to the well is optimised if the mobility ratio is favourable (less than 1). If an unfavourable mobility ratio is obtained, the gas or water (displacing fluid) to flow passes the displaced fluid giving rise to a phenomenon known as ‘viscous fingering’ thereby causing early break through and thus decreasing sweep efficiency (Baker,

1997; Ahmed, 2006). In enhanced oil recovery, the mobility ratio can be made less than 1 by the following means.

- Decrease the viscosity of the displaced fluid.
- Increase the effective permeability of the displaced fluid.
- Decrease the effective permeability of displacing fluid.
- Increase the viscosity of the displacing fluid.

2.10 Evaluation of surfactants for enhanced oil recovery

It is important to characterise the surfactant used in enhancing oil recovery to ensure that the surfactant is favourable to the reservoir conditions and can interact with reservoir fluid to mobilise residual oil.

2.10.1 Critical micelle concentration (CMC)

It is important to determine the critical micelle concentration of surfactants used for enhanced oil recovery to estimate the concentration at which a very low interfacial tension will be obtained. At the CMC, the surfactant molecules begin to form aggregates known as micelles shown in Figure 2-9. When a surfactant is introduced into a two-phase system, the surfactant will initially partition into the interface of the system lowering the energy of the interface and removing the hydrophobic part of the surfactant from water. When the surface coverage of the surfactant increases, the surface free energy decreases, and the surfactant starts aggregating into micelles. This further decreasing the energy at the interface and removing the hydrophobic part from water. Upon reaching the CMC of a surfactant in an aqueous solution, a further increase in surfactant concentration will just increase the number of micelles.

CMC is one of the most important parameters of a surfactant system. It is important to make the concentration of the surfactant higher than the critical micelle concentration to obtain a very low interfacial tension (IFT). As this concentration, will determine the point at which a surfactant solution can effectively influence oil recovery. This is because the greatest effect of the surfactant in lowering interfacial tension is achieved when a significant number of micelles are present (Donaldson et al, 1989).

For recovery mechanisms involving surfactant, gas, and oil, some researchers have shown that using surfactant concentration above the critical micelle concentration,

can form foam with gas and this presents a wide mobility control (Kulman et al, 1992). Rafati et al (2016) from conducting foam stability test showed that at surfactant concentrations above the CMC can form stable foam and the collapse of foam is a function of the surfactant concentration. They also observed that at a surfactant concentration lower than the critical micelle concentration, unstable foam was formed. Figure 2-9 shows the plot of surface tension against surfactant concentration and the point of deviation on the curve is the critical micelle concentration.

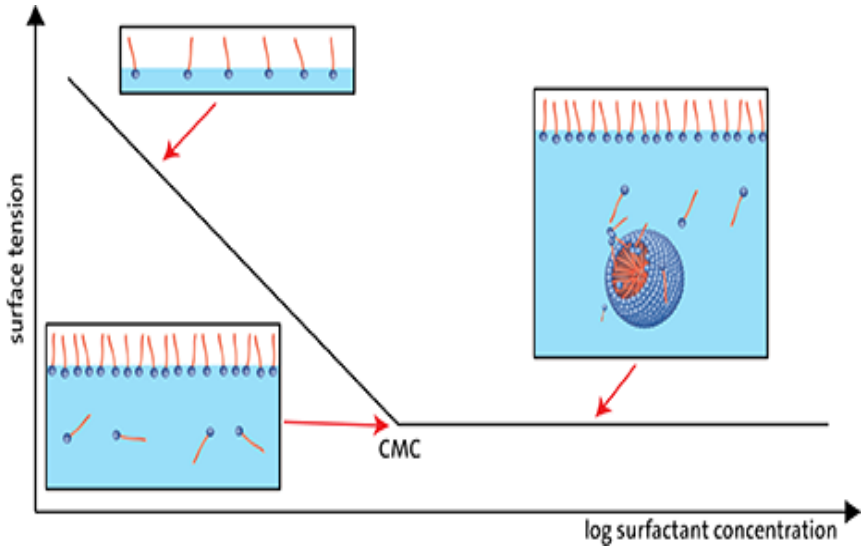

Figure 2-9: Surface tension as a function of surfactant concentration (www.dataphysics.de).

2.11 Surfactant retention and adsorption

Surfactant retention has been known to be one of the important variables affecting the economics of using surfactants in enhanced oil recovery. For enhanced oil recovery with surfactants to be successful, adsorption on the rock surface should be minimal. The retention ability of surfactant on the rock requires evaluation before injection into the reservoir. High surfactant loss will reduce the efficacy of the project. Bera et al (2013) studied surfactant adsorption on sand surfaces using cationic, anionic and non-ionic surfactants. They discovered that pH and salinity play an important role in surfactant adsorption. High adsorption efficiency was measured for anionic and non-ionic surfactant at low pH, an opposite trend was observed for cationic surfactant. The mechanism of retention of surfactants is complex and is as a

result of many factors. These factors include the rock mineralogy and clay content, salinity, pH, microemulsion viscosity, crude oil type, temperature and co-solvent. Adsorption takes place when surfactant micelles and aggregates form on the surfaces of the reservoir rock. A monolayer begins to form and when the equilibrium monolayer adsorption has been reached, the system will form an additional layer (Solairaj et al, 2012).

Figure 2-10 shows the different regions of adsorption of a negatively charged surfactant on a positively charged reservoir rock.

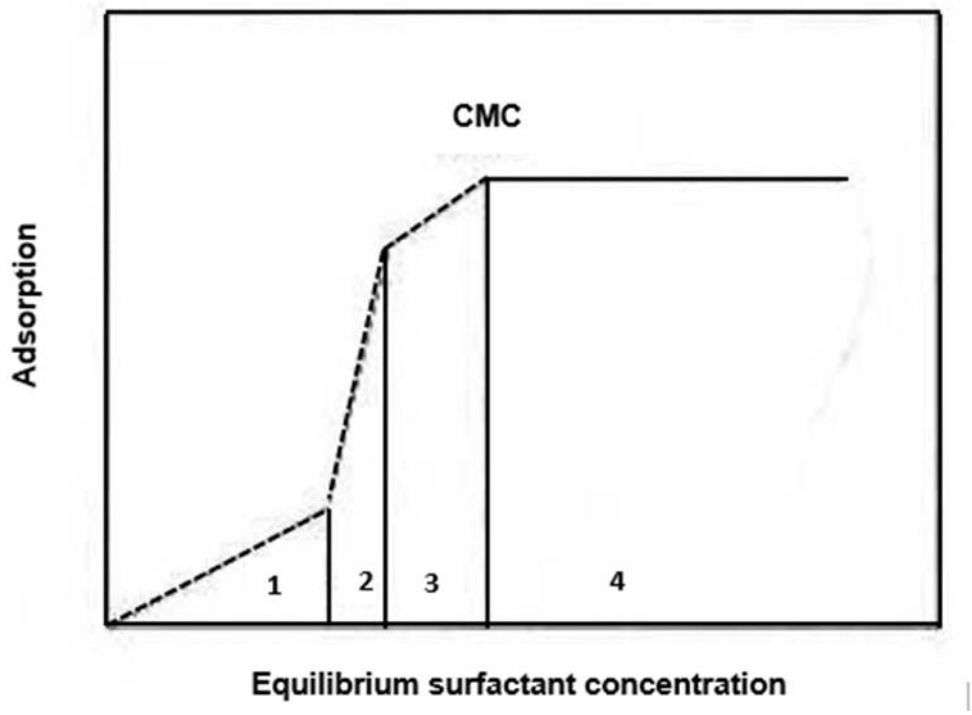

Figure 2-10: Surfactant adsorption on reservoir rock (Azam et al, 2013).

Region 1 on the plot occurs at lower surfactant concentration. The monomers are adsorbed onto the substrate due to the electrostatic interaction between the head group charge and net charge present onto the surface of the adsorbent.

In region 1, the slope of the curve is approximately 1 until it reaches region 2. In region 2, a sharp increase in adsorption density is experienced due to the formation of surface aggregates, called colloids. These colloids include hemi-micelles and ad-micelles. The surface aggregates are formed due to lateral interactions between

hydrocarbon chains and monomers found at the surface. Due to the additional driving force which emerges from the lateral interaction of monomers, the adsorption density increases rapidly. The adsorption density increases with a lower gradient in region 3, this is because the solid surface is electrically neutralised by the surfactant monomers that have been adsorbed. Adsorption takes place due to lateral interactions only. The surfactant reaches the critical micelle concentration in region 4. Hence any further increase in surfactant concentration contributes to the increase in micelles in the surfactant solution making adsorption constant. In this region, surfactant molecules adsorb onto the surface with reverse orientation and this results in the decrease of hydrophobicity of the particles (Somasundaran and Zhang, 2006; Paria and Khilar, 2004).

2.12 Surfactant microemulsion phase behaviour

Mobilising the residual oil saturation from the reservoir to the producing well is understood to occur when the water flood brine is replaced by a surfactant solution. The surfactant solution reduces the interfacial tension between the residual oil and the aqueous phase. Surfactants are transported in the reservoir in the form of microemulsion during surfactant flooding. This is because of the interaction between the aqueous phase containing the surfactant and the hydrocarbon phase. It has been shown that the key factor in determining the success of oil recovery is by interpreting the oil/brine/surfactant system (Sheng, 2011; Flaaten et al, 2009).

Microemulsions are thermodynamically stable, hence do not require high energy input or shear conditions for their formation. The microemulsion phase is transparent, has low viscosity and can create low interfacial tension. The aqueous phase may contain salts and the oil can contain complex hydrocarbons. Winsor first described the behaviour of microemulsion as type I (oil in water) which has a lower phase microemulsion in equilibrium with excess oil, type II (water in oil) with upper phase microemulsion in equilibrium in excess brine and the type III which has middle phase microemulsion in the water/oil region. To find regions where ultra-low interfacial tension is created by high solubilisation ratio, the microemulsion phase behaviour needs to be investigated. This established relationship between interfacial tension and microemulsion is what is used to screen surfactants suitable for chemical flooding.

The transition of surfactants from one phase to another phase is dependent on the several factors such as temperature, surfactant type and structure, oil properties and brine electrolyte. The low interfacial tension is measured by examining the phase behaviour of the microemulsion system where a high solubilisation ratio is obtained. It is crucial that the surfactant forms a three-phase system (middle phase microemulsion) when it is injected into the reservoir to achieve the very low interfacial tension. This is because the lowest interfacial tension is achieved when a middle phase microemulsion is formed (Hirasaki et al, 2008; Buijse et al, 2010).

To increase surfactant solubility of anionic surfactants in brine and to prevent the formation of viscous phases, co-solvent such as alcohol and co-surfactants can be added. The solubilisation parameter indicates the amount of water and oil that has been solubilised in the microemulsion phase per volume of surfactant (Spildo et al, 2012). The oil or water solubilisation is defined as the volume of oil or water that has been solubilised into the microemulsion phase per unit weight of the surfactant. Oil solubilisation ratio can be expressed as the ratio of the volume of oil to the volume of the surfactant (V_o/ V_s) and water solubilisation ratio as the ratio of the volume of water to the volume of surfactant (V_w/V_s) (Elraies, 2014).

In 1976, Healy represented oil and water solubilisation ratio graphically. They measured each volume of solubilised oil and water in neat surfactant solution to obtain water and oil solubilisation ratios. This data was used in obtaining optimal salinity by plotting the solubilisation ratio of oil and water as a function of the salinity for salinity scans that look promising. The point at which equal oil and water volume have been solubilised is the point on the graph where the solubilisation ratio of oil and water intersects. This defines the optimal salinity (Iglauer et al, 2010). This same method is used in this paper to obtain solubilisation ratio and optimal salinity. Figure 2-11 is a diagram showing microemulsion phase formed when surfactant is in equilibrium with oil and water.

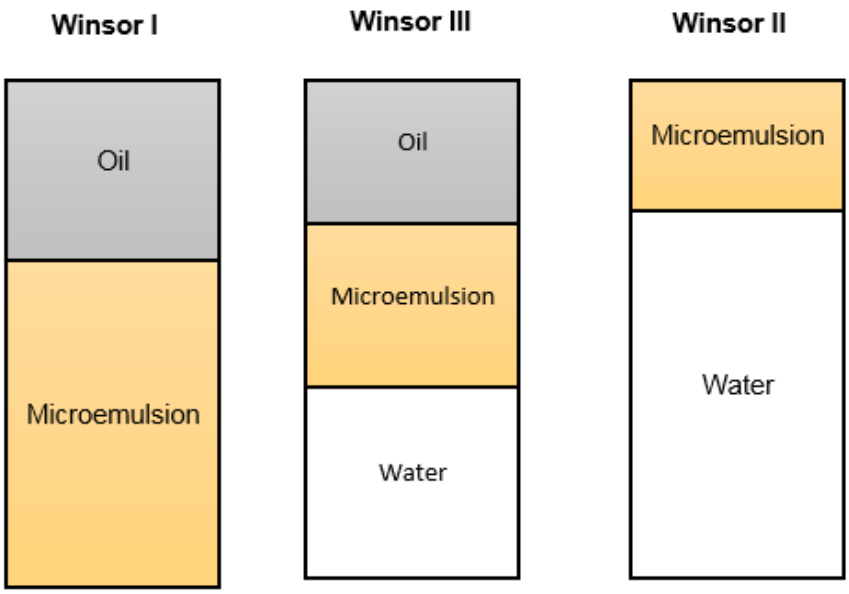

Figure 2-11: Winsor microemulsion phases (Bera and Mandal, 2014).

Healy also defined optimal salinity as the salinity at which the interfacial tension between oil and microemulsion phase is equal to the interfacial tension between the microemulsion and water phase. As a result of the relationship between the optimal salinity and interfacial tension, it is necessary to estimate both properties when choosing a surfactant blend for chemical flooding (Elmofty, 2012). Huh in 1979 proposed a correlation that relates the interfacial tension to the solubilisation ratio and the interfacial tension at optimum salinity. This equation proposed by Huh proposed a correlation relating the solubilisation ratio to interfacial tension which can be used for accurate estimation of interfacial tension form surfactant phase behaviour experiment (Levitt et al, 2006).

$$\gamma = \frac{c}{\sigma^2} \qquad [2.47]$$

Where c is a constant and is approximately 0.3m N/m for most crude oil. σ is solubilisation ratio and is γ the interfacial tension (Fuseni et al, 2013). Figure 2-12 presents the optimal salinity plot for surfactant phase behaviour.

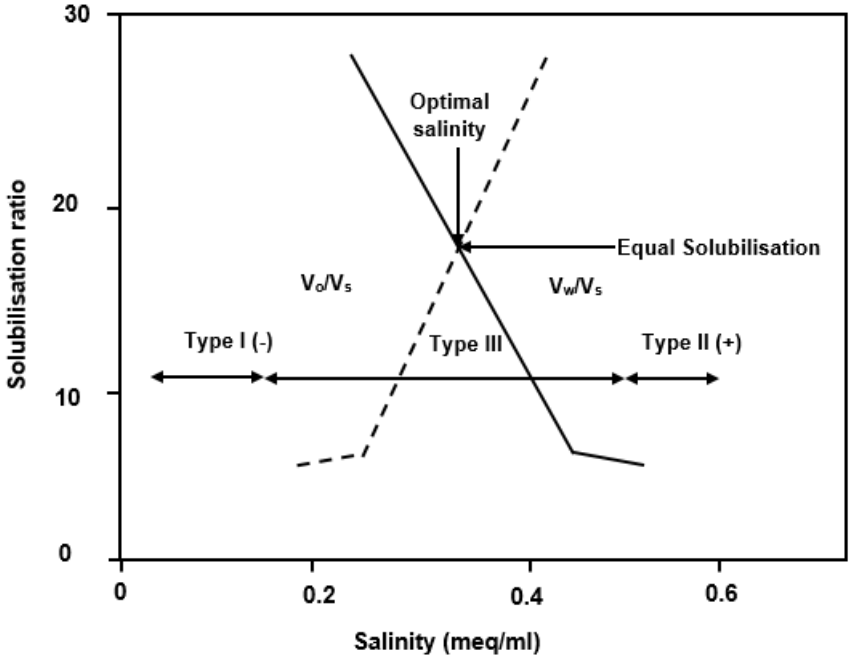

Figure 2-12: Surfactant solubilisation ratio against salinity (Sheng, 2011).

Elraies (2014) studied the mechanism of surfactant in microemulsion phase behaviour using a commercial anionic surfactant alcohol alkoxy sulphate, soft brine (NaCl) and light crude oil. Their results showed that alcohol alkoxy sulphate can create a type III microemulsion phase and then using Healy's method they could obtain the optimal salinity of the surfactant and calculate the interfacial tension with Huh's correlation. They concluded that the concentration of surfactant in a microemulsion phase decreases with increase in salinity. Hence a type III formation at low salinity is more prone to surfactant loss.

Co-surfactants are usually used in conjunction with surfactants. This is because most single chain surfactants are incapable of decreasing the interface tension of oil and water to form a microemulsion phase. The most common co-surfactants are medium chain alcohols, which can increase the fluidity of the oil/water interface, thereby increasing the entropy of the system. Non-ionic surfactants can also be used as co-surfactant. These medium chain alcohols and non-ionic surfactants also increase the mobility of the surfactants' non-polar tail region. Hence, allowing greater penetration by oil molecules and therefore stabilising the system and speed the formation of a microemulsion (Attwood and Florence, 1983).

2.13 Surfactants in water-alternating-gas flooding (SAG)

Chemical flooding of oil reservoirs over the years have been one of the most successful enhanced oil recovery methods in low pressure reservoirs. The use of chemicals in WAG has been studied over the years by researchers (Salehi et al, 2014). The process of alternating water and gas aids the control of gas mobility but unfortunately, the reduction of oil/gas contact reduces in the presence of water this is as a result of the blocking phenomena and high water/oil interfacial tension. This water blocking is a strong function of water wet rocks. In highly viscous oil, the water is displacing highly viscous oil, the water injected has a low viscosity compared to that of the reservoir oil this causes an unstable front behind the oil bank which leads to viscous fingering of injected water and thus the gas having higher mobility and early breakthrough which bypasses many portions of the reservoir.

In this condition, the WAG mobility ratio becomes unfavourable. For this reason, the effectiveness of WAG is decreased (Kulkarni, 2003; Rao et al, 2004).

Falls et al (1988) discussed that surfactant can be injected as a chemical slug during WAG process to reduce the water blocking effect by lowering the IFT and to improve the mobility ratio. The interaction of surfactant and gas during SAG leads to the creation of foam. Foam generated in the porous media is defined as the dispersion of gas in a liquid such that the liquid phase is continuous and at least some part of the gas is made discontinuous by thin liquid films called lamellae. The foam is created as the gas disperses within the surfactant solution and reduces the mobility of the gas and aqueous phase). In surfactant alternating gas injection, a surfactant solution and gas are injected alternatively in slugs. If the slugs are small, they mix near the well and (if gravity segregation has not occurred) at a sufficiently large radius approximate injection at a fixed foam quality. Oil recovery by SAG injection can be effected in three different ways:

A) Stabilising the displacement process as the displacing fluid (gas or foam) viscosity increases.
B) Blocking the high-permeable swept zones and diverting the fluid into the unswept zones.
C) Reduction of the capillary forces by reducing the interfacial tensions with the presence of a surfactant (Majidaie et al, 2015).

The advantage of SAG over WAG injection for the improvement of mobility is that it can contain higher gas saturation (over 85 to 95% gas). This means that a relatively small amount of water is used to decrease gas mobility. The creation of foam has other properties that are favourable to oil recovery, particularly in CO_2 flooding. The apparent foam viscosity is greater than the viscosity of its components which increases oil recovery due to improved mobility ratio. It also increases the saturation of gas trapped and decreases the oil saturation. The trapping of high gas saturation usually leads to a reduction in gas mobility (Syahputra et al, 2000). SAG injection has proved to be an efficient injection procedure. Operating of SAG is similar to WAG and requires little extra effort.

Salehi et al, 2013 conducted an experimental study on SAG injection versus WAG. The compared results obtained from both experiments. Their results show that oil recovery factor for SAG was 20% higher when compared to WAG. The increase in oil recovery in SAG was a result of stable foam formed and viscous fingering was delayed.

For any chemical oil recovery process involving surfactants, a compatible surfactant formulation needs to be designed to prevent problems associated with surfactant flooding such as the formation of gels and precipitates that can clog the pore space of the rock. In this research, to select the suitable surfactant formulation, the Barnes et al (2010) methodology will be used. Phase behaviour studies will be conducted and the solubilisation ratio and optimal salinity will be obtained. Different surfactant blends will be evaluated and the most promising of all the blends will be used for the research.

Surfactant effect on two-phase (water/oil, gas/oil and gas/water) relative permeability will be evaluated in this research using the unsteady state two-phase displacement experiment as discussed in the literature. The two-phase relative permeability curves will be obtained by history matching experimental data with Sendra software using the Sigmund and McCaferry correlation in the literature.

The extension of JBN/Welge theory will be used to estimate experimental three-phase relative permeability and surfactant effect on three-phase relative permeability. Three-phase relative correlations in the literature review available in Eclipse reservoir simulator will also be used to study surfactant effect on three-phase relative

permeability. The correlations are Stone 1, Stone 2, Stone exponent, saturated weighted interpolation and linear interpolation displayed in equations [2.27] to [2.43].

Evaluation of the correlation that best predicts three-phase relative permeability in the presence of surfactants will be carried out by comparing the experimental prediction to of surfactant effect of three-phase relative permeability to results obtained using correlations.

Chapter 3 Materials and methods

This chapter describes the equipment, materials and methodology used for this research. 3.1, 3.2 and 3.3 will describe the properties of materials, chemicals, fluids and equipment used in the experiments. 3.4 and 3.5 will discuss the methodology used in measurements involving fluids (oil and brine) characterisation (viscosity, density and interfacial tension measurement) and selecting surfactant formulation for this research.

The experiments required to evaluate the surfactants involves the determination of critical micelle concentration, surfactant salinity scan, and surfactant adsorption and phase behaviour experiments. Core sample characterisation and the displacement experiments conducted to obtain two and three-phase relative permeability data will also be discussed in 3.6 – 3.8. 3.9 discusses the software used for this research.

The objective of the two-phase displacement experiment was to investigate surfactant effect on fluid flow existing when only two-phases are present and correlate with three-phase flow in the porous media. The two-phase relative permeability data is needed to estimate three-phase relative permeability using the three-phase correlations present in the literature. The following displacement experiments have been conducted for this research:

- Two phase gas/water displacement experiment.
- Two phase gas/oil displacement experiment.
- Three phase oil/gas/water displacement experiment.
- Three phase surfactant/oil/gas displacement.

3.1 Materials

Core sample properties

All experiments were performed using Berea sandstone core samples. A total of 5 core samples were used for this study.

The properties of the rock are listed in Table 3-1. The absolute permeability of the rock was measured at 25 °C after plotting differential pressure versus flow rate and applying Darcy's law. It should be noted that the absolute permeability and porosity values presented in Table 3-1 are average values after several measurements.

Table 3-1: Core properties

Absolute Permeability (mD)	100
Length (cm)	10.2
Diameter(cm)	2.5
Pore Volume (ml)	9.00
Bulk volume (cm^3)	49.5
Dry weight (g)	104.5
Saturated weight (g)	113.5
Porosity	0.18

3.2 Fluid properties

The brine used for this research is hard brine containing several divalent and monovalent ions. The composition of the brine is presented in Table 3-2. Crude oil is from the North Sea with 21° API gravity, which indicates a medium crude oil. The properties of the crude oil are given in Table 3-3.

Table 3-2: Hard brine composition

Salts	**Concentration (g/litre)**
NaCl	56.6
$CaCl_2.2H_2O$	6.3
KCl	0.56
$MgCl_2.6H_2O$	8.16

Table 3-3: Crude oil properties

API	21
Density (g/cm^3)	0.93

Surfactant

All surfactants used for this research are anionic. They include alcohol alkoxy sulphate (AAS), internal olefin sulfonate (IOS), methyl ester sulfonate (MES) and anionic olefin (AO).

Gas

Nitrogen gas is used for this study and it is assumed to be completely immiscible with the oil.

3.3 Details of experimental apparatus

3.3.1 Core flood set up

The experimental setup is a customised core flood apparatus which has been designed and fabricated to perform sequential injection of water, oil, and gas at constant temperature at a specified pressure. A schematic of the core flood apparatus is shown in Figure 3-1 and it comprises of the following components.

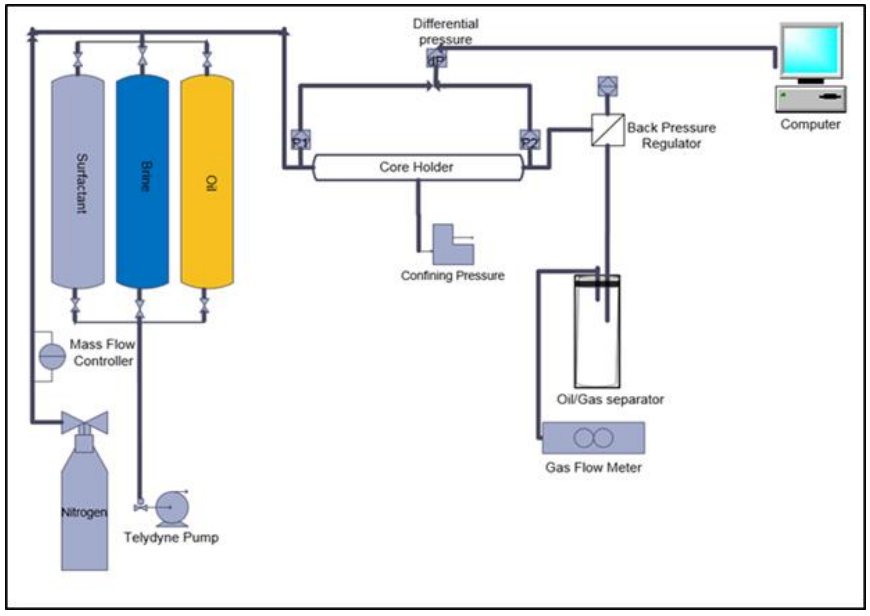

Figure 3-1: Schematic of core flood system.

3.3.2 Core holder

All experiments were conducted using a high pressure, stainless steel cylindrical core holder. This is a typical hydrostatic core holder, as depicted in the appendix A3, with two steel end plugs on two sides and a rubber sleeve inside to hold core samples.

This core holder was designed for gas and liquid permeability testing and for experiments involving chemicals. The reservoir overburden pressure is mimicked in this experiment by applying confining pressure. The confining pressure was exerted in the core holder using hydraulic oil, which was injected through a hydraulic pump into the annulus space of the core holder. On the top of the core holder there is an opening which is sealed with a knob to hold pressure in the core holder and prevent the hydraulic oil from draining out.

3.3.3 Fluid injection system

The fluid injection system consists of three accumulators used to store fluids (oil, brine, and surfactant solutions) and then supply these fluids through the tubing into the core sample. A pump connected to the accumulators is used to push the fluids in the accumulator by moving the piston inside the accumulator and tubing flow lines. The transfer cylinder, tubing flow, lines and fitting valves connect the flow lines to the core holder. The pump is a Teledyne Isco (D Series with a flow accuracy of 0.5 % of set-point) syringe pump, shown in Appendix A2. It has a digital controller front panel. Flow rate, flow pressure, and operating mode could be controlled by user input. In this research, the pumps were operated in a constant flow rate mode.

3.3.4 Pressure transducer system

The Bronkhorst pressure transducers data acquisition system was responsible for receiving and recording the signals of pressure from the injection and production point of the core holder. The pressure transducer sends an electronic signal which is proportional to pressure, to the computer. The Bronkhorst software such as flow view, flow plot and flow DDE which have been installed in the computer transforms these signals to a text file. The Flow DDE receives the signals from the pressure transducers and converts the signals to pressure data. The flow plot digitally records pressure data in a text file while the flow view is used to manually monitor pressure measurement.

3.3.5 Fluid collection system

A Back-Pressure Regulator (BPR) was mounted in the fluid discharge line (as shown in Figure 3-1) to control the pressure in the core flood system during experiments. This is to maintain a constant pressure drop during the experiment. The BPR was

operated via a balanced pressure system. In this system nitrogen, at the desired pressure, was injected into the dome of the regulator. Once the fluid flow pressure exceeds the pre-set dome pressure, the metal diaphragm inside the back-pressure regulator will flex to allow fluids to flow and to maintain the system pressure.

Effluent fractions were collected in graduated test tubes for water/oil displacement to obtain the volume of oil and water produced during the experiment. For gas/oil and gas/water displacements, a conical flask placed on a balance was used to collect the effluent. The conical flask was connected to the outlet of the core flood system and then sealed at the top using a rubber plug. The plug has two openings at the top. One of the openings is connected to the core flood outlet to collect the effluent while the second opening was connected to the gas flow meter to measure gas breakthrough time. The mass of the fluid is measured using the balance and divided by the density to obtain the volume.

3.3.6 Heating system

The core flood apparatus was housed in an oven to keep the temperature constant during the experiment. The temperature controller is used to set temperature in the oven. The temperature range of the oven is between 40 – 250 ºC.

3.3.7 Gas injection system

Gas injection was conducted using a custom-made precise Bronkhorst (accuracy within 0.5 %) gas flow controller. This controller can be visualised in the appendix A7. It was fed with a constant pressure of 30 psi from a nitrogen cylinder to accurately inject gas at constant rates. This gas flow controller can inject any gas at a constant flow rate up to 8 ml/min and can function up to a maximum pressure of 500 psi.

3.4 Experimental procedures for fluid characterisation

Experimental procedures have been divided into two sections. The first section describes the procedures involved in fluid characterisation and surfactant formulation design, while the second part describes experimental procedures for two and three-phase displacement experiments.

3.4.1 Density Measurement

A 50 ml pycnometer was used to measure the density of the brine and oil. The diagram of a pycnometer is shown in the appendix. To measure the density, the following steps were taken.

- Rinse the pycnometer thoroughly with distilled water three times.
- Fill the pycnometer completely with distilled water.
- Place carefully so that the excess fluid flows through the jet orifice of the cap.
- Clean up the exterior of the pycnometer until completely dry, and then measure the mass.
- Fill the pycnometer with water and register the mass. Subtract the mass of the empty pycnometer from the weight of the filled pycnometer to get the mass of water.
- Use the equation [3.1] to calculate volume of water.

$$V = \frac{M_{H20}}{\rho_{H20}} \qquad [3.1]$$

- Empty the pycnometer and pour in the fluid to be tested.
- Repeat the same procedure for water and then measure the mass of the tested fluid in the pycnometer.

The volume of the liquid can be calculated from the equation

$$V = \frac{M_L}{\rho_L} \qquad [3.2]$$

Combining equations [3.1] and [3.2] yields the equation that provides the density of the measured liquid.

$$\frac{M_{H20}}{\rho_{H20}} = \frac{M_L}{\rho_L} \qquad [3.3]$$

Nitrogen gas density calculation

The ideal gas equation was used to calculate the density of gas.

$$\rho_{nitrogen} = \frac{PM}{ZRT} \qquad [3.4]$$

Where

ρ- Density of nitrogen

M- Molecular weight

P- Pressure

R- Gas constant

T- Temperature

Z- Gas compressibility

3.4.2 Fluid viscosity measurement

The viscosities of the oil, brine, and surfactant were measured using Bohlin 200 rheometer. Fluid viscosity is required for permeability calculations and for simulation of oil recovery in Eclipse reservoir simulator. The Bohlin rheometer measures the viscosity as a function of shear rate. Fluid viscosities were measured at room temperature and 60 ºC. See appendix A10 for the diagram of the rheometer.

Gas viscosity measurement

Gas viscosity at 60 ºC was calculated using Sutherland's equation. The theory is based on the kinetic theory of ideal gas (Memon et al, 2016).

$$\mu = \mu_o \left(\frac{a}{b}\right) \left(\frac{T}{T_O}\right)^{3/2} \quad [3.5]$$

Where $a = 0.555T_O + C$

$b = 0.555T + C$

For nitrogen gas, viscosity at reference temperature $\mu_o = 0.017$ cp,

Reference temperature $T_O = 527.6$ ºR

Sunderland constant C = 240

Experimental temperature T= 599.67 ºR

3.4.3 Interfacial tension measurement using pendant drop method

The surfactant formulation should be able to reduce water/oil interfacial tension. The pendant drop method is used to measure initial water/oil interfacial tension before surfactant reduction. The mechanism behind the pendant drop method is to analyse the drop shape formed when the oil meets water/brine through the needle. Figure 3-2 shows a pendant drop for interfacial tension measurement.

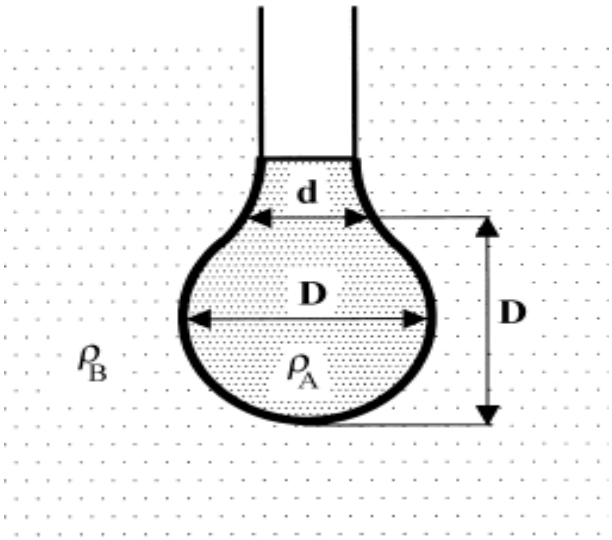

Figure 3-2: Pendant drop (Drelich et al, 2002).

A transparent cell which has the needle attached to it at the bottom is half filled with water or brine while oil is injected through a syringe into the cell. The cell is half filled with brine/water to make allowance for the oil to form a drop. As the oil meets the water from the needle it forms a drop shape. This drop is captured by the camera. The cell is placed in a position where the oil drop can be captured properly by the video camera. The video camera is connected to a computer where a drop analysing software has been installed. See Figure 3-3 below for the schematic of the setup for interfacial tension measurement. Several drops were captured and analysed to get a good image of the drop.

The interfacial tension is calculated from the dimensions of the pendant drop. The pendant drop method involves the measurement of the two parameters known as equatorial diameter D and the diameter d of the distance D (equatorial diameter) from the top of the drop of the drop. The interfacial tension is then calculated form equation [3.7]. In equation [3.6], the parameter H is dependent on the value of a shape factor S. S is the ratio of d/D. The shape factor S is used to calculate the shape dependent parameter H by obtaining the empirical constants for a range of S values given in Table 3-4 (Drelich et al, 2002). The shape dependent parameter H depends on the value of the shape factor S. The values for 1/H can be calculated from the empirical formula below.

$$\frac{1}{H} = \frac{B_4}{S^a} + B_3\,S^3 - B_2 S^2 + B_1 S - B_0 \qquad [3.6]$$

Where B_i (= 0, 1, 2, 3, 4) and 'a' are empirical constants for a certain range of values.

Table 3-4: Empirical Constant (Drelich et al, 2002).

Range of S	A	B4	B3	B2	B1	B0
0.401–0.46	2.566	0.327	0	0.975	0.840	0.180
0.46 – 0.59	2.597	0.319	0	0.468	0.500	0.132
0.59–0.68	2.624	0.315	0	0.117	0.157	0.052
0.68–0.90	2.642	0.313	0	0.091	0.147	0.058
0.90–1.00	2.846	0.307	- 0.691	-1.083	- 0.183	-0.209

The interfacial tension is the calculated with this equation:

$$\gamma = \frac{\Delta\rho g D^2}{H} \qquad [3.7]$$

Where

ρ- Density

g- Gravity

D- Equatorial diameter

H- Shape parameter

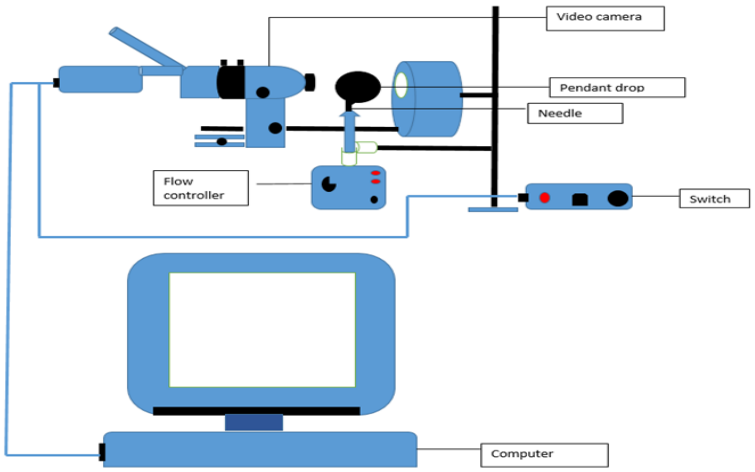

Figure 3-3: Video camera and set-up for interfacial tension measurement.

3.5 Surfactant formulation selection

3.5.1 Measurement of critical micelle concentration (CMC)

To measure the CMC, surface tension is measured at very dilute concentrations of surfactant using a DCA (Direct contact angle) tensiometer. The DCA tensiometer measures the surface tension of a fluid at its interface with gas. A du-nuoy ring which is connected to the tensiometer is dipped into the surfactant solution inside a beaker placed on the sample stage of the tensiometer. The surface tension is measured when the ring is dipped into the fluid and the pulled to the surface. This is repeated for different concentrations to obtain the different surface tension values. A plot of surface tension against surfactant concentration was used to determine the critical micelle concentration. When the plot is made, the point of deviation on the plot where the lowest surface tension is achieved is known as the critical micelle concentration. After this point, the surface tension measured becomes almost constant. This deviation point at lowest surface tension is the CMC.

Error analysis has been examined for the surface tension measurements using the tensiometer. The measurement for surface tension was repeated twice and the error analysis are shown in appendices A13-15. One can see from the plots surface tension measurements against the surfactant concentration(A13-15) that the uncertainty between the two measurements were very low. This could be due to the ring in the tensiometer still have some traces of surfactant from the previous measurement after being cleaned with distilled water. Usually heat is applied to the ring after cleaning but for this research, tissue was used to dry the ring. This could also be the source of error. This error margin was calculated using the standard deviation method proposed by Pipes and Lawrence (2014).

For this study, surfactant concentration used will be above the critical micelle concentration. Several types of research have shown that using surfactant concentration above critical micelle concentration is more effective in surfactant enhanced oil recovery processes. Creation of foam by surfactants has been investigated by Jones et al (2016) and Vikingstad et al (2005). They also concluded that the stability of foam generation is achieved when the concentration is above the critical micelle concentration. Donaldson et al (1989) have agreed that it is important to make the concentration of the surfactant higher than the critical micelle

concentration to obtain a very low interfacial tension for water/oil system. This is because the greatest effect of the surfactant in lowering interfacial tension is achieved when a significant number of micelles are present (Donaldson et al, 1989). Since the two mechanisms involved in SAG are the reduction in interfacial tension and generation of foam from surfactant interaction with gas, a concentration of 0.15 vol% was used in all experiments.

3.5.2 Surfactant salinity scan

The salinity scan experiment was conducted at room temperature. Brine and surfactant are mixed in a test tube. The surfactant concentration is kept constant while the salinity of the brine is varied. The solution of surfactant and brine in test tubes, were monitored for five days to observe if there was precipitation or if the solution becomes hazy. If the solution remained clear for the five days, this indicates that the surfactant is compatible with the brine and can be used for phase behaviour experiment. If precipitates are formed or the solution becomes hazy, the surfactant should be discarded and a new surfactant should be selected. Figure 3-4 shows the chart for surfactant salinity scan test. The chart shows the steps involved in selecting a surfactant formulation for chemical enhanced oil recovery.

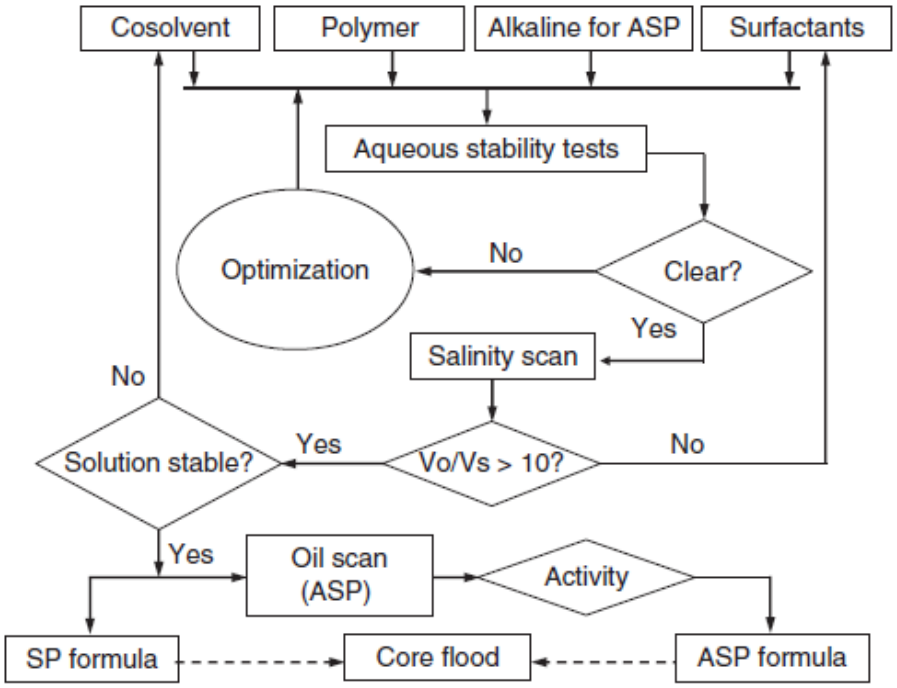

Figure 3-4: Surfactant salinity scan chart (Sheng, 2011).

3.5.3 Surfactant phase behaviour experiment

The Phase behaviour experiment is conducted with surfactants that do not form precipitates. The essence of conducting a phase behaviour experiment is to study the surfactant interaction with the brine and oil by the ability of the surfactant to create microemulsion phase. A suitable surfactant should be able to form a stable microemulsion phase. The experiment was conducted using a 5 ml glass pipette with an equal volume of the aqueous phase and oil phase (2.5 ml each). The bottom of the pipette was flame sealed and a stopper was used to seal the top of the pipette.

The aqueous phase was introduced into the pipette when no precipitation was observed. Crude oil was introduced into the pipette. The salinity of the brine in the aqueous phase was varied keeping in the range of 1- 6.7 % while the concentration of the surfactant was kept constant. The pipette was placed in an oven with the samples in them at a temperature of 60 °C. The temperature was fixed at 60 °C because this is the temperature at which the core flooding experiment with surfactant will be conducted.

Equilibration time was monitored as well as oven temperature. The pipettes were agitated and inverted at time intervals of 30 minutes to ensure complete mixing of the different phases. The pipettes were arranged in order of increasing salinity. The equilibration time, as well as change in volume of the aqueous phase and oil phase, were recorded at different intervals (days to weeks) and the microemulsion phase change were also monitored and recorded. Phase behaviour tests were conducted at room temperature and at 60 ºC.

Phase behaviour experiments were conducted using internal olefin sulfonate surfactant, methyl ester sulfonate and alcohol alkoxy sulphate with co-surfactants methyl ester sulfonate and internal olefin sulfonate. For the phase behaviour experiment, surfactant concentration used was above the critical micelle concentration.

3.5.4 Determination of solubilisation ratio and optimal salinity

The optimum salinity was determined by plotting the solubilisation ratio as a function of the salinity for promising surfactant/oil formulations in the pipette. The point at which equal oil and water volume have been solubilised on the graph is where the solubilisation ratio of oil and water intersects. This point is known as the optimal salinity. The solubilisation ratio was determined from the surfactant phase behaviour experiment by using the ratio of the oil volume to the volume of the surfactant solubilised for oil solubilisation ratio. Water solubilisation ratio is the ratio of the volume of the aqueous phase to neat surfactant volume solubilised. A solubilisation ratio greater than 10 indicates that the surfactant can create very low interfacial tension of about 0.001 mN/m using Huh's correlation. A surfactant formulation with solubilisation ratio less than 10 should be discarded. Equations [3.8] and [3.9] were used to calculate oil and water solubilisation ratios. The plot of solubilisation ratio versus salinity has been discussed in Figure 2-12.

$$\textit{Oil solubilisation ratio} = \frac{\textit{Volume of oil } (V_o)}{\textit{Volume of surfactant solubilised}(V_s)} \quad [3.8]$$

$$\textit{Water solubilisation ratio} = \frac{\textit{Volume of water } (V_w)}{\textit{Volume of surfactant solubilised } (V_s)} \quad [3.9]$$

3.5.5 Measurement of low interfacial tension using solubilisation ratio from phase behaviour experiment

After the phase behaviour experiment, the solubilisation ratio obtained can be used to estimate interfacial tension created by the surfactant. Huh (1979) proposed a correlation that relates the interfacial tension to the solubilisation ratio and the interfacial tension (Levitt et al 2006). Huh correlation has been discussed in equation [2.47].

3.5.6 Adsorption of surfactant Using UV spectrometer

For this research, the surfactant adsorption experiment was conducted using the core flood apparatus. Surfactant solution was injected into a core sample that was fully saturated with injection brine. The effluent was collected in glass bottles until the differential pressure becomes constant and effluent concentration was the same as the injected surfactant. Surfactant concentration was measured using a UV spectrometer until the concentration of the effluent was almost the same as the surfactant solution. See appendix for the diagram of UV spectrometer. Surfactant adsorption was calculated using equation [3.11].

$$Adsorption = (C_o - C) \times PV / W_{sg} \qquad [3.11]$$

Where
C_o- Initial surfactant concentration
C- Surfactant effluent concentration
PV- Pore volume
W_{sg}- Weight of sample
Adsorption: Surfactant adsorption on the rock sample (Zhang et al, 2013).

3.6 Two and three-phase relative permeability measurement

3.6.1 Core sample cleaning

The core was cleaned using toluene and methanol in a soxhlet extractor. The core sample was placed in a soxhlet with toluene in the round bottom flask placed on a heating mantle. When the heat was switched on, the toluene starts to boil. As toluene

gets to its boiling point, the vapour goes to the condenser in the soxhlet. Through the condenser, the vapour turns back to liquid (toluene or methanol) and flows back to the soxhlet where the core sample was positioned and cleans the sample. When the soxhlet gets filled with toluene at a particular level, the liquid drains back to the round bottom flask and continues to boil. This cycle continues until the core sample becomes completely cleaned. The core sample is said to be clean when the toluene in the soxhlet becomes colourless meaning all the crude oil has been removed from the sample. The cleaning repeated with methanol after using toluene. When cleaning is complete with toluene and methanol, the core sample was flushed continuously with distilled water and then placed in the oven to dry.

3.6.2 Core sample preparation

The weight of the dry core sample is measured using a weighing balance and a calliper is used to measure the diameter and the length of the core sample. The core sample is saturated in brine and kept in a vacuum to displace air from the core sample and enhanced saturation.

3.6.3 Porosity and absolute permeability measurement

- The length and diameter of the core sample was measured using a calliper
- The weight of the sample was measured using a balance
- The core was then saturated in water in the vacuum
- The saturated weight was obtained using the balance
- The porosity of the core sample was estimated from the difference between the saturated weight and the dry weight divided by the bulk volume and density of the brine.

To calculate the bulk volume of the core sample, equation [3.12].

$$\text{Bulk volume} = \frac{\pi d^2}{4} l \qquad [3.12]$$

The first test which is the simplest and yet very important one is measuring the absolute permeability. The absolute permeability of a core can be determined by injecting a single-phase fluid at different flowrates. The pressure drop across the core was measured and with the viscosity of the fluid, Darcy's law was used to estimate

the absolute permeability of the core. The permeability tests were conducted at room temperature and a confining pressure of 500 psi was applied. Eight different flowrates of water starting from 1- 8 ml/min were applied until steady state pressure drops across the core was achieved. Darcy's equation is expressed in equation [3.13].

$$\mathrm{K} = -\frac{Q\mu L}{A\Delta P} \qquad [3.14]$$

Where

K- Permeability

Q- Flowrate

μ- Viscosity

A- Area

L- Length

ΔP- Differential pressure

3.6.4 Capillary end effects

Capillary end effects can have a significant impact on core flooding experiments. The end effects occur at the outlet face of a core during a simultaneous flow of two or three phases. This simultaneous flow of fluid can give rise to a discontinuity in capillary pressure which exists when flowing phases are about to leave the core and enter the non-porous space with zero capillary pressure. The discontinuity in capillary pressure affects the wetting phase more than the non-wetting phase, this makes it difficult for the wetting phase to leave the outlet face of the core. The build-up of the wetting phase which occurs at the outlet of the core can influence the end-point saturation values and end-point permeabilities.

In calculating the relative permeabilities from core flood experimental data, theoretically it is possible to include the effect of the capillary pressure. In most cases the required capillary pressure versus saturation data are not available for the rock-fluid systems which are under investigation. Under certain conditions, capillary end effects can be neglected (Maini and Okazawa, 1987). It is, therefore, necessary to set appropriate criteria and run the core flood experiment. A scaling coefficient can be used to determine a critical value above which the capillary end effects can be neglected. The equation for the scaling coefficient is defined as Lvμ >1. Where L is the length of the core (cm), v is the Darcy velocity (cm/min) and μ is the viscosity of

displacing fluid (cp). In a core flood experiment where Lvμ >1, it is reported that the capillary end effects will be small and they can be neglected (Haugen, 1990). In each displacement process, the injection flow rates must be high enough to maintain this criterion. For this study, the above-mentioned criteria have been considered while setting the flow rate to prevent the capillary end effects. The rates were set to hold the condition Lvμ >1.

3.6.5 Dead volume of the core flood apparatus

In assembling any core flood apparatus for core flood experiments, in addition to the real pore volume of the core sample, there is going to be some extra volume associated with injection/production and pressure lines which are called dead volume. The dead volume consists of two different types which are static and dynamic dead volume. The static dead volume consists of pressure lines in which there is no fluid flow while the dynamic volume includes the injection and production lines right before and after the sand faces. In designing the core flood system, there must be maximum effort to minimise the dead volume. The dead volume must be measured and recorded to be deducted after core flood experiment to get the actual fluid production. For the core flood system used for this study, the dead volume includes the tubing connecting the accumulator to the core holder, the tubing connecting the production line to the core holder. The dead volume of this system has been measured to be 7.5 ml.

3.7 Two-phase water/oil experiment

The following procedures were carried out for the water/oil displacement experiment

- The length and diameter of the clean dried core were first measured using a calliper and then the weight was taken with a balance
- The weighed sample was saturated in brine for 18 hours and weighed again to obtain the saturated weight and then placed into the core holder
- After placing the core in the core holder, a confining of 500 psi was applied to the core sample to account for reservoir overburden pressure
- The core sample was flooded continuously with brine at different flow rates to measure the absolute permeability

- A back-pressure regulator was connected at the production end of the core flood apparatus. The back pressure was maintained at 30 psi
- The core was aged using 10 pore volumes of brine at a low rate of 0.1ml/min to restore any wettability alteration by cleaning.
- The desired temperature was set on the temperature controller and the accumulator was filled with oil
- Oil was injected at a constant rate of 0.3 ml/min via a transfer cylinder
- Oil injection was continued until irreducible water saturation was established
- During oil injection, effluent was collected in the graduated test tubes while recording time

3.7.1 Two-phase surfactant /oil experiment

The same procedure for two-phase water/oil displacement experiment was followed for the surfactant but instead of brine, surfactant was continuously injected into the core sample for one hour and left to equilibrate for 6 hours. To fulfil surfactant retention on the core sample. Oil was injected to displace surfactant to irreducible saturation. Surfactant was then injected until residual oil saturation.

3.7.2 Two-phase gas/oil experiment

The experiment started with oil injection into the core sample at a steady flowrate of 0.3 ml/min until connate water saturation which resembles a natural petroleum reservoir. To simulate gas flow into the reservoir, nitrogen was injected into the core sample at a constant flowrate of 8 ml/min. The gas flow rate is controlled by the gas flow controller. The oil was flooded by gas to the production end of the core flood apparatus. To obtain surfactant gas/oil relative permeability and study the effect of surfactants on gas/oil relative permeability, the core flood experiment was conducted in the presence of surfactant.

3.7.3 Two-phase gas/oil flooding with surfactant

The surfactant is injected into the core sample continuously for 4 hours and the sample is left to equilibrate with the surfactant for another 6 hours. Oil is then injected into the sample to displace the surfactant. The oil injection is stopped at breakthrough

leaving the surfactant solution at irreducible value in the pore spaces of the core sample. Gas is then injected to displace the oil from the core sample.

3.7.4 Two-phase gas/water experiment

The core sample was first saturated with brine. The brine was injected continuously into the core sample for one hour and let to equilibrate. Gas was then injected into the core sample from the gas flow controller to displace the water to connate water saturation. To study the effect of surfactant on gas/water relative permeability, the core sample was replaced with a clean saturated sample in brine.

3.7.5 Two-phase surfactant/gas experiment

Surfactant was continuously injected into the core sample for 3 hours continuously and kept to equilibrate. Gas is then injected into the sample to displace the surfactant to irreducible value. Surfactant production is collected using a test tube and the differential pressure is measured using the pressure transmitters.

3.8 Three-phase displacement experiment

3.8.1 Water-alternating-gas flooding

- The length and diameter of the clean, dried core were first measured using a calliper and then weighed with a balance
- The weighed sample is saturated in brine for 18 hours and weighed again to obtain the saturated weight and then placed into the core holder
- After placing the core in the core holder, a confining pressure of 500 psi was applied to the core sample to account for reservoir overburden pressure
- The core sample was flooded continuously at different flow rates to measure the absolute permeability
- A back-pressure regulator was connected at the production end of the core flood apparatus. The back pressure was maintained at 30 psi
- The core was aged using 10 pore volumes of brine at a low rate of 0.1 ml/min to restore any wettability alteration by cleaning
- The desired temperature was set on the temperature controller and the accumulator was filled with oil and allowed to equilibrate for 8 hours

- Oil was injected at a constant rate of 0.3 ml/min via a transfer cylinder
- Oil injection was continued until irreducible water saturation was established
- Brine was injected into the core sample until residual oil saturation. Then the brine accumulator was isolated completely for gas injection
- Gas injection into the core sample continued to produce residual oil saturation. The gas was supplied into the core sample through a Bronkhorst gas flow controller until gas breakthrough. Gas breakthrough is monitored using a gas meter
- After gas injection, another cycle of water was injected into the core sample until oil production ceased completely and there was only water production
- Effluents were collected using a test tube and the total volume of oil was collected after oil and water segregation in the test tube

The same procedure for WAG was followed but in the case of surfactant. After saturating the core sample with brine, the core was placed in the core holder a continuously flushed with surfactant to account for surfactant retention on the core sample. The core sample was kept to equilibrate for 8 hours before oil was injected into the sample. Oil was continuously injected at 0.3 ml/min until connate water saturation. The surfactant was then injected into the core sample until breakthrough. The surfactant accumulator was completely isolated for gas injection. Gas was injected until residual oil saturation and then another cycle of surfactant was injected into the core sample.

3.9 Software used for research

3.9.1 Sendra software

Sendra is a two-phase core flooding simulator which has been specially designed to simulate and verify special core analysis (SCAL) experiments. Sendra covers all common experimental approaches which include unsteady-state and steady-state flow experiments, single and multi-speed centrifuge experiments, and porous plate experiments. It can be utilized for oil-water experiments, gas-oil or gas-water experiments, and imbibition and drainage processes. The main application of Sendra is to determine relative permeability from experimental data through an automated history matching approach. Sendra can simulate all common SCAL experiments and can be used as a tool for planning and successful execution of your SCAL projects

(Sendra user guide, 2011). Sendra is tailored for SCAL and options necessary for laboratory applications have been included in the software. Sendra is not constrained by limiting assumptions such as zero capillary pressure which analytical methods are. Consequently, Sendra provides a very good means of quality control of analytical methods (Sendra user guide, 2011). In this study, Sendra software has been used to history match experimental data using two-phase relative permeability correlations present in the software to obtain two-phase relative permeability curves.

3.9.2 Eclipse reservoir simulator

Schlumberger Eclipse is a reservoir simulation software. It is used in relation to black oil, compositional, thermal, and streamlines reservoir problems. It offers a robust set of numerical solutions for fast and accurate prediction of dynamic behaviour for all types of reservoirs and development schemes. The ECLIPSE simulator suite consists of two simulators, ECLIPSE100 and ECLIPSE300. Eclipse 100 is the black oil simulation software, this model treats the three-phase oil, gas and water as mass components in which the gas is only allowed to dissolve in oil and water while E300 is the compositional simulation software. Eclipse 300 allows modelling multicomponent hydrocarbon flow to get a detailed description of phase behaviour and compositional changes. This model defines not just the three phases (water, gas, and oil) but the actual compositions of the oil and gas phases are explicitly acknowledged due to their more complicated PVT behaviour. That is separate hydrocarbon components (C1, C2, C3, etc.) in the oil and gas phases (Eclipse100 manual, 2013). Eclipse can be used to calculate three-phase relative permeability using existing three phase correlations present in the software by simulating WAG flooding and inputting the three-phase relative permeability keyword (Melby, 2014).

Chapter 4 Experimental results and discussion

This chapter presents the results obtained during this research following the methodology described in Chapter 3. The first set of results presented in 4.1 and 4.2 are measurements of fluid properties such as viscosity, interfacial tension and density of oil, brine and gas. Viscosities of oil, brine, and surfactant measured at room temperature and 60 ºC. The gas viscosities were calculated using Sutherland's equations.

The next series of results in 4.3 - 4.3.5 corresponds to the surfactant evaluation, to select the best surfactant formulation that is compatible with the brine and oil used in this research. This is followed by the discussion of results in 4.4- 4.4.6 obtained from two-phase oil/water, gas/water and gas/oil displacement experiments. The effect of surfactant on two-phase gas/water, gas/oil and water/ oil relative permeability is also being analysed in this section. Comparisons of surfactant effect on gas relative permeability has also been evaluated in this chapter to give a better understanding of the interaction that occurs in the reservoir during gas flow involving surfactant.

4.1 Fluid property measurement results

4.1.1 Viscosity

Viscosity measurement for brine, oil and surfactant are shown in Figures 4-1, 4-2, 4-3, and 4-4. Figure 4-1 is a plot of viscosity against time for brine at 25 ºC and 60 ºC. While Figures 4-2 is the plot for surfactant viscosity at 25ºC and 60 ºC and figures 4-3 and 4-4 are plots for oil viscosities at 25 ºC and 60 ºC. Oil viscosity at 60ºC was 26 cp while at 25 ºC the viscosity was 100 cp. The viscosity values obtained for brine at 25 ºC and 60 ºC were 1.05 cp and 1.07 cp respectively. The values for surfactant viscosities are the same as brine viscosities. Table 4-1 shows the calculated nitrogen gas viscosity using equation [51] in Chapter 3.

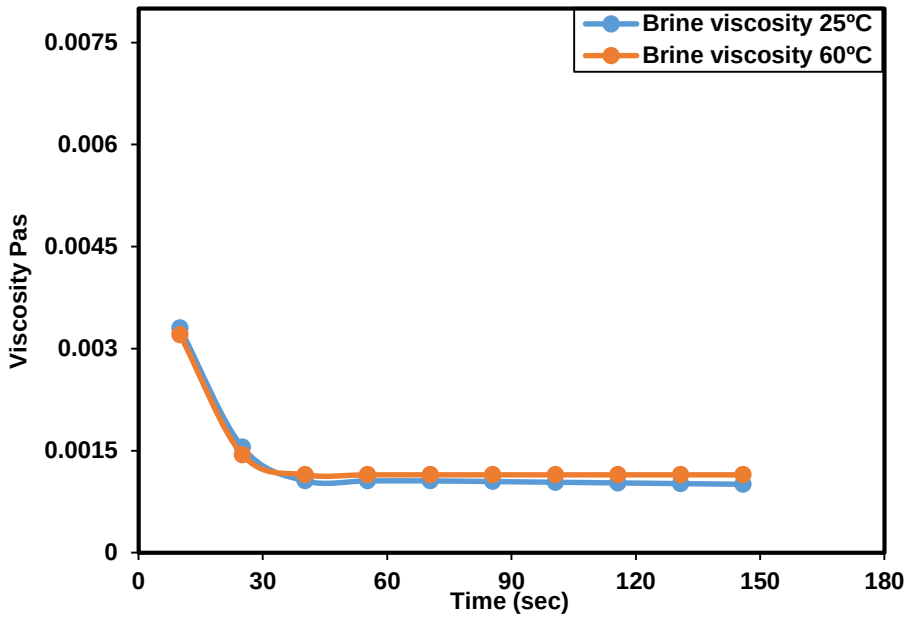

Figure 4-1: Brine viscosity versus time.

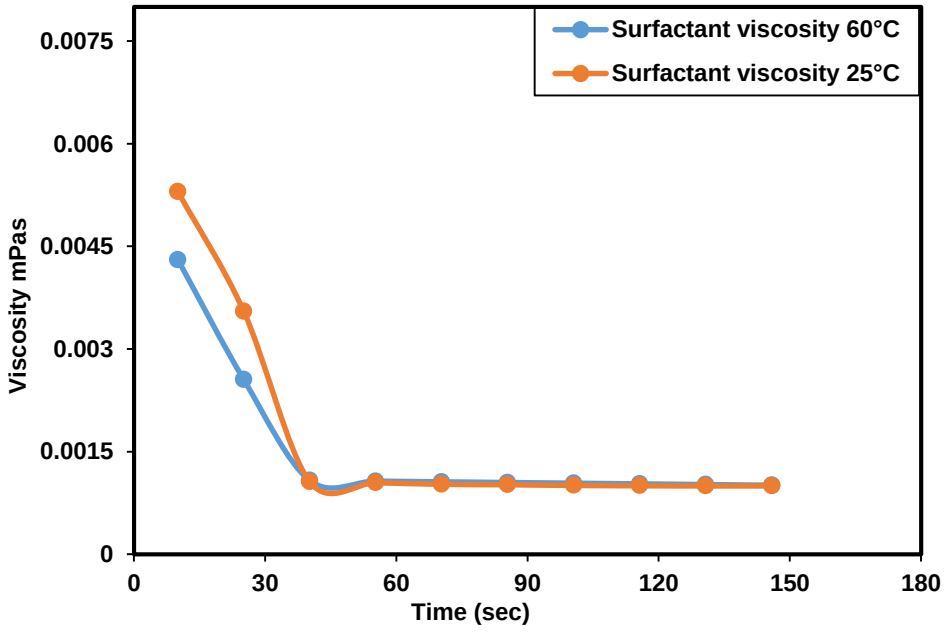

Figure 4-2: Surfactant viscosity versus time.

Table 4-1: Calculated nitrogen viscosity using Sutherland's equation

Fluid	Viscosity (cp)
Calculated nitrogen viscosity @ 60ºC	0.014
Calculated nitrogen viscosity 25ºC	0.017

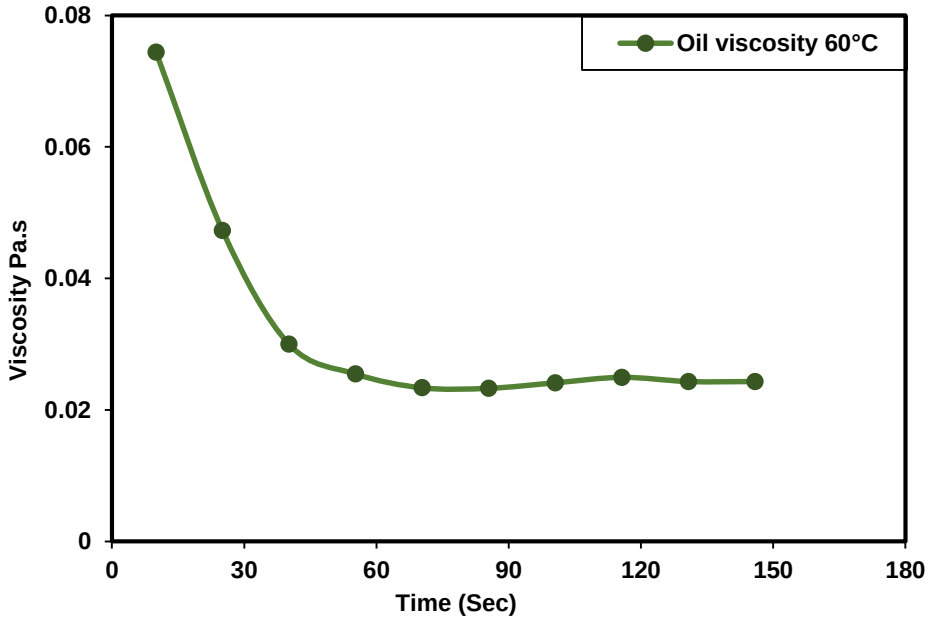

Figure 4-3: Oil viscosity versus measurement time at 60 ºC.

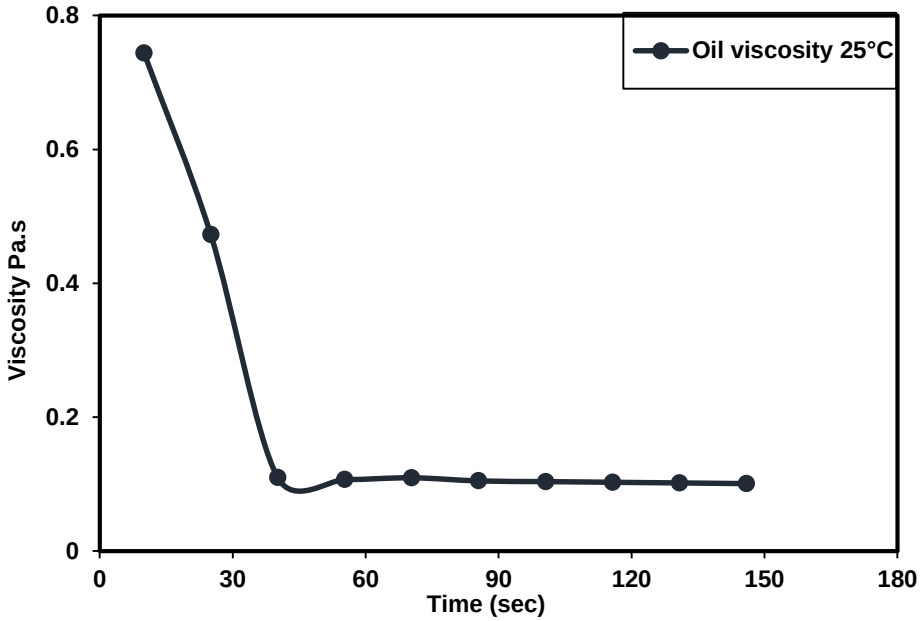

Figure 4-4: Viscosity of oil versus measurement time at 25 ºC.

4.1.2 Fluid Densities

Table 4-2 is the measured densities of oil and brine and calculated density of gas. Density measurements are used as input data in Sendra and Eclipse to obtain two and three-phase relative permeability curves.

Table 4-2: Density of oil, brine and gas at 60 degrees Celsius.

Fluid	Density(g/cm³)
Brine	1.01
Oil	0.92
Gas	0.03

4.2 Interfacial tension measurement

One of the most important properties of surfactant formulation in enhanced oil recovery is the ability to reduce water/oil interfacial tension and increase the capillary number. To examine surfactants ability to reduce interfacial tension, the initial water/oil interfacial tension has been measured using the pendant drop method

explained in chapter 3. Table 4-3 shows the measured interfacial tension between oil/brine and oil/water.

Table 4-3: Interfacial tension measurement.

Phases	Needle diameter	D(mm)	d	S= d/D	ϒ(mN/m)
Oil/water	0.78	3.28	1.3	0.41	22.7
Oil/brine	0.78	2.33	1.1	0.46	11

Where D- Equatorial diameter.

d- Distance from the top of the drop.

ϒ- Interfacial tension.

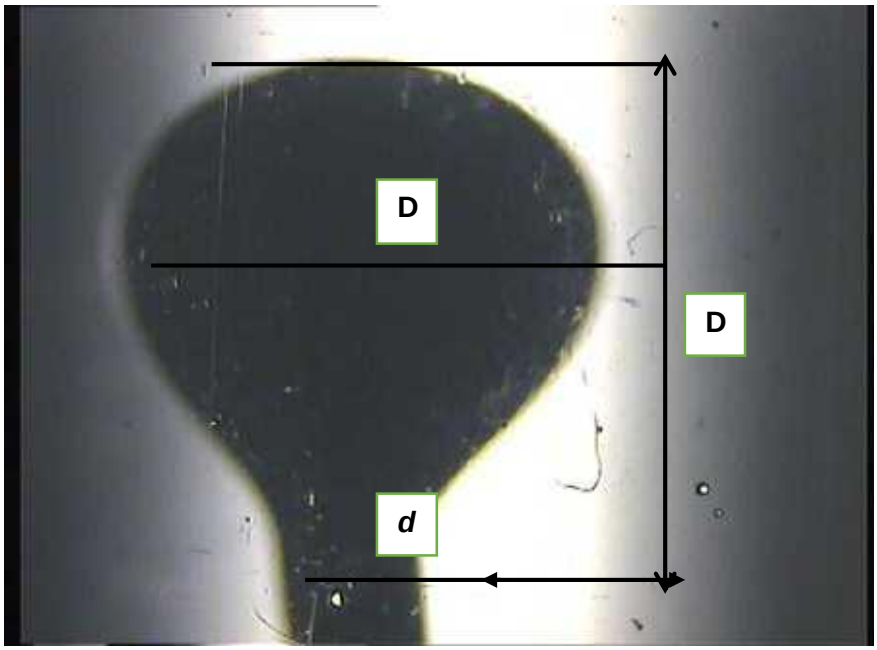

Figure 4-5: Pendant drop for water/oil interfacial tension measurement.

Figure 4-5 is an image of oil drop captured during water/oil interfacial tension measurement. An interfacial tension of 22.7 mN/m was measured for oil/water before surfactant injection. This is in the range of 20-30 mN/m reported by Donaldson et al (Donaldson et al, 1989). The effect of brine ions on water/oil interfacial tension was

evaluated using the synthetic brine made for this study. The results showed that interfacial tension between brine and crude oil was lower compared to the measured interfacial tension obtained between water and oil. The interfacial tension reduced to 11 mN/m. The reduction of interfacial tension between brine and oil is because of the divalent and monovalent ions present in the brine. These ions present in the brine accelerate the diffusion of the surface-active components of the crude from the bulk phase to the interface (Bai et al, 2010). Although the interfacial tension of the brine/oil reduced compared to oil/water, it is still not low enough to improve oil recovery. An interfacial tension of 10^{-3} mN/m is required to mobilise trapped oil.

4.3 Surfactant Evaluation

4.3.1 Critical micelle concentration (CMC)

For this study, five different surfactant solutions were analysed to select the most suitable for oil recovery. The first step in characterising a surfactant solution is to determine the CMC. The CMC for the different surfactant solutions were determined by plotting the surface tension measured using the tensiometer against surfactant concentration. This measurement to determine the concentration at which the surfactant can reduce interfacial tension and have effect on enhanced oil recovery. Figures 4-6 - 4-10 show the plot of surface tension against surfactant concentration to obtain the CMC for anionic olefin (AO), internal olefin sulfonate (IOS), methyl ester sulfonate (MES), alcohol alkoxy sulphate (AAS), and alcohol propoxy sulphate (APS).

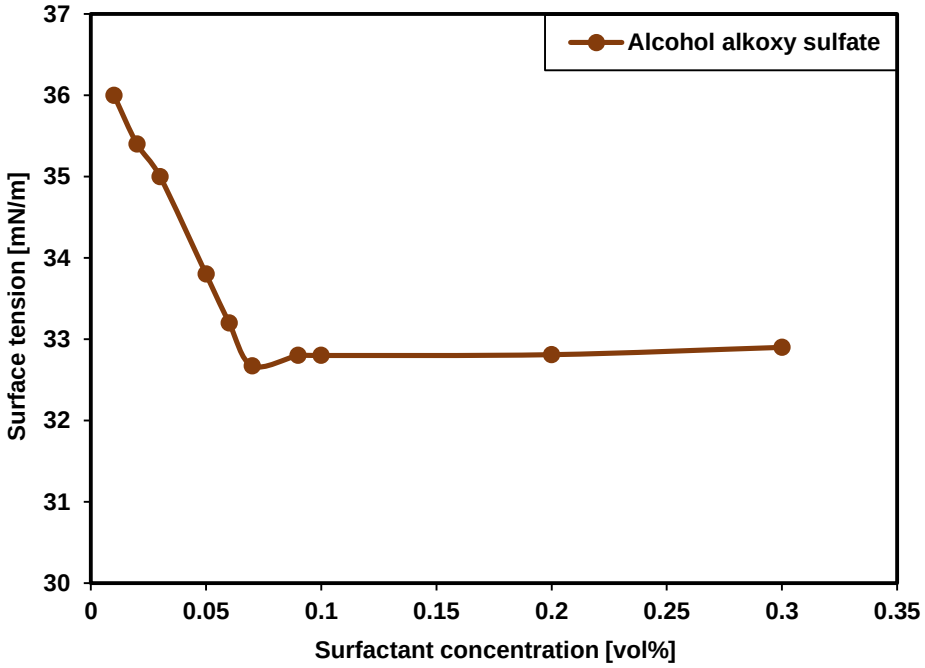

Figure 4-6: Surface tension versus surfactant concentration for AAS.

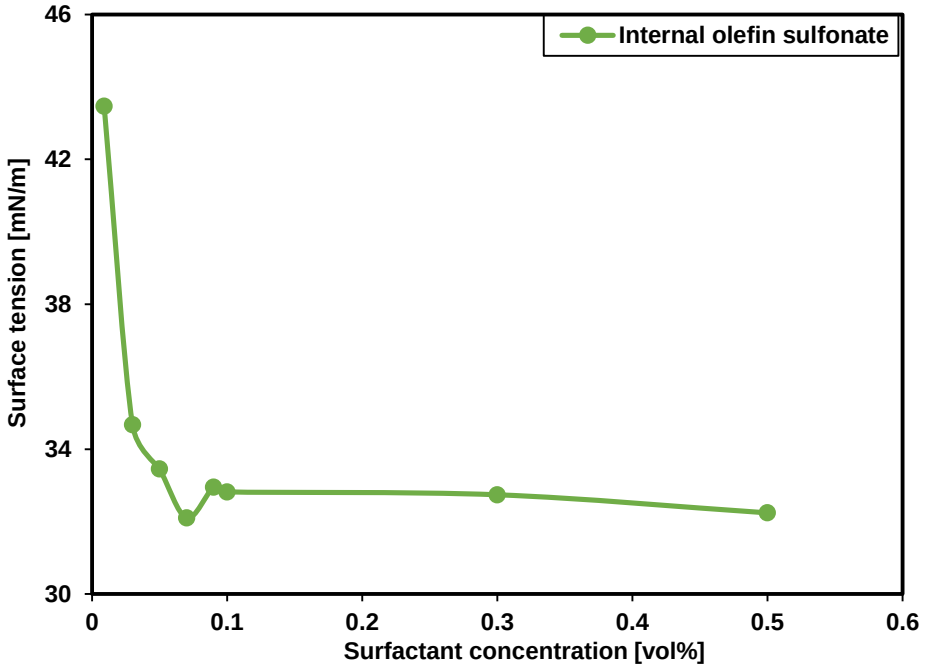

Figure 4-7: Surface tension versus surfactant concentration for IOS.

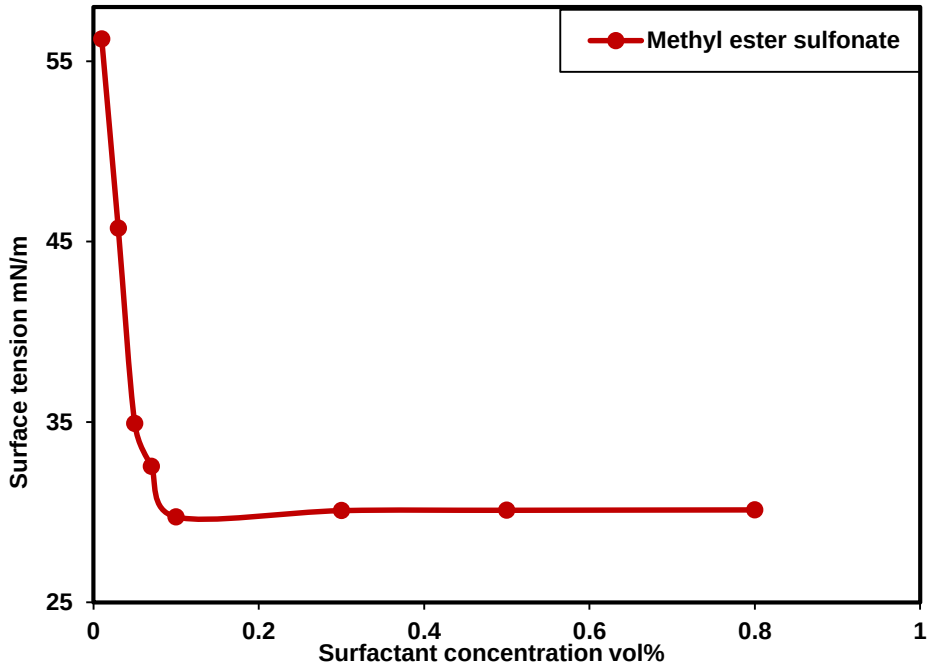

Figure 4-8: Surface tension versus surfactant concentration for MES.

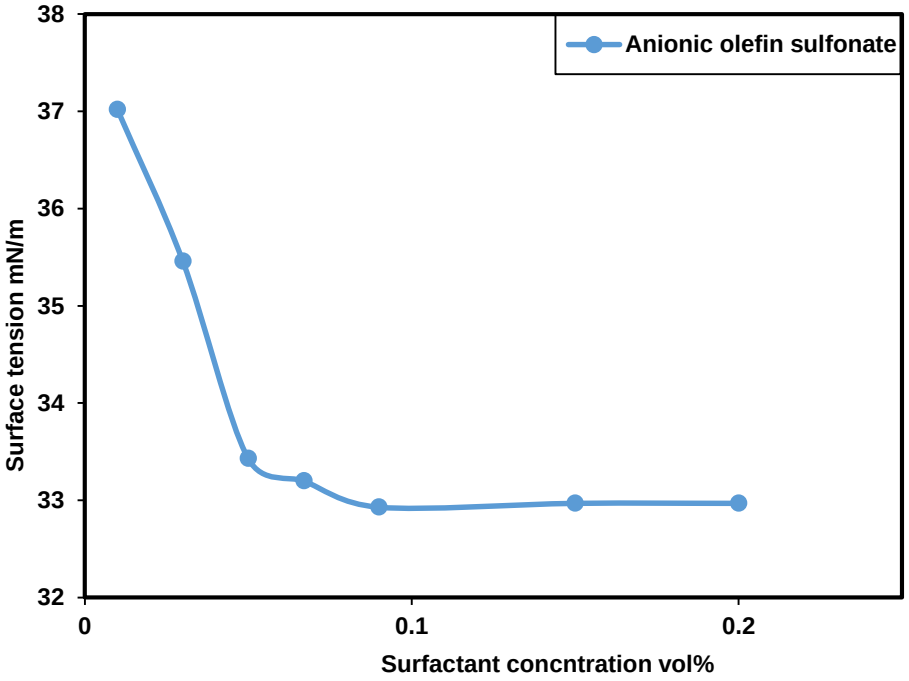

Figure 4-9: Surface tension versus surfactant concentration for AO.

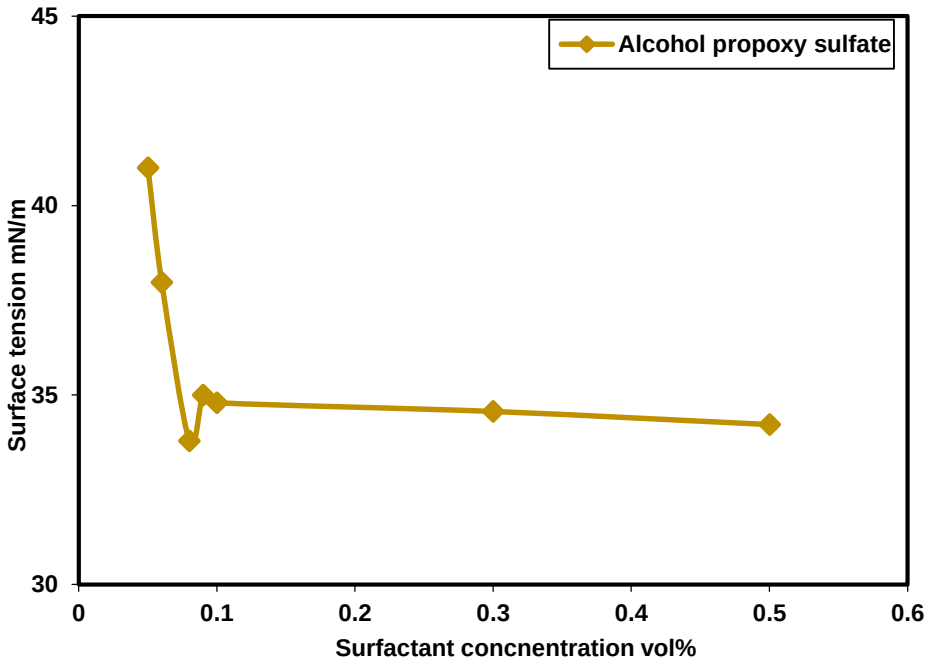

Figure 4-10: Surface tension versus surfactant concentration for alcohol propoxy sulphate.

The same trend was observed for all surfactants. As the concentration of the surfactant increases, the surface tension decreases.

For AO, the CMC is 0.06 vol% while IOS and AAS have their CMC at 0.07 vol%. MES has the highest critical micelle concentration at 0.1 vol%. CMC for APS was found at 0.08 vol%. After the critical micelle concentration, continuous increase in surfactant concentration does not have much effect on the surface tension as the surface tension becomes almost constant.

4.3.2 Aqueous stability test for surfactant

Figures 4-11 and 4-12 show the stability of AAS in hard brine with and without a co-surfactant. Results show that AO and APS solutions became cloudy when introduced into the brine at salinity ranges of 3.56 - 6.7 %. AAS was stable up until 4.8 % salinity. The surfactant must be compatible with the injection brine to prevent the formation of precipitates during injection. When the surfactant is mixed with the brine, it should stay clear and transparent at different salinities up to the salinity of the injection brine. In this case, the salinity of the injection brine is 6.5 %. If the surfactant stays cloudy in the brine, it needs to be discarded as this will not be suitable for injection. Before a

surfactant solution is discarded, Levitt (2006) stated that it is advisable to add either an alkaline or a co-surfactant into the solution to improve the stability of the surfactant. IOS and MES stayed stable for two days in salinity ranges of 1- 6.7 % salinity. IOS and MES were used as co-surfactants as they stayed stable in hard brine without forming precipitates. These two surfactants were added separately into solutions of AO at different salinities. This was also repeated for APS and AAS. The stability of APS and AO became clear from 2.1 – 4 % salinity which is still not up to the salinity of the injection brine. While AAS stability improved to 6.7 % salinity. The stable surfactant solutions were selected for further investigation in the phase behaviour experiment.

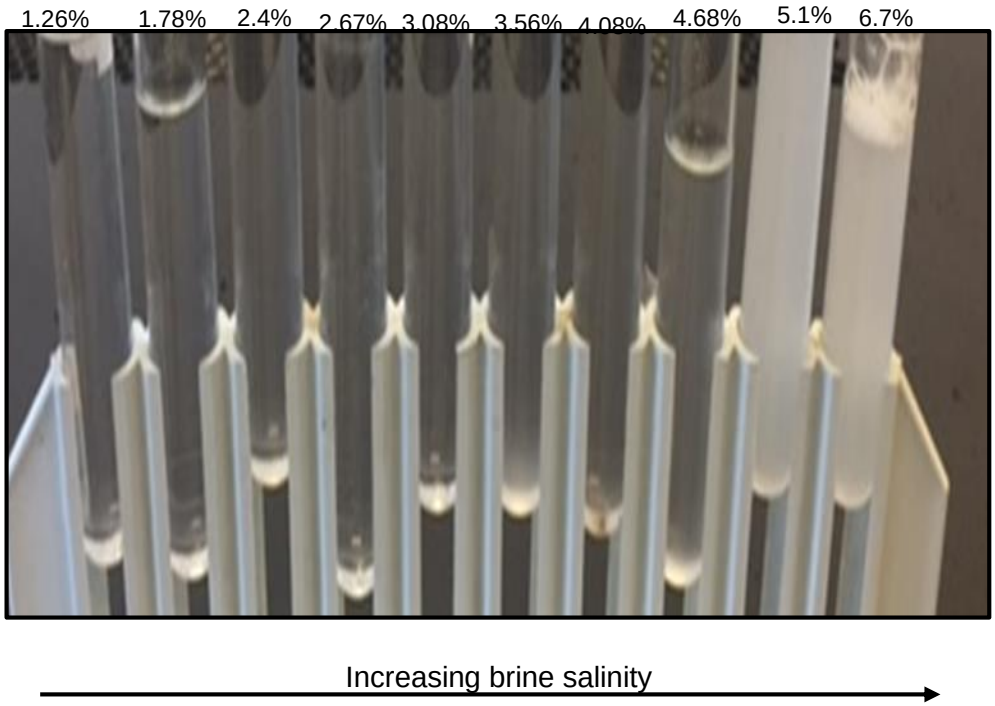

Figure 4-11: Aqueous stability test for AAS.

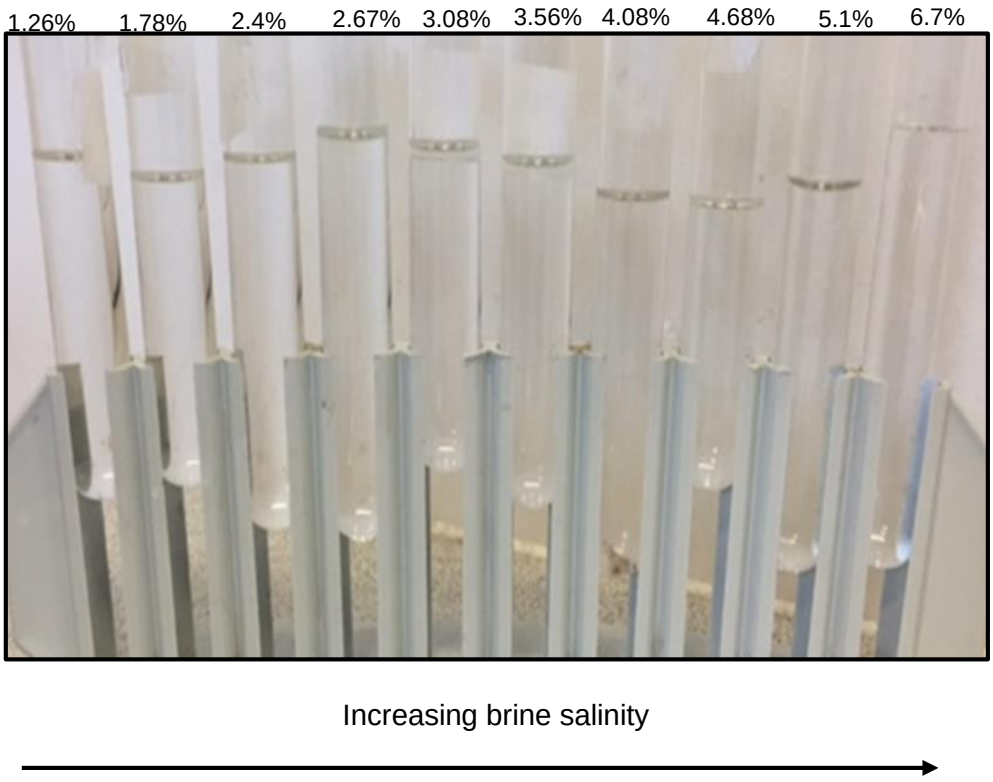

Figure 4-12: Aqueous stability test for alcohol AAS/IOS.

4.3.3 Surfactant phase behaviour experiment

Figure 4-13 shows a pipette set containing surfactant, brine and oil at different salinities with the different microemulsion phases. The microemulsion phases formed followed the typical Windsor phase behaviour by forming type I microemulsion phase at low salinities and began to form type III microemulsion phase at intermediate salinities from 3 % salinity to higher salinities of 6 %. The type II microemulsion phase was not formed in this experiment. The ability of the surfactant blend of AAS/IOS to form a type III microemulsion phase shows that the surfactant blend can reduce interfacial tension. Figure 4-14 shows a tilted pipette with non-viscous microemulsion phase formed. Tilting of the pipette was used to examine the viscosity of the microemulsion phases in the pipette. A non-viscous microemulsion phase will flow freely in the pipette while a viscous microemulsion phase will not flow.

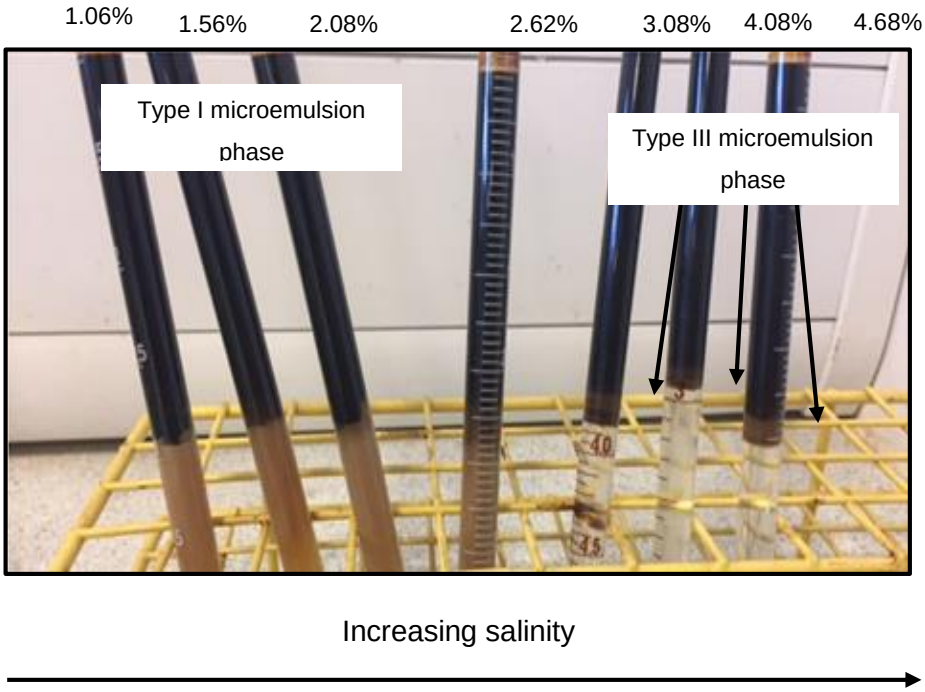

Figure 4-13: Microemulsion phase formed during surfactant phase behaviour experiment for AAS/IOS blend.

Figure 4-14 Tilted pipette showing non-viscous microemulsion phase formed.

4.3.4 Optimal salinity and solubilisation ratio for internal olefin sulfonate

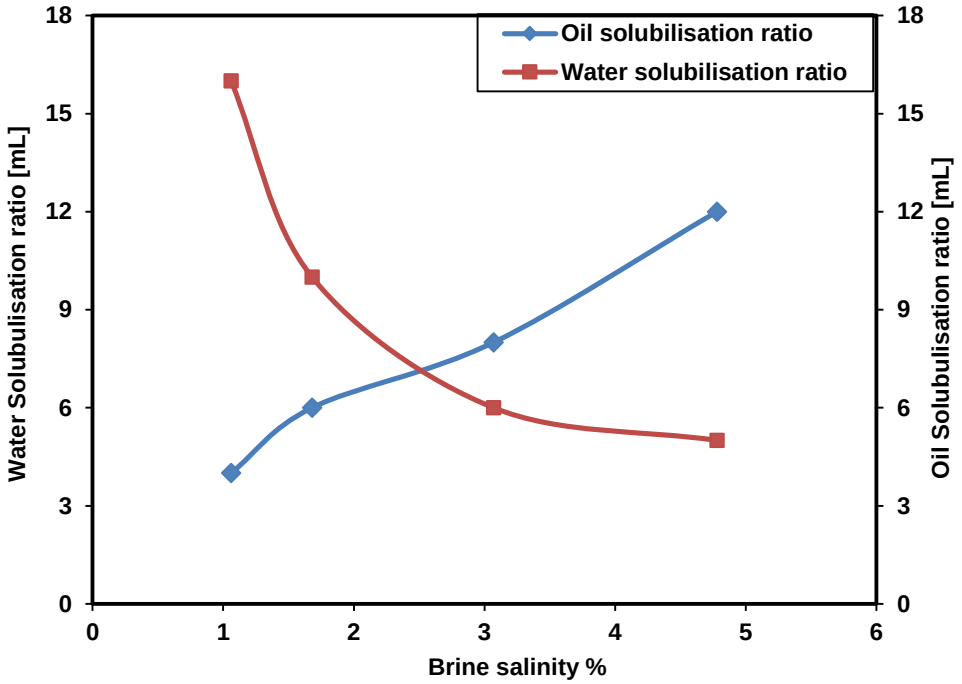

Figure 4-14: Water and oil solubilisation ratio for IOS.

Figure 4-15 shows the plot of solubilisation ratio against salinity for IOS surfactant. IOS could not form microemulsion phase at room temperature but started forming microemulsion phase when the temperature was increased to 60 ºC. The microemulsion phase formed was non-viscous as it flowed easily in the pipette. A high viscosity microemulsion phase will create local fluid heterogeneities that will be bypassed by subsequent chase fluids, thus causing high phase trapping in the porous media. Also, high viscosity microemulsion phase is difficult to pump through perforations causing injectivity problems (Sheng, 2011). The formation of low viscosity microemulsion shows that the surfactant has a good interaction with hard brine and medium crude oil used for this research.

The solubilisation ratio obtained from phase behaviour experiment was 7 which is below 10, indicating that internal olefin sulfonate alone cannot create very low interfacial tension. For a surfactant to create low interfacial tension it should have a solubilisation ratio of 10 or greater (Sheng, 2015). The low solubility of internal olefin sulfonate in saline and reservoir brines which can be one of the reasons for low solubilisation ratio has been discussed by Barnes et al (2013). They attributed the inability of the surfactant to solubilise to be because of the increase in carbon chain

length and hydrophobicity of the surfactant. To increase its solubility, they have suggested the addition of a non-ionic surfactant into the solution containing internal olefin sulfonate. The low solubilisation of ratio <10 could also be because of the temperature used for phase behaviour experiments as other researchers such Barnes et al (2010) have conducted phase behaviour experiments with this same surfactant under very high temperatures of about 80-90 ºC and have obtained higher solubilisation ratios.

4.3.5 Solubilisation ratio for methyl ester sulfonate

In Figure 4-16, MES formed very low volumes of microemulsion phase. This surfactant was the slowest to form a microemulsion phase compared to IOS and AAS. A solubilisation ratio of 4 was obtained which is very low.

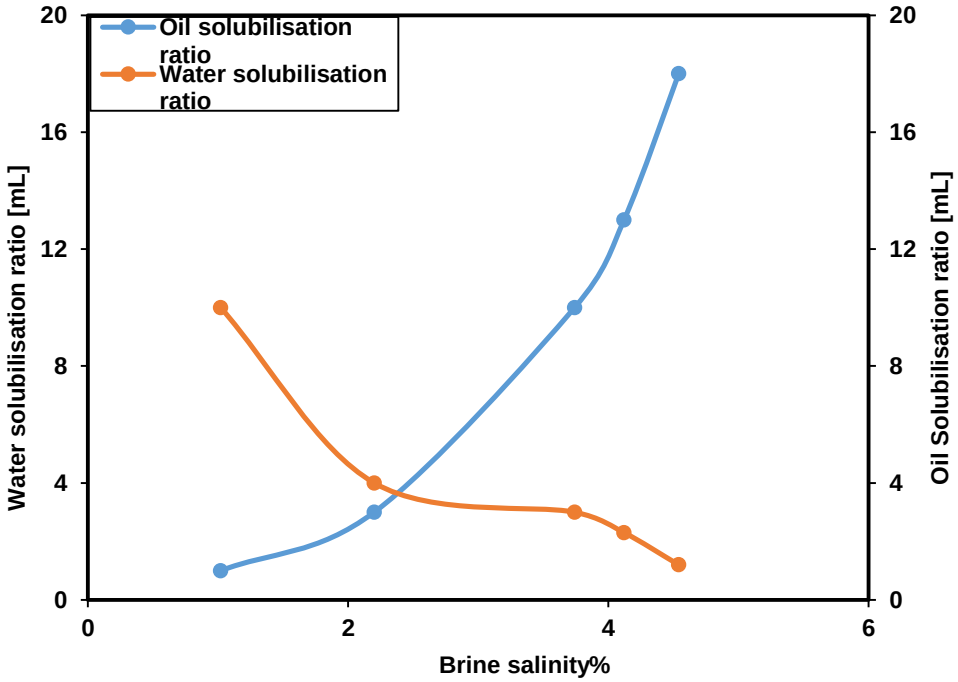

Figure 4-15: Water and oil solubilisation ratios for MES.

4.3.6 Optimising AAS by adding MES and IOS as co-surfactants

The most promising of all surfactant blends tested in this research was the AAS/IOS. Formation of microemulsion phase started 30 minutes after the surfactant blend was mixed with into the oil in the pipette. As the solutions in the pipettes were placed in the oven at 60 ºC, equilibration time for microemulsion phase became quicker

compared to the other surfactant blends with oil. The micro emulsion phase formed was also non-viscous. The microemulsion phase transitioned from type1 at low salinities (1- 3.08 %) while at higher salinities (3.54 - 4.8 %), the middle phase type III microemulsion phase was formed. The phase behaviour plot in Figure 4-17 shows the solubilisation ratio at optimum salinity in the AAS/IOS blend obtained at 15 compared to a solubilisation ratio of 8 obtained with internal olefin sulfonate.

The result shows that optimising AAS with IOS creates even a less viscous microemulsion phase as compared to internal olefin sulfonate. Thus, a solubilisation ratio greater than 10 can lead to a very much lower interfacial tension because a solubilisation ratio of 10 can create an interfacial tension of 0.03 mN/m (Levitt et al, 2006). Using Huh's correlation discussed in chapter 3, the calculated interfacial tension of this surfactant blend is 1.0 x 10^{-3} mN/m.

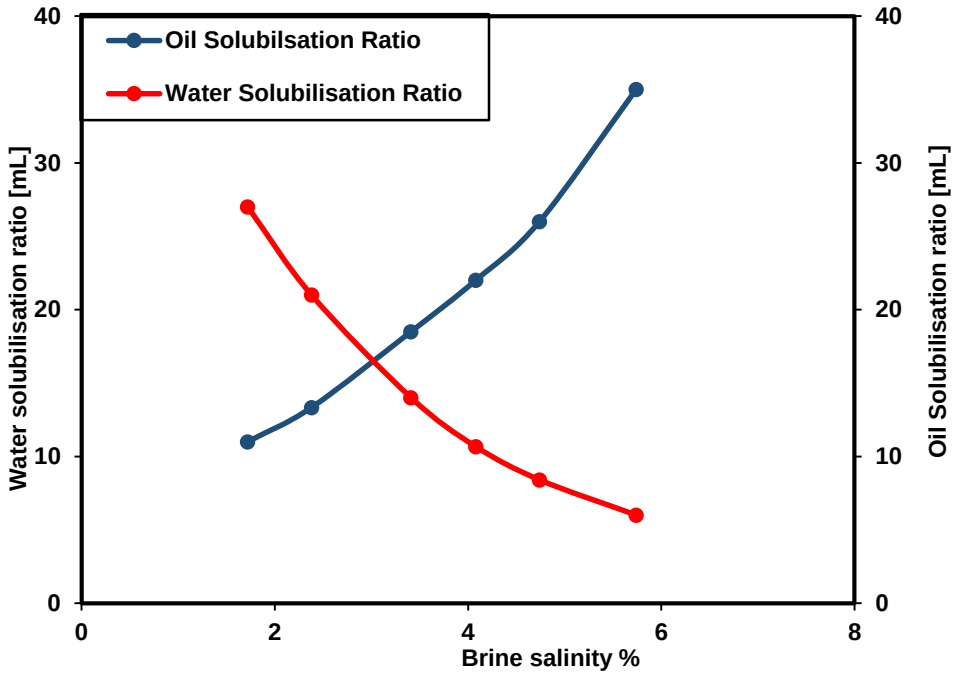

Figure 4-16: Water and oil solubilisation ratio for surfactant blend AAS/IOS.

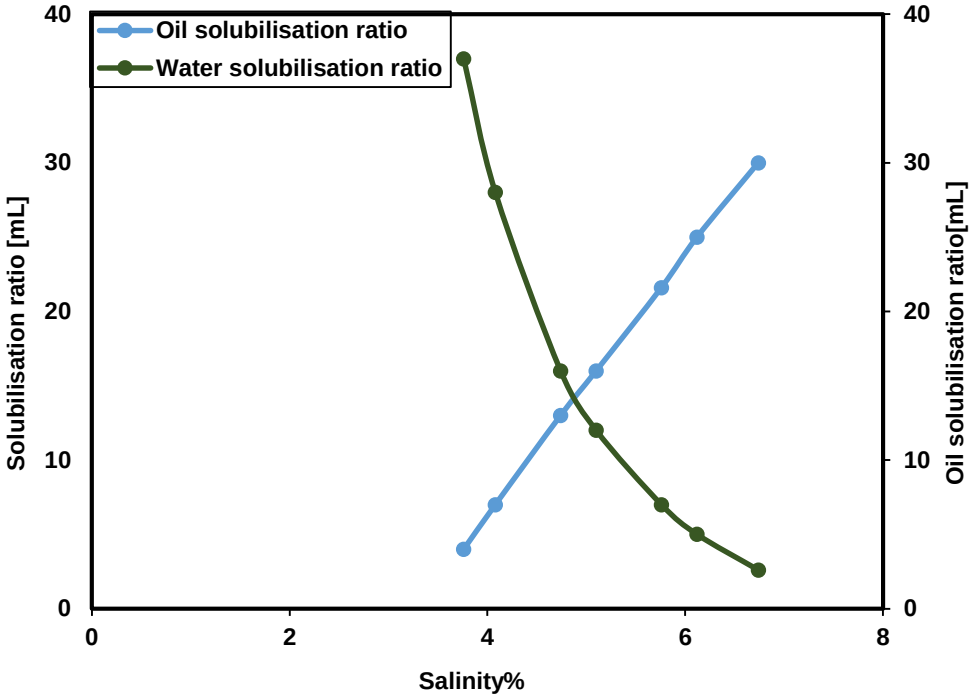

Figure 4-17: Water and oil solubilisation ratio for surfactant blend AAS/MES.

Figure 4-18 shows the plot of solubilisation ratio against salinity for the AAS/MES surfactant blend. The formation of microemulsion phase for the AAS/MES blends was slower compared to the AAS/IOS blend, but formation of microemulsion phase was quicker compared to MES alone in combination with oil. The type III microemulsion phase formed from 3.8 - 5.1 % salinity. There was no microemulsion phases formed in the pipettes at very low salinities after seven days for this surfactant blend. No type I or Type II microemulsion phases were formed for this surfactant blend. AAS/MES blend formed a gel-free and less viscous microemulsion phase. The solubilisation ratio obtained at optimal salinity was 12. Using Huh's correlation to calculate interfacial tension, the interfacial tension of this surfactant blend is $1.5x10^{-3}$ mN/m.

4.4 Flow in the porous media

4.4.1 Surfactant Adsorption

Figure 4-19 shows the plot of surfactant adsorption against surfactant concentration injected into the Berea sandstone core sample to determine the concentration of surfactant adsorbed on the rock sample during injection. Region 1 is usually observed at very low surfactant concentrations. Surfactant adsorption begins to increase in

region 2. Adsorption increases from region 3 until it gets to the stage of region 4. In region 4 the adsorption becomes constant at the CMC concentration of the surfactant. This shows that there is no further increase in surfactant adsorption after the critical micelle concentration. The calculated adsorption of the surfactant blend of AAS/IOS in Berea sandstone core is very low at 0.00135 mg/g. There loss of the surfactant on the core sample is very minimal. The adsorption data will be used to build the surfactant model for simulation of SAG in Eclipse software.

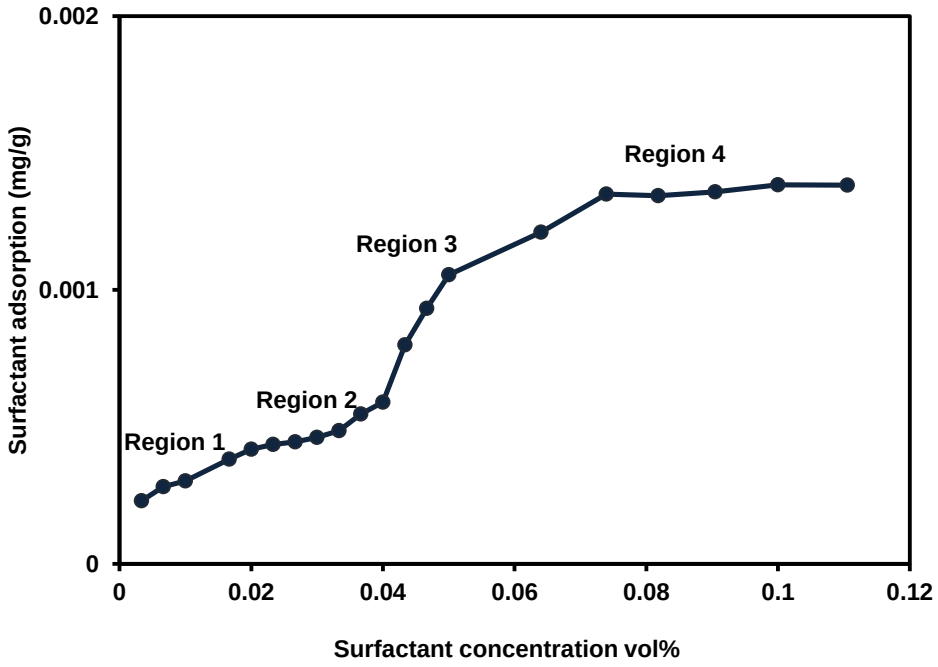

Figure 4-18: Adsorption of surfactant blend AAS/IOS on Berea sandstone core sample.

4.4.2 Absolute permeability measurement

The plot in figure 4-20 was used to obtain the absolute permeability of the core sample which was 100 mD.

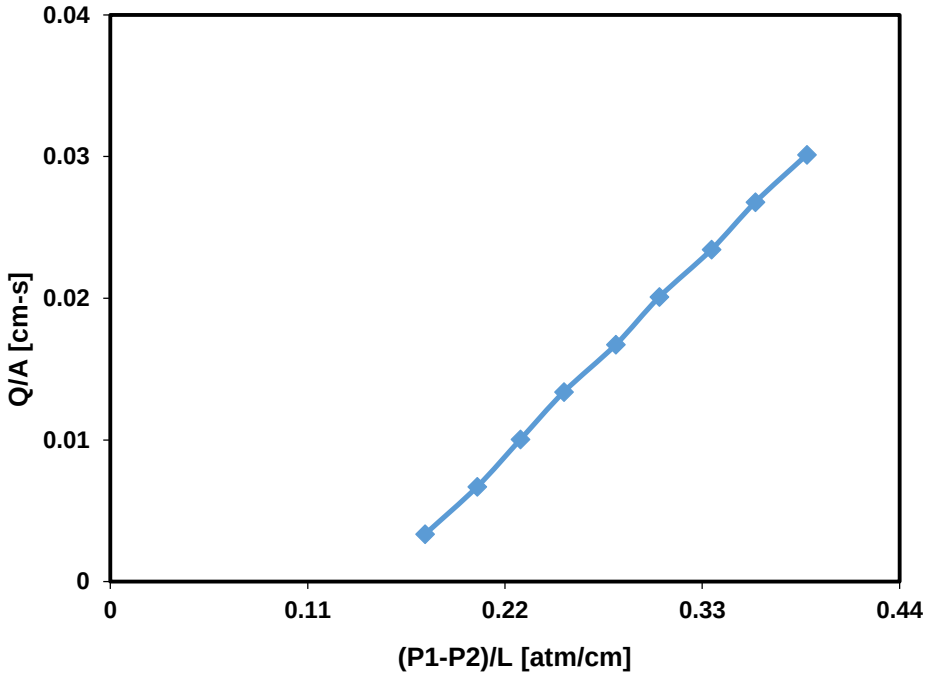

Figure 4-19: Absolute permeability measurement.

4.4.3 Effect of surfactant on two phase relative permeability water/oil relative permeability

The relative permeability curves obtained from two-phase displacement experiments are presented in Figures 4-21 and 4-22. The relative permeability curve in Figure 4-21 shows that the core sample is moderately water-wet. This behaviour is supported by the observation of the cross over point of the water and oil relative permeability curves. The residual oil saturation obtained from water/oil displacement experiment was 40 % while residual oil saturation decreased to 33 % with surfactant/oil displacement experiment. The relative permeability for surfactant flooding is presented in Figure 4-22. The result shows that the presence of surfactant increases the oil relative permeability but the water relative permeability was not affected. It can also be deduced from the cross over point in the relative permeability curve for surfactant displacement experiment moved further to the right.

Abesinghe et al (2012) while studying surfactant/oil relative permeability curves reported the same shift of the relative permeability curves to higher water saturation value. The curves for surfactant/oil have less curvature when compared to water/oil relative permeability curves. Lower interfacial tension results to less curvature. This

effect on relative permeability curves by low interfacial tension has also been reported by Shen et al, 2010. The production rate of oil increased by 30 % when about 0.5 pore volumes of surfactant solution was injected into the core sample. Oil recovery increased in Figure 4-23 when surfactant was injected into the core sample when compared to water flooding. The plot showed that oil recovery increased by 25 %.

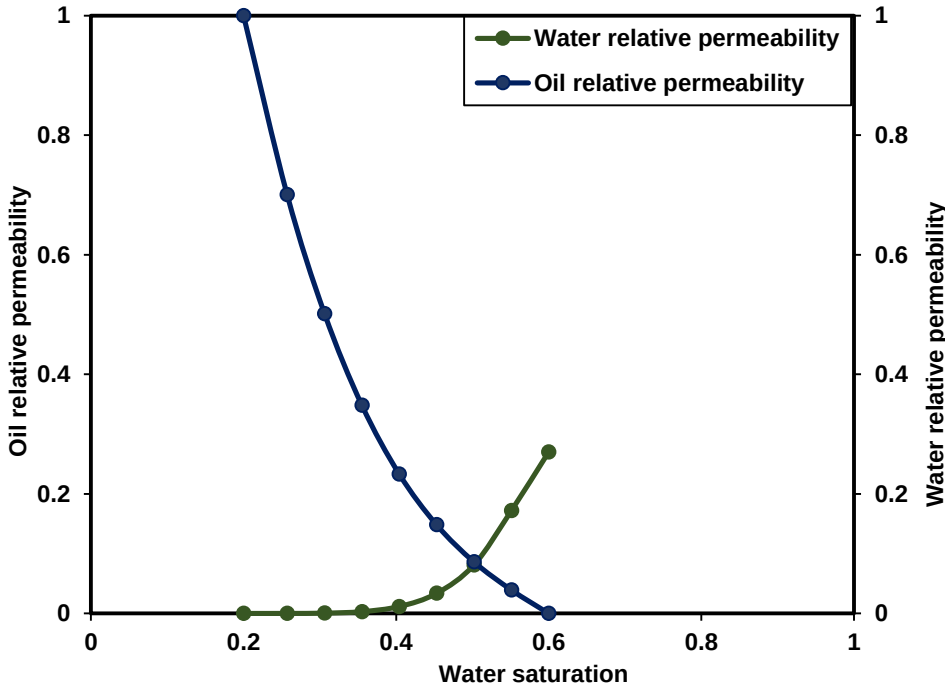

Figure 4-20: Water/oil relative permeability curves.

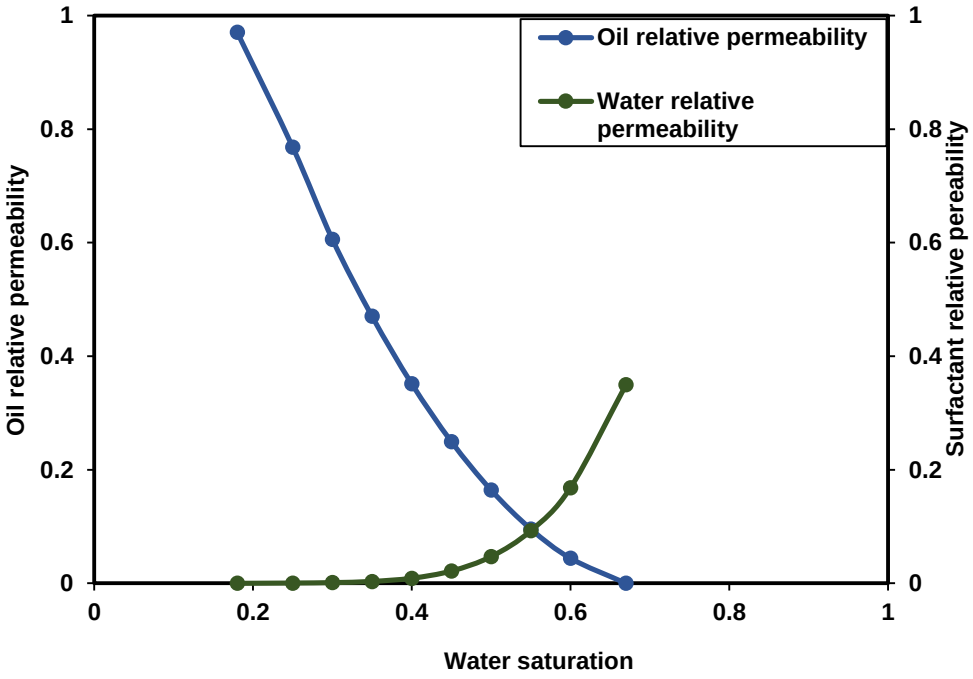

Figure 4-21: Surfactant/oil relative permeability curve.

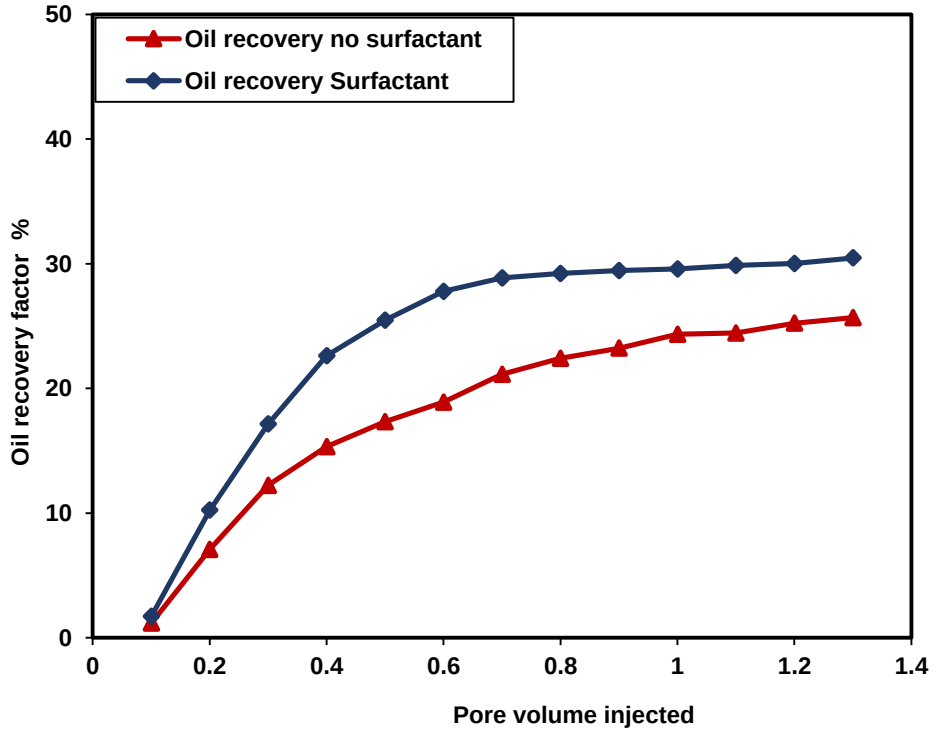

Figure 4-22: Surfactant effect on oil recovery in water/oil displacement experiment.

Figure 4-24 shows the plot of pressure gradient against pore volume of water and surfactant injected into the core sample. Pressure gradient in surfactant/oil displacement is lower compared to water/oil displacement experiment. The reduction in differential pressure shows that a decrease in interfacial tension leads to a reduction in pressure during displacement. This shows that surfactant reduces the capillary pressure that traps oil in the reservoir improving the mobility of oil.

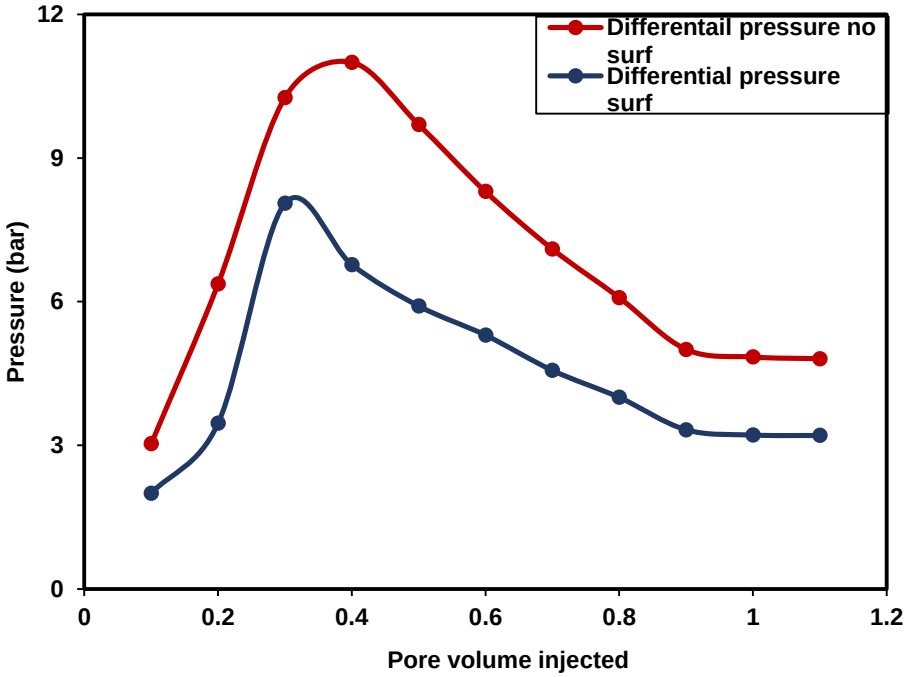

Figure 4-23: Differential pressure versus pore volume of surfactant injected in water/oil and surfactant/oil displacement experiment.

4.4.4 Effect of surfactant on gas-water relative permeability

Figure 4-25 presents the results from the gas/water displacement experiment with and without surfactants. The plot shows that water production increased in the presence of surfactant. Water production continued in the presence of surfactant until gas breakthrough which was delayed when compared to gas/water displacement without surfactants. Higher water production in the gas/surfactant displacement experiment can be attributed to the even displacement of surfactant by gas until breakthrough and the reduction of gas mobility by surfactant. In the gas/water experiment, gas fingering was encountered at the early stages of the experiment. Similar results were obtained by Santamarina and Kim (2014). They observed in their

micro-model experiment that pore scale displacement efficiency is higher when surfactant is present in gas/water displacement.

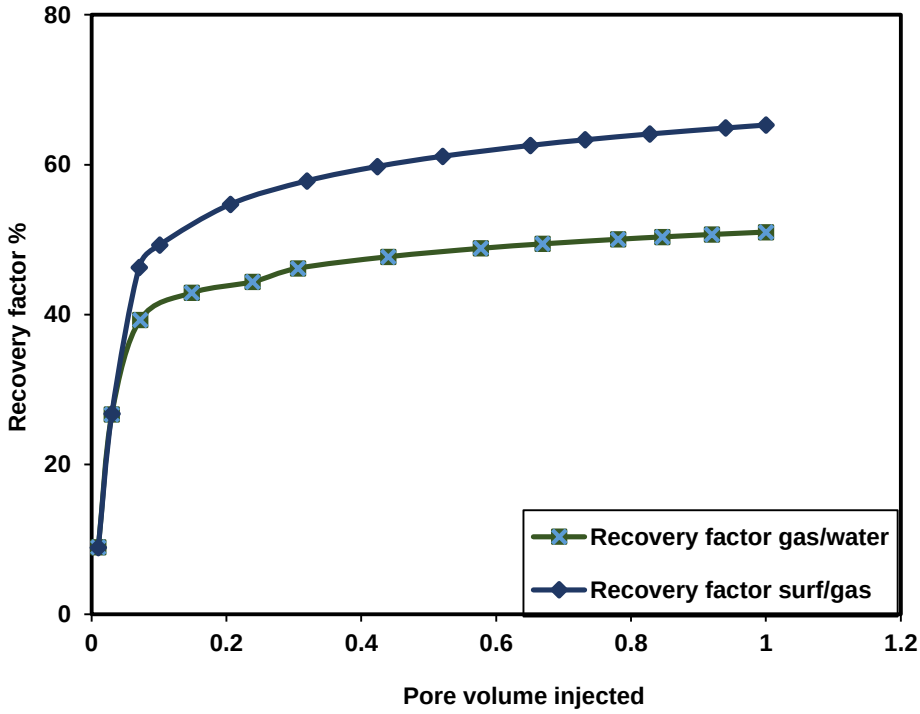

Figure 4-24: Effect of surfactant in water/gas displacement experiment.

Relative permeability curve for gas/ water displacement experiments is shown in Figure 4-26, while relative permeability curve for surfactant/gas is presented in Figure 4-27. The relative permeability of water in the presence of surfactant increased when compared to the results without surfactant. This is to further prove that the increase in water production in the surfactant/gas displacement experiment is because of the increase gas trapping by the surfactant which allows the gas to effectively displace the water. The increased gas trapping is attributed to the creation of foam by the gas interaction with the surfactant. This creates a better trapping effect when compared to gas/water experiment. The relative permeability curves in Figure 4.27 shows that the gas relative permeability for surfactant/ gas displacement is lower compared to gas/ water displacement experiment. The presence of surfactant does not permit high permeability of gas.

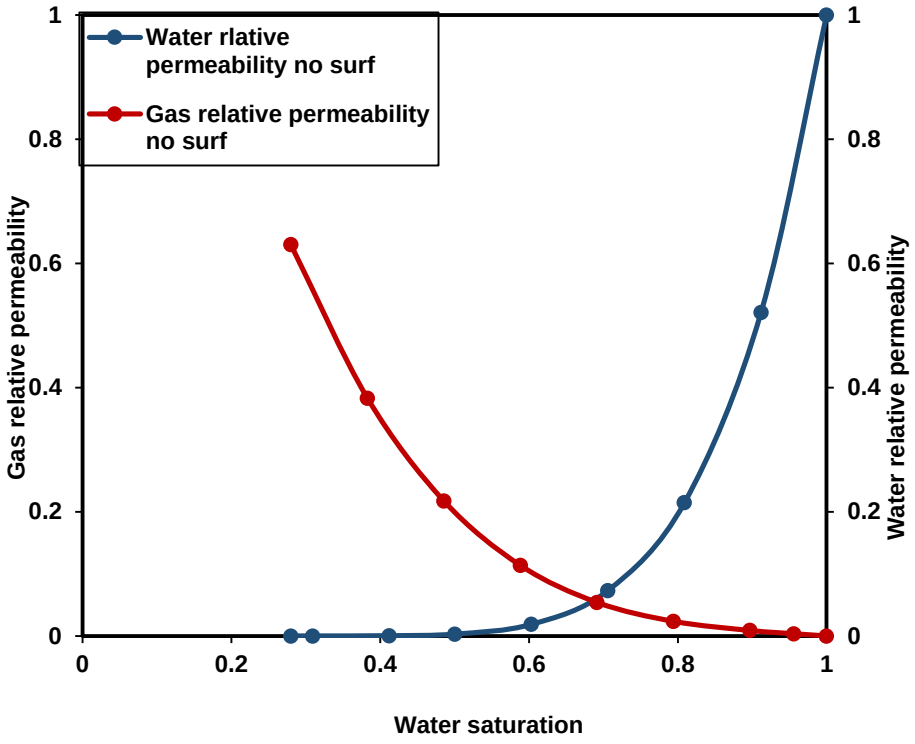

Figure 4-25: Gas/water relative permeability curves.

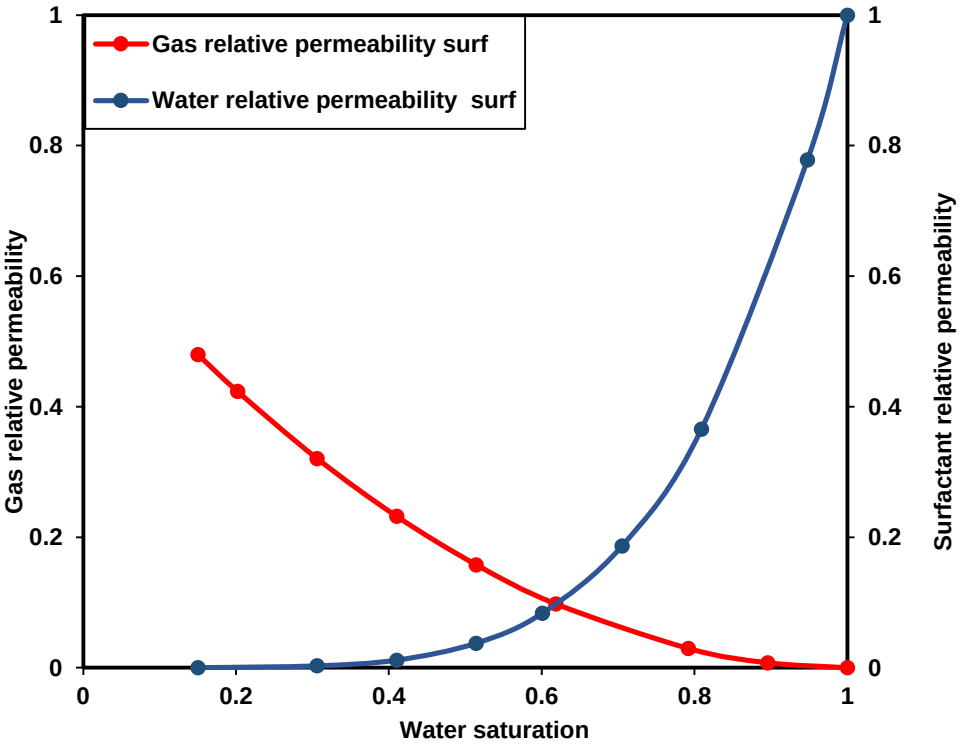

Figure 4-26: Surfactant/gas relative permeability curve.

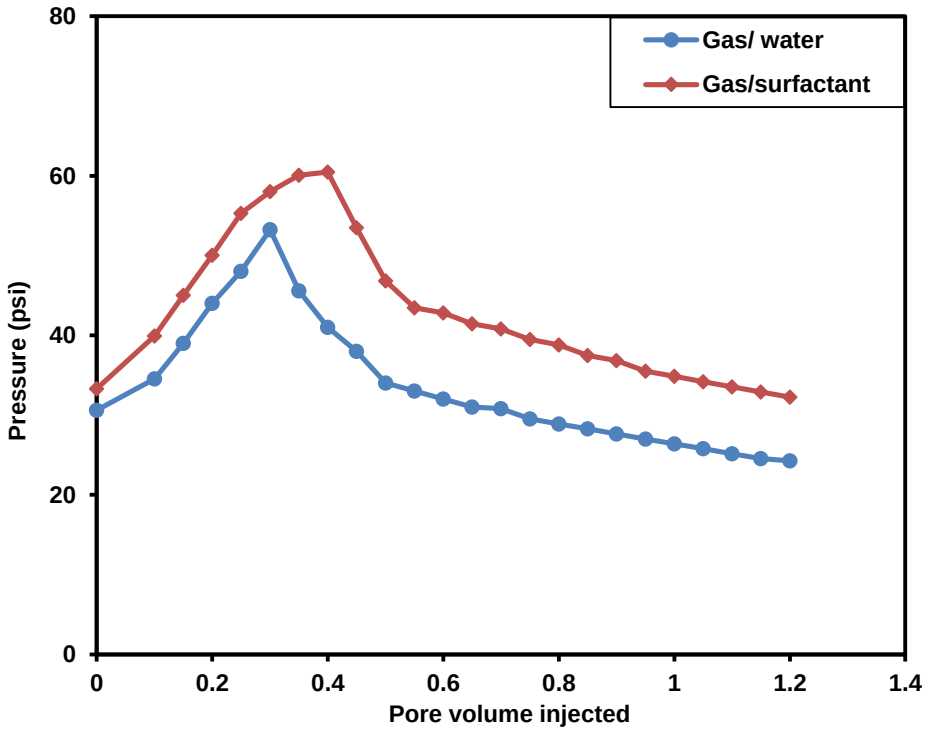

Figure 4-27: Differential Pressure versus pore volume injected for gas/water and gas/surfactant displacement experiments.

The plot in Figure 4-28 shows the plot of differential pressure for gas/water and gas/surfactant displacement experiments. The result shows that the pressure increased by 38 % in the presence of surfactant. Similar results were achieved by Sagir et al, 2016. They discussed that the increase in pressure gradient in surfactant /gas experiment was because of the reduction in gas mobility by the surfactant when compared to the pressure gradient generated in gas/water experiments. Nguyen (2011) in his work on gas trapping during foamed flow in porous media also concluded in his results that the higher-pressure gradient achieved in gas/surfactant displacement is due to foam generation.

4.4.5 Effect of surfactant on gas/oil relative permeability

Figure 4-29 shows oil recovery curves for gas/oil displacement experiment. The gas/oil relative permeability curves with and without surfactant are presented in Figures 4-30 and 4-31 respectively. In the oil recovery curves, the production rate of oil increased by 10 % in the presence of surfactant during gas injection than when there was no surfactant. The increase in oil recovery was due to the core sample

being more water-wet by the injection of surfactant. The remaining surfactant in the pore spaces traps some of the gas, this allowed oil to flow freely through the core sample. Reduction in gas mobility by the remaining surfactant in the core also aided oil recovery by stabilising the gas front to effectively displace the oil. The relative permeability curves shown in Figures 4-30 and 4-31, reveal a decrease in residual oil saturation by 20 % in surfactant gas/oil experiment when compared to gas injection without surfactant.

The relative permeability curves in Figures 4-30 and 4-31 also indicates a reduction in gas relative permeability by 20 % in the presence of surfactant when compared to the experiment without surfactant. As the gas interacts with the remaining surfactant in the porous media, gas is trapped by the films of liquid lamellae. This results in the decrease of gas velocity. The gas and liquid phases will move together at the same velocity if a case of stable foam has been achieved (Al-Mossawy et al, 2011). Oil recovery stopped immediately after gas breakthrough in the gas/oil displacement experiment without surfactant. This was due to gas channelling through the oil because of its very low viscosity.

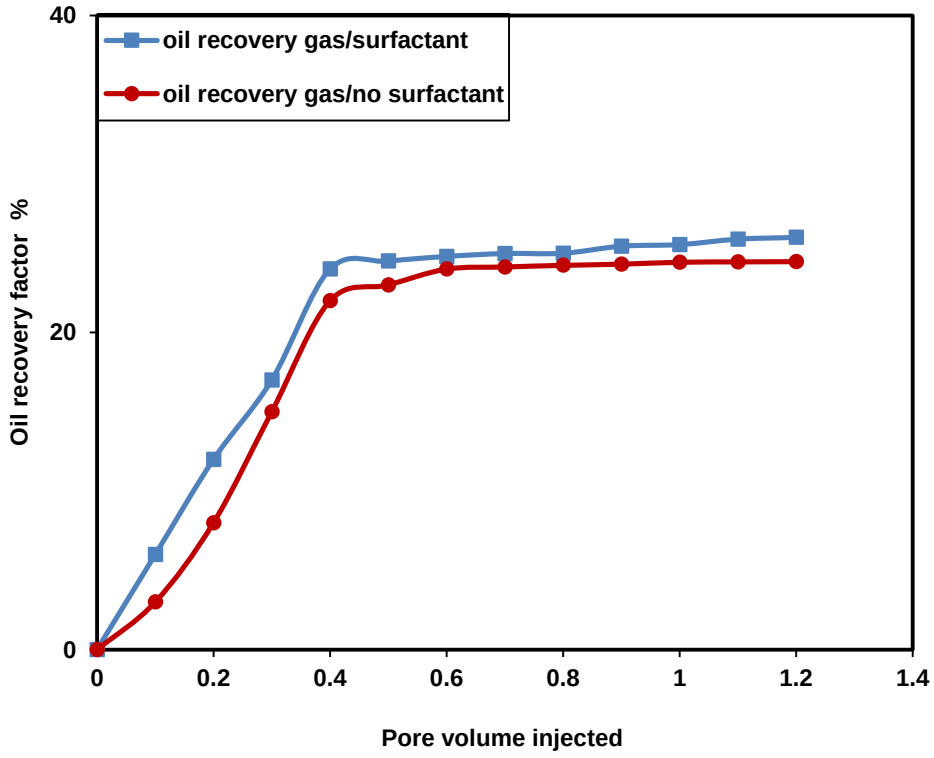

Figure 4-28: Surfactant effect on oil recovery in gas/oil displacement experiment.

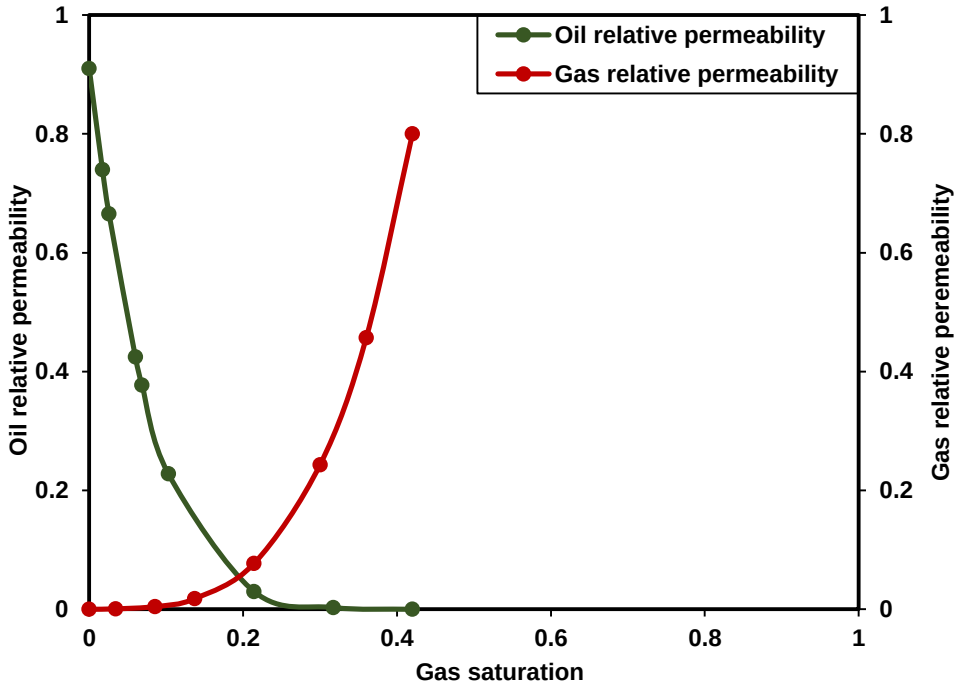

Figure 4-29: Gas/oil relative permeability curves.

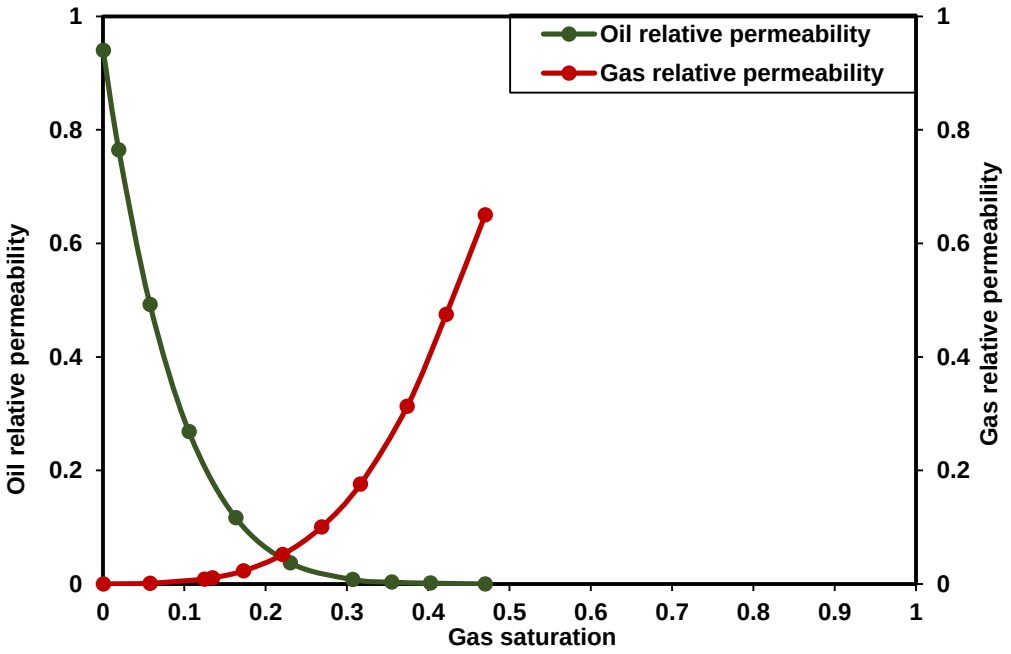

Figure 4-30: Surfactant effect on gas/oil relative permeability curves.

4.4.6 Comparison of the effect of surfactant on gas/oil and gas/water relative permeability

In Figure 4-32 the relative permeability to gas in gas/surfactant displacement experiment is much lower compared to the gas/oil core flooding experiment in the presence of surfactant. The higher gas relative permeability in the gas/oil injection compared to the gas/water is because of the reduction of the foaming capability of the surfactant with the gas in the presence of oil. Jensen and Friedman (1987) also confirmed in their work that the presence of oil saturation greater than 20 % in foam flooding is unfavourable for foam generation and propagation of preformed foam. Oil presence destabilises the formation of foam as discussed by Lobo et al (1989) and Osei-Bonsu et al (2015, 2017). They demonstrated in their work that the oil solubilises in the micelles of the surfactant resulting in the increase of Van der Waal forces between the micelles. This leads to a decrease in micellar volume concentration and suppression of the film stratification thus decreasing the stability of foam that can aid gas trapping. These results show that the presence of oil can affect the interaction between gas and surfactant.

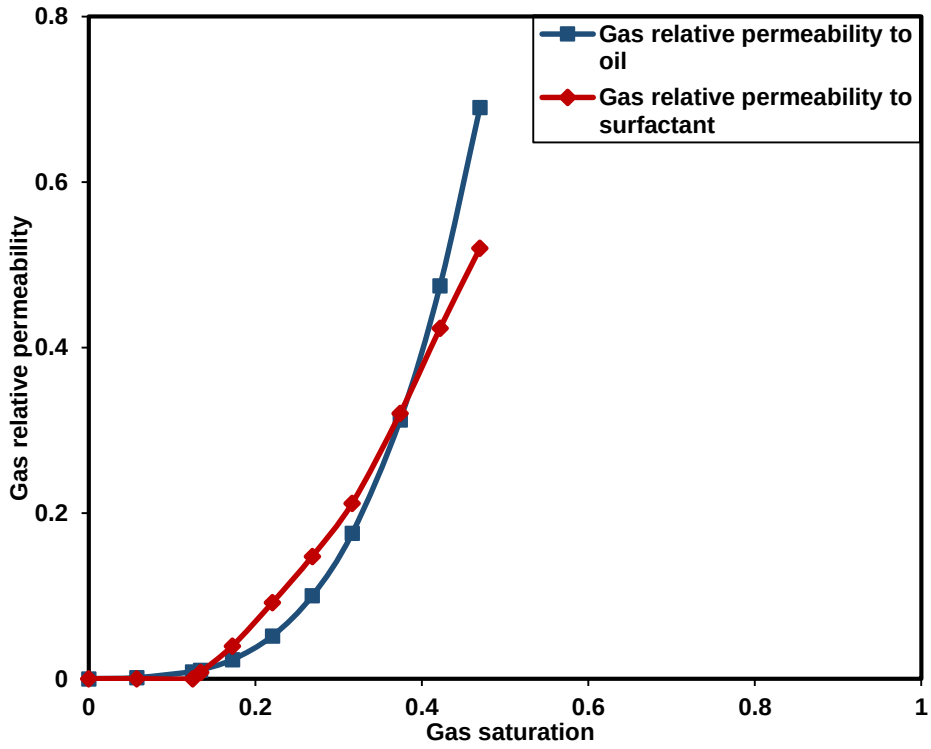

Figure 4-31: Surfactant effect on gas relative permeability.

Chapter 5 Estimation of three-phase relative permeability and surfactant effect on three-phase relative permeability

This chapter discusses the two methods used in estimating three-phase relative permeability and surfactant effect on three-phase relative permeability in WAG.

The first method described in this chapter is the extension of JBN/Welge theory to three immiscible fluids by Grader and O'Meara (1988). This method has been used to calculate three-phase relative permeability and surfactant effect on three-phase relative permeability using recovery data from WAG and SAG.

The second section of this chapter will present these correlations to study surfactant effect on three-phase relative permeability. Three-phase relative permeability correlations present in Eclipse have been discussed in the literature. These correlations will be used to predict surfactant effect on WAG and comparisons will be made with experimental results to determine which correlation best predicts surfactant effect on three-phase relative permeability.

The last section of this chapter will present the results obtained from experimental estimation of surfactant effect on three-phase relative permeability and the results will be compared to estimated surfactant effect on three-phase relative permeability using correlations.

5.1 Extension of the JBN/Welge method to three-phase flow

This proposed method by Grader and O'Meara (1988) mentioned in the literature review makes it possible to calculate three phase relative permeabilities along each saturation trajectory in displacement experiments. This method is a mathematical extension of the JBN/Welge theory and it invokes the simplifying assumptions made in Buckley-Leverett theory such as one dimensional, incompressible, immiscible three- phase flow with no capillary pressure (Cao and Siddiqui, 2011). Siddiqui et al (1995), Cao and Siddiqui (2011), Cinar (2005), Skauge and Larsen (1999) have used this method proposed by Grader and O'Meara to estimate three phase relative permeability experimentally.

The experimental data collected from WAG and SAG displacement experiments that will be used calculate three-phase relative permeability using this method are

differential pressure, pore volume of gas injected and pore volume produced (oil, water, and surfactant).

The saturation of each phase j (oil, water, gas and surfactant) can be calculated as a function of the initial saturations of that phase, pore volume injected, the pore volume produced and the slope of the recovery curves. The equation for saturation of each phase is given in equation [5.1].

$$S_{j=}\ S_j^0 - L_j\ +\ Q\frac{dL_i}{dQ} \qquad [5.1]$$

Where

S_{j-} Saturation of each phase

S_j^0- Initial saturation of a phase

L_j - Pore volume produced

Q – Pore volume injected

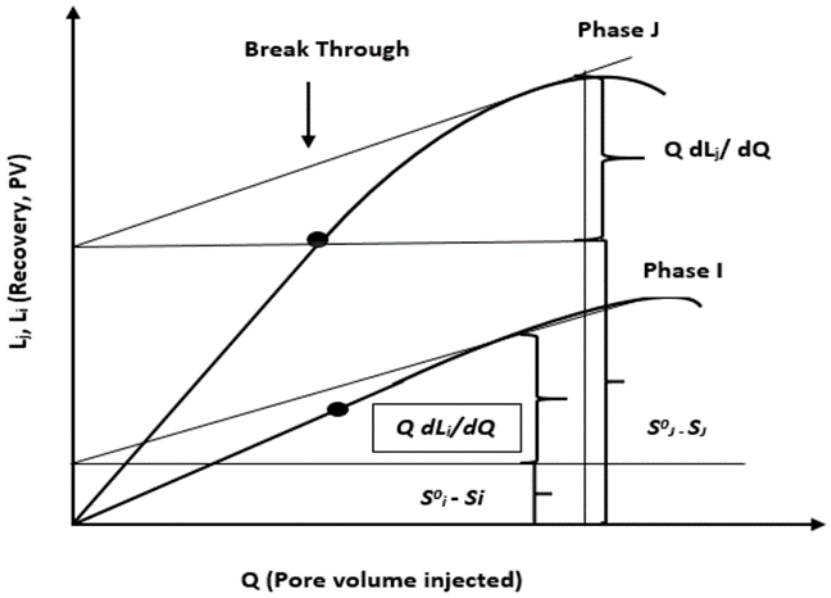

Figure 5-1: Recovery of two phases displaced by a third phase as a function of pore volume (Siddiqui et al, 1995).

Figure 5-1 shows graph of pore volume of fluid injected (Q) against pore volume produced (L_j). Equation [59] is applied to determine the saturation at the end of the

core. This graphical representation is known as the Welge tangent construction method. The relative permeability to a phase i, K_{ri} is calculated using equation [5.2]:

$$K_{ri} = \frac{q_t \mu_i L}{K_{abs}} \frac{f_i}{A(\Delta p - Q\frac{d(\Delta p)}{dQ}} \quad [5.2]$$

Where

q_t – Total flowrate

$\mu_{i\_}$ Viscosity of a phase

L - Length of core

K_{abs}- Absolute permeability

A – Cross sectional area

Δp – Differential pressure

The graphical representation of equation of equation [5.2] is shown in Figure 5-2. The graph shows a plot of differential pressure differential pressure against pore volume injected. The pressure rises before breakthrough and falls after breakthrough. The differential pressure values at the intercepts of the tangents to this graph allows for the calculation of the term in the bracket in equation [5.2].

The fractional flow f_i in equation [5.2] is derived from the slope of the tangent drawn across the recovery curves in Figure 5-1.

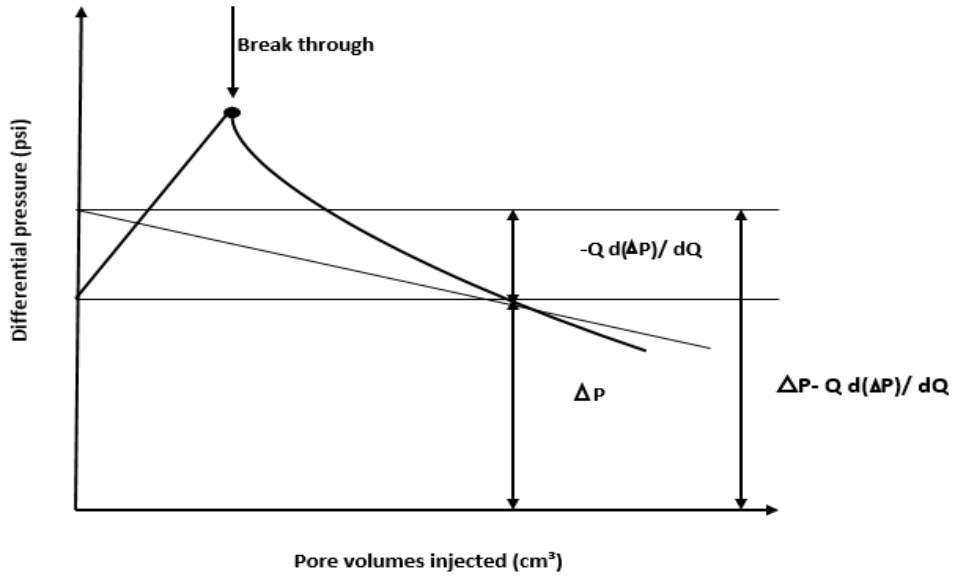

Figure 5-2: Differential pressure as a function of pore volume.

The expression $(\Delta p - Q\frac{d(\Delta p)}{dQ})$ in Figure 5-2 can be obtained from the slope of the tangent across the pressure as shown on the plot.

5.2 Estimation of three-phase relative permeability from two-phase relative permeability curves

This method involves simulating WAG and SAG using Eclipse software. The relative permeability curves data are obtained from the WAG and SAG displacement experiments. In the model built using Eclipse software, keywords for three-phase relative permeability correlations are included to calculated three-phase relative permeability during simulation. The relative permeability curves required for the simulation are water/oil and gas/oil. To study the effect of surfactant on three phase relative permeability, the two-phase relative permeability of surfactant/oil and gas/oil displacement experiments will be used. The different three-phase correlations will be used estimate surfactant effect on three-phase relative permeability and oil recovery. Oil recovery predicted from simulation will be compared to oil recovery from experiments to estimate which correlation can match experimental oil recovery.

5.3 Reservoir simulation model description

A one-dimensional model with grid size 100x1x1 was used for this research to simulate SAG and WAG in Eclipse software. The input data used for simulation have been obtained from laboratory experiments discussed in Chapter 3. The reservoir is homogeneous with porosity of 0.18 and absolute permeability of 100 mD. This is done to represent the core sample properties used in the SAG and WAG displacement experiments. One injector well and producer well were assigned to this model. Capillary pressure was ignored; as capillary pressure has been neglected in the equations used for experimental estimation of three-phase relative permeability.

For this simulation and a simple PVT data of immiscible dry gas and dead oil was used. Relative permeability curves obtained from surfactant alternating gas flooding has been used in this model. The reservoir was initially saturated with oil at connate water saturation with initial pressure of 500 psi. Three-phase relative permeability correlations (Stone 1, Stone 2, linear interpolation, saturated weighted interpolation

and Stone exponent) will be included in the Eclipse data file to estimate three phase relative permeability.

5.4 Experimental investigation of three-phase flow

Figures 5-3 shows the plot of pore volume of oil produced against pore volume of gas injected in WAG and SAG. The results show that oil recovery improved in SAG when compared to WAG. Figure 5-4 is the plot of pore volume of water and surfactant produced against pore volume of gas injected, the volume of surfactant produced is slightly higher than the volume of water produced. Oil, water and surfactant saturations are calculated from the recovery curves. Figure 5-5 is the plot of pore volume of gas produced versus pore volume injected. The plot shows that gas break-through was delayed when SAG. In WAG injection, gas breakthrough occurred at 0.34 pore volume of gas injected while in SAG gas breakthrough occurred at 0.48 pore volume of injected gas. Gas produced in WAG is also higher when compared to surfactant WAG. This is because of increased gas trapping by surfactant.

Figure 5-6 presents the plot of pressure gradient in WAG compared to the pressure gradient of SAG. The results show that there is an increase in pressure in SAG when compared to WAG. The increase in pressure gradient in the gas/surfactant injection indicates that there was a significant reduction in the gas relative permeability. The surfactant could create the required resistance to gas flow in the core sample and reduce the mobility (Sagir et al, 2015).

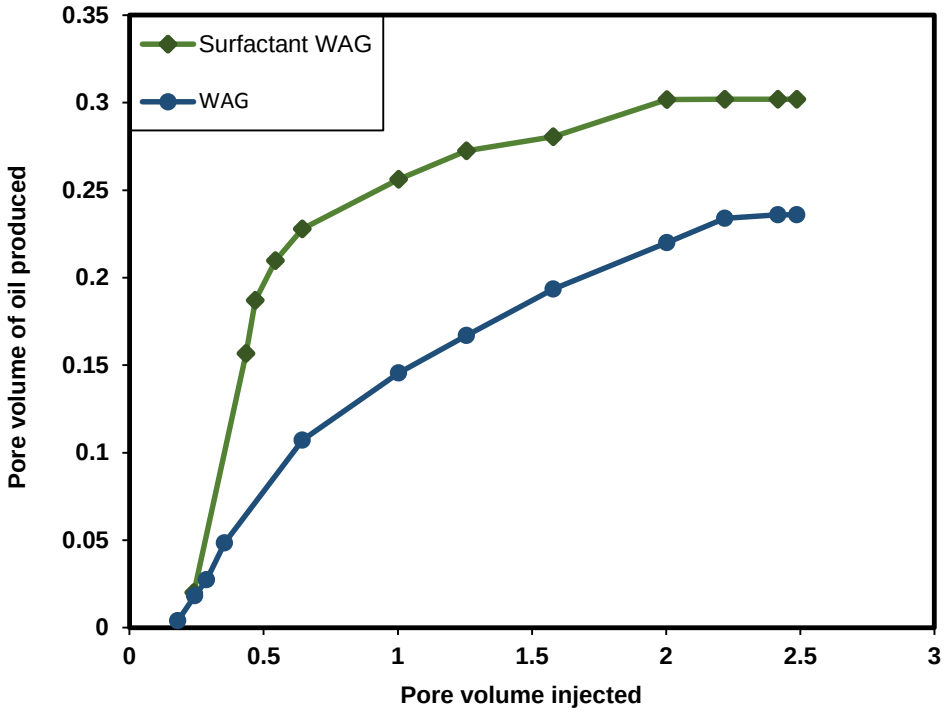

Figure 5-3: Comparison of oil production in WAG and SAG displacement experiments.

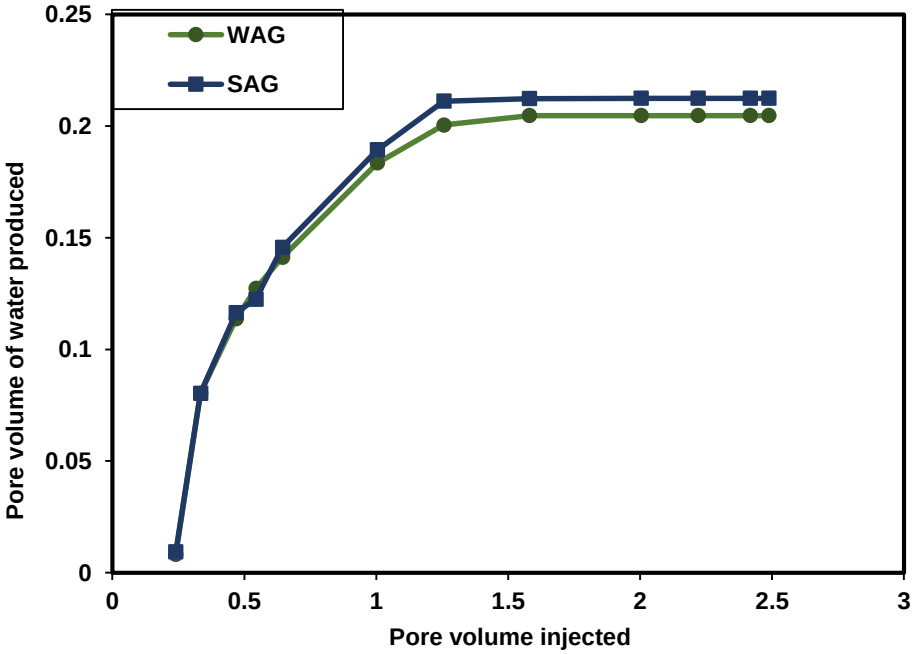

Figure 5-4: Comparison of water production in WAG and SAG displacement experiments.

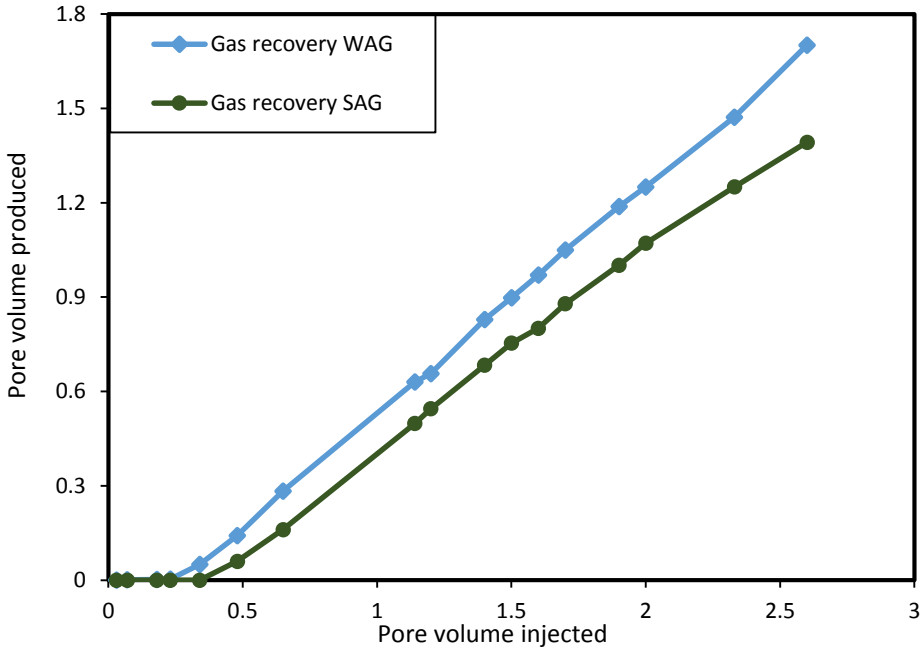

Figure 5-5: Comparison of gas produced in WAG and SAG displacement experiments.

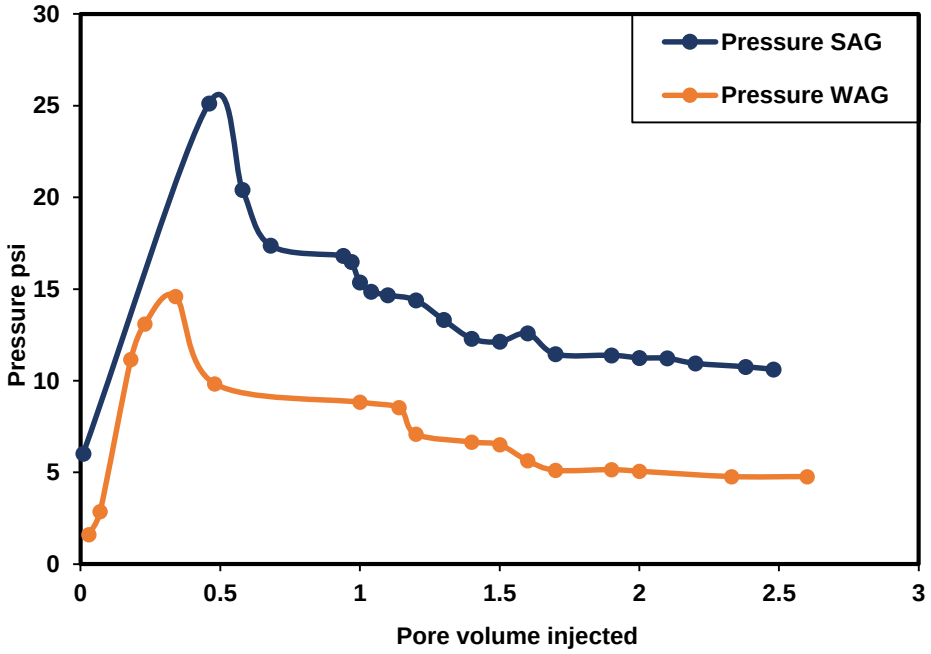

Figure 5-6: Pressure gradient in WAG and SAG displacement experiments.

5.5 Experimental investigation of surfactant effect on three-phase relative permeability

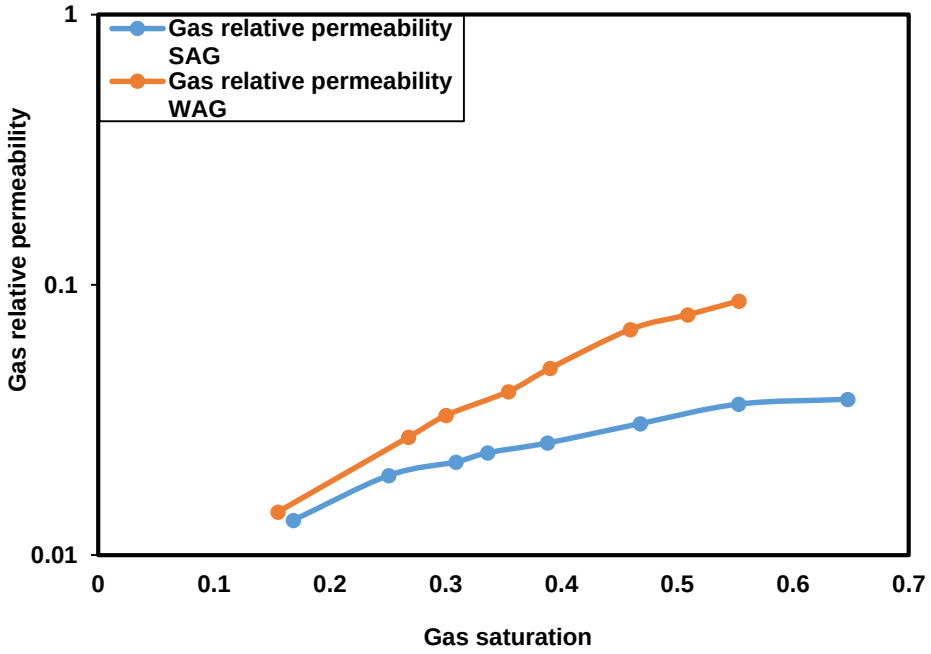

Figure 5-7: Surfactant effect on three-phase gas relative permeability

The three-phase relative permeability plots for all phases have been presented in semi-log graphs. Figure 5-7 presents the plot of gas relative permeability in WAG and SAG versus gas saturation. Results from the experiments show that gas relative permeability in three-phase flow is a function of its saturation and that of water and oil. As the presence of water and surfactant can reduce the gas mobility by trapping and depending on the oil saturation, the oil can minimise gas and surfactant interaction. The gas relative permeability in SAG is a lot lower compared to WAG. Surfactant can create foam when it meets gas increasing the gas viscosity and reducing the gas mobility. This result contradicts the assumption of the channel flow theory discussed in the literature which states that the gas relative permeability is a function of its saturation only.

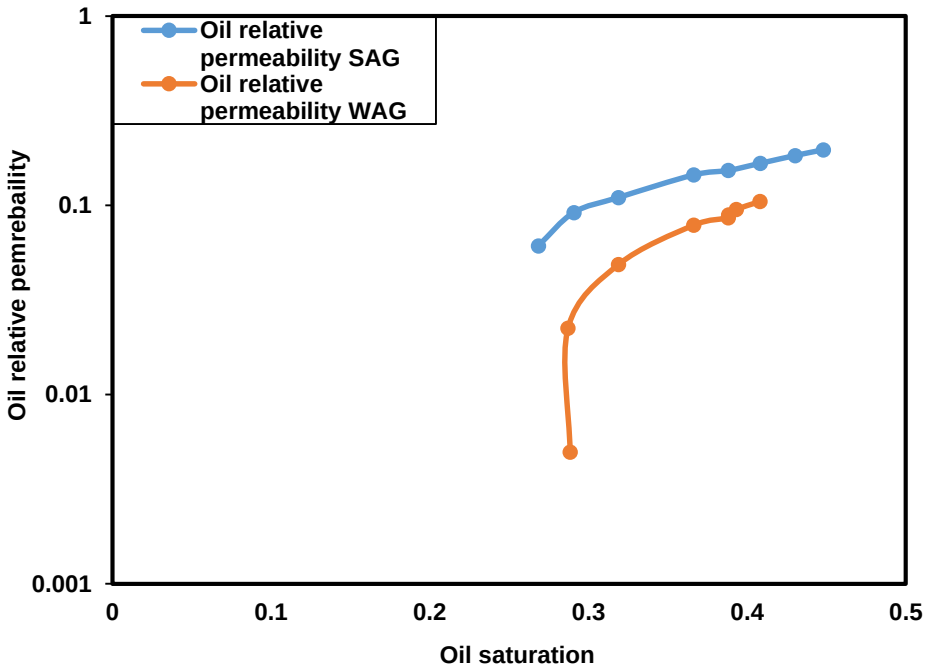

Figure 5-8: Surfactant effect on three-phase oil relative permeability

Figure 5-8 shows three-phase oil relative permeability in SAG and WAG. The oil relative permeability results clearly indicate that oil relative permeability is a function of the other two phases (gas/water or gas/surfactant). The plot also shows that the oil relative permeability increases in the presence of surfactant/gas as compared to water/gas. The SAG injection combines the two mechanisms of interfacial tension reduction and gas trapping to effectively displace oil. The first gas injection is conducted after an initial surfactant flooding for SAG. As the gas saturation increases, the remaining surfactant in the porous medium interacts with the gas, hence increases the gas viscosity and reduces the water blocking effect encountered during WAG which prevents the trapped gas from encountering the oil. This increase in gas viscosity allows the gas to create a front behind the oil causing an increase in oil flow. Cinar and Orr (2005) in their study of three-phase relative permeability in interfacial tension variation also reported an increase in oil relative permeability in three-phase flow when the oil and water interfacial tension is reduced.

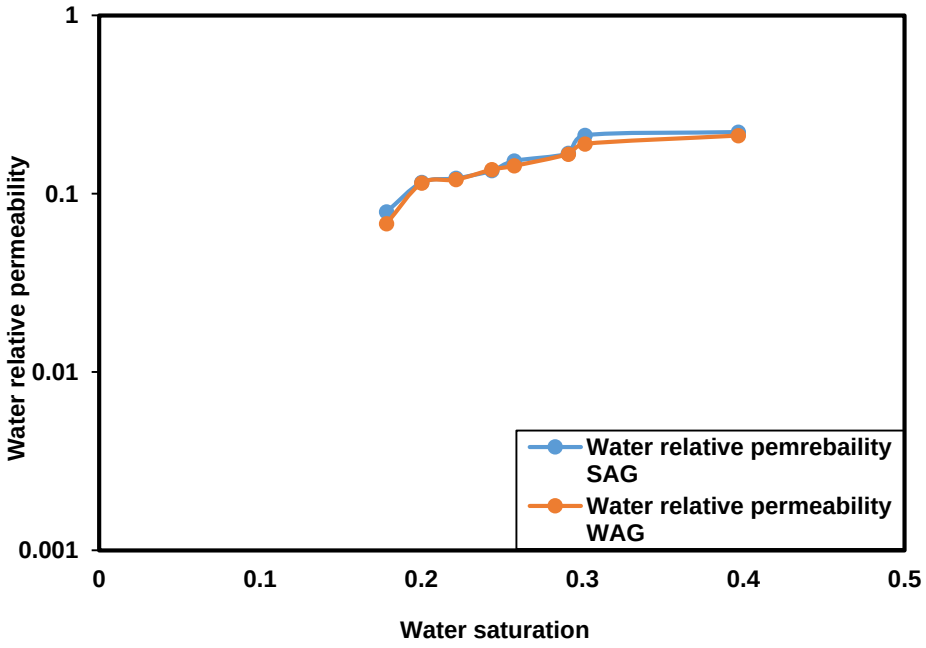

Figure 5-9: Surfactant effect on three-phase water relative permeability

Figure 5-9 presents the plot of water relative permeability in SAG and WAG. The plot of relative permeability curves shows that water relative permeability in three-phase flow is a function of only its saturation and the presence of surfactant does not have any effect on the flow of water in the porous medium. As the change in water relative permeability in the presence of surfactant is very minimal. Compared to oil and gas three phase relative permeability, water and surfactant seem to have the higher values. When compared to two-phase water and surfactant relative permeabilities the values are of the same range. Further proving that water relative permeability is a function of only its saturation.

5.6 Effect of rock absolute permeability on three-phase relative permeability with surfactants

The affected fluids in three-phase flow with surfactants are gas and oil. Further experiments were conducted to study rock permeability effect in oil and gas three-phase flow with surfactant. Figure 5-10 shows the plot of gas three-phase relative permeability in a 100 mD core sample and 50 mD core sample. The results show that gas relative permeability is higher in 100 mD core sample when compared to 50 mD core sample. While oil relative permeability in 100 mD core sample in Figure 5-

11 is also higher than that of 50 mD. The reason for this is because of the effect of capillary force that is more pronounced in the 50 mD core sample. The capillary force significantly affects the distribution of fluids in the porous media.

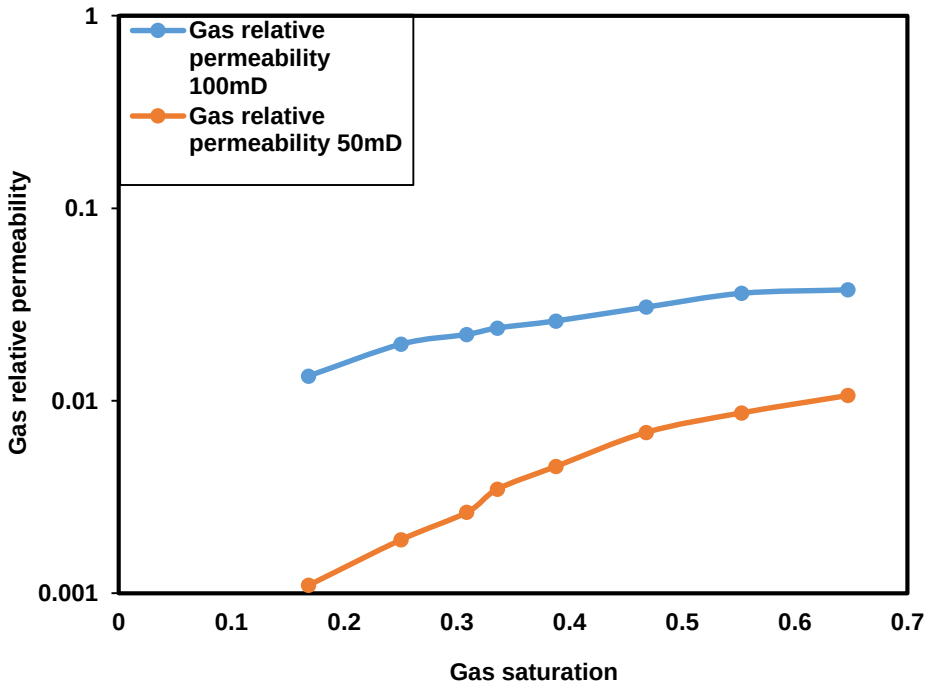

Figure 5-10: Rock permeability effect on three-phase gas flow

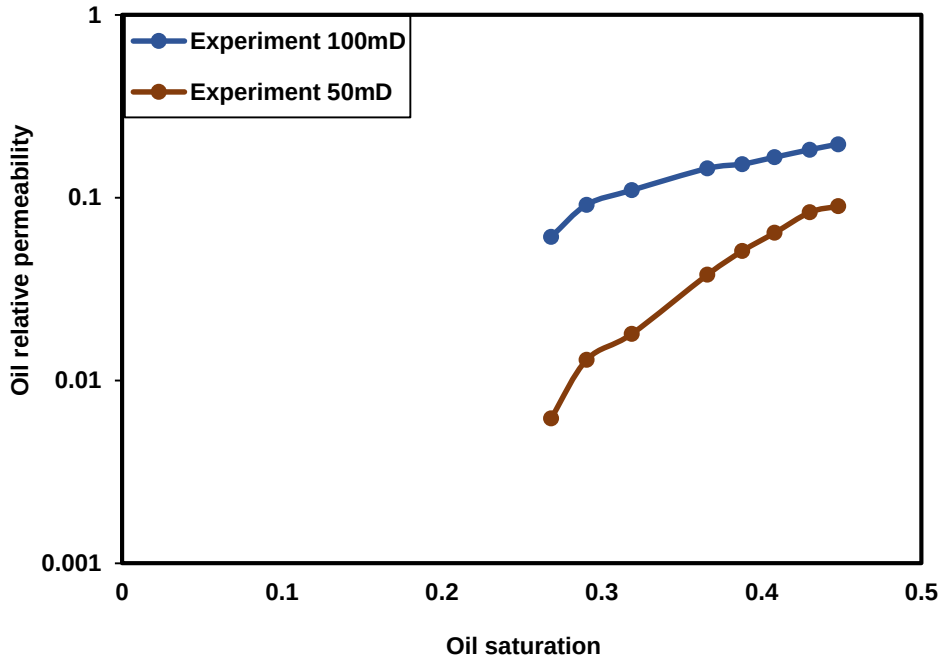

Figure 5-11: Rock permeability effect on three-phase oil flow.

5.7 Estimation of surfactant effect on three-phase relative permeability using empirical correlations

The three-phase relative permeability correlations used for this research will be the ones present in Eclipse reservoir simulator. The correlations are Stone 1, equation [2.27], Stone 2, equation [2.38], Stone Exponent, equation [2.27], saturated weighted interpolation, equation [2.39], and linear interpolation, equation [2.42]. Since the correlations assume the channel flow theory which states that in three-phase flow, the water and gas relative permeabilities are functions of their saturations only and oil relative permeability is a function of both saturations, the correlations will only be used to predict three-phase oil relative permeability in comparison to experimental results. Table 5 shows the rock properties while used for the simulation. The relative permeability curves used for the simulation were obtained from the surfactant-alternating-gas injection flooding experiment. All other fluid properties used in the simulation were obtained from laboratory experiments described in Chapter 3.

Table 5-1: Reservoir rock properties.

Parameters	Value-Units
Reservoir size	10 x 2x 3(cm)
Reservoir grid	100 x1x1
K_x x K_y x K_z	100
Porosity	0.18
Initial pressure	500psia
temperature	60ºC
Net to gross	1

Figure 5-12 presents the synthetic model built for surfactant water alternating gas flooding using the different three-phase relative permeability correlations. The colours represent the active cells in the grid block. The comparison of three-phase oil relative permeability prediction by correlations with experiment are given in Figures 5-13 and 5-14. Figure 5-13 and 5-14 show the comparison between experimental three-phase relative permeability to oil and predicted oil relative permeability by correlations.

The results show that there is no match between experimental and predicted SAG three-phase relative permeability by correlations. Saturated weighted interpolation equation [2.39], linear interpolation, equation [2.42], Stone 1, equation [2.27] and Stone 2, equation [2.38] predicted higher relative permeabilities. Stone exponent correlation, equation [2.33] predicted similar relative permeabilities at higher saturations but at lower saturations, the relative permeabilities differ greatly. Overall none of the three-phase relative permeability correlations could effectively predict three-phase relative permeability in SAG. This is because none of the correlations put into account the interactions between gas and surfactant which is the gas tapping and creation of foam. The correlations also do not put into consideration the reduction of gas relative permeability as a result of hysteresis which occurs due to continuous cyclic injection of water and gas. The correlations are based on channel flow theory which assumes water and gas relative permeabilities are functions of only their saturations only. This assumption has been not to be accurate and discussed in the experimental estimation of three-phase flow in this research. Figure 5-15 shows oil

recovery factor predicted by correlations and experiment. Only the Stone exponent could predict recovery factor close to the experiment. The other correlations over estimated oil recovery factor.

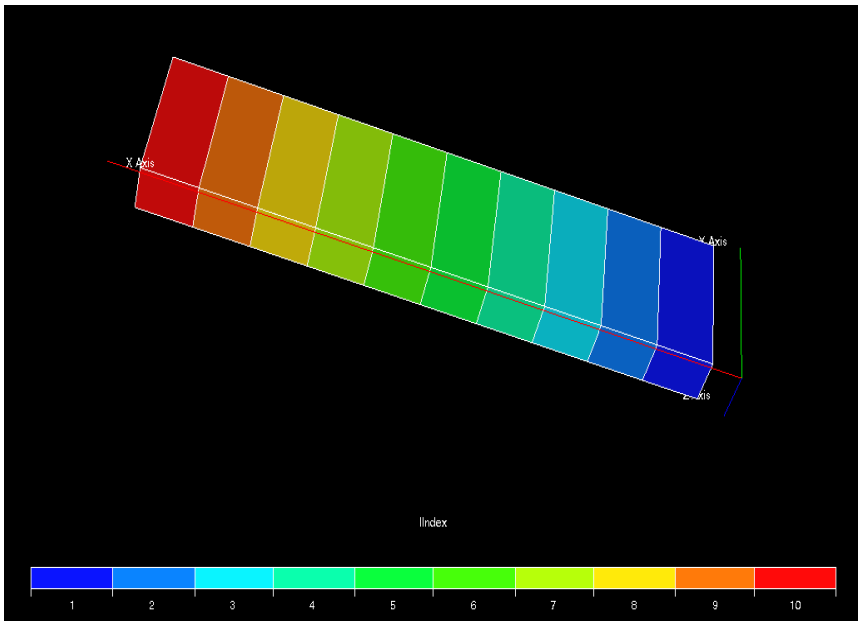

Figure 5-12: Synthetic reservoir model built in Eclipse for SAG.

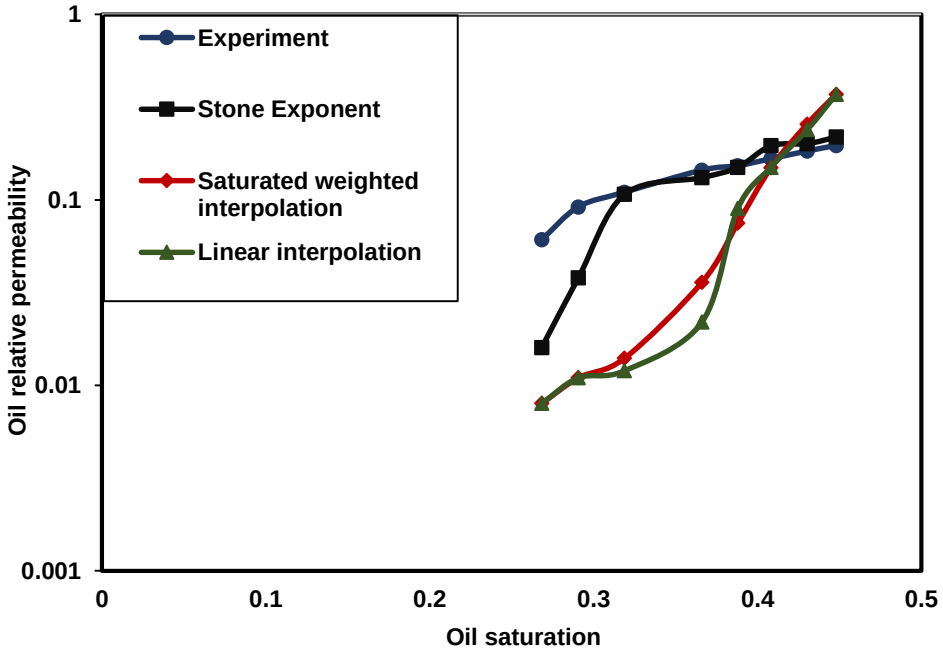

Figure 5-13: Comparison of SAG three-phase oil relative permeability predictions by linear interpolation, saturated weighted interpolation, Stone exponent models and experiment.

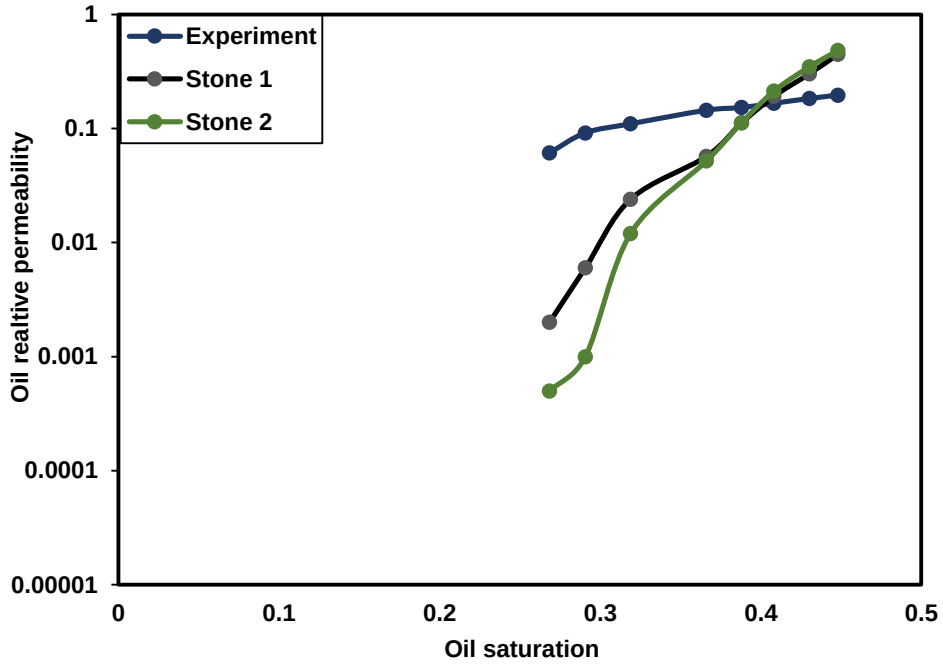

Figure 5-14: Comparison of SAG three-phase oil relative permeability predictions of Stone 1 and Stone 2 models and experiment.

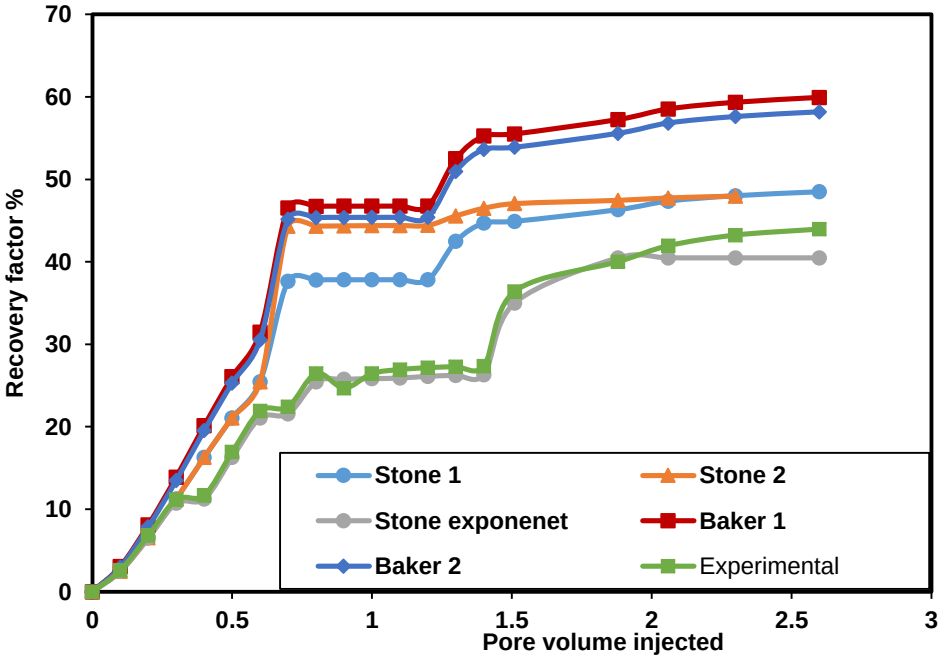

Figure 5-15: Oil recovery factor predictions by models and experiment.

Chapter 6 Conclusions and recommendations

In this research, an experimental investigation of surfactant effect on three-phase relative permeability in water-alternating-gas flooding has been studied. To do this, experiments were conducted to analyse different surfactant blends to select the surfactant formulation that is compatible with the brine and oil used in this research.
Two phase core flood experiments were conducted to study the effect of surfactants on two phase gas/oil, water/oil and gas/water relative permeability.
Water-alternating-gas flooding and surfactant-alternating-gas flooding experiments were conducted and the extension of Buckley-Leveret theory proposed by Grader and O'Meara (1988) and confirmed by Siddiqui et al (1995) was used to calculate experimental three-phase relative permeability. Surfactant effect on three-phase relative permeability was evaluated by comparing experimental prediction of three-phase relative permeability in WAG and surfactant WAG. Two-phase relative permeability curves obtained from surfactant WAG were used in Eclipse reservoir simulation to estimate three-phase relative permeability with surfactants and the results were compared with that obtained from experiments.

6.1 Conclusions

The following conclusions have been made from this research:

- For this research, alcohol alkoxy sulphate surfactant was optimised by introducing internal olefin sulfonate as a co-surfactant. This improved the stability in hard brine containing divalent ions. The surfactant blend gave the lowest interfacial tension and could form a non-viscous type III microemulsion phase. Making this surfactant blend the most suitable for displacement experiments.
- The presence of surfactant in two-phase water/oil displacement experiment increases oil relative permeability but does not influence water relative permeability.
- In two-phase gas/water displacement experiment, surfactant increased gas trapping, thus decreasing gas relative permeability and increasing water relative permeability.
- The presence of surfactant in two-phase gas/oil displacement experiment increases oil relative permeability. The increase in oil relative permeability is

due to the increase in water wetness of the rock which allows oil to flow freely. Gas relative permeability decrease, but the decrease in gas relative permeability is more pronounced in gas/water displacement because the presence of oil limits gas contact with surfactant.

- Surfactant effect on oil mobility is more pronounced in two-phase flow, than in three-phase flow because of the fluid interactions that occur in three-phase flow. In two-phase flow, oil relative permeability is higher compared to three phase flow and gas relative permeability also.
- In SAG, oil and gas relative permeabilities are not functions only their saturations but are functions of the saturations of all the fluids present in the reservoir.
- Water and surfactant relative permeability in SAG are functions of their saturations alone. Water relative permeability for three-phase flow in the presence of surfactant is similar to that of two-phase flow and the presence of surfactant does not affect water relative permeability.
- The presence of surfactant in experimental three-phase flow increases gas trapping and reduces the viscosity of gas. This causes the reduction in three-phase gas relative permeability in SAG when compared to WAG.
- Three-phase relative permeability correlations cannot predict surfactant effect on three-phase relative permeability accurately as the correlations do not consider the gas trapping by surfactant and reduction in water/oil interfacial tension by surfactant.

6.2 Recommendations

Based on the results from this work, the following are lists of recommendations that may be considered in the future:

- More core flooding experiments to study surfactant effect on three-phase relative permeability should be conducted using CO_2 and methane gases. These are the gases that can be found in oil field processes.
- Gas interaction with surfactant should be evaluated by conducting foam creation experiment using alcohol alkoxy sulphate and nitrogen to determine the foam properties such as the strength and viscosity.

- Capillary pressure should be incorporated in future work as it plays a very important role in enhanced oil recovery processes.
- To gain better insight and understanding on fluid saturation distributions in cores during experiments in three-phase flow with surfactants, a CT scanner should be used during experiments to capture fluid distribution as three-phase flow with surfactants follow a completely different saturation path unlike two-phase flow.
- Building a more advanced compositional simulator that puts into account gas trapping and microemulsion phase in predicting surfactant effect on three-phase relative permeability and to capture the interaction between oil, water and surfactant and gas. More flexible correlations for estimating SAG three-phase relative permeability that puts into consideration the mechanisms involved in three-phase flow involving surfactants.
- Reveal software can be used to match experimental and simulated three-phase relative permeability as it can include the phases and interactions that occurs when surfactant is present in WAG.

References

Abaci, S., Edwards, J.S. and Whittaker, B.N., (1992) Relative permeability measurements for two-phase flow in unconsolidated sands. *Mine water and the environment*, 11(2), pp.11-26.

Abdi, M., Moradi, S., Habibnia, B. and Kord, S., (2014) Improving oil recovery during water injection and WAG processes in asphaltenic oil reservoirs by using non-ionic surfactants. *International Journal of Science & Emerging Technologies,* 7(4).

Abeysinghe, K.P., (2013) A novel approach to surfactant flooding under mixed-wet conditions.

Aghdam, K.A., Moghaddas, J.S., Moradi, B., Dabiri, M. and Hassanzadeh, M., (2013) Maximizing the oil recovery through miscible water alternating gas (WAG) injection in an Iranian oil reservoir. *Petroleum science and technology*, 31(22), pp.2431-2440.

Ahmed, T., (2006) Reservoir Engineering handbook, 3rd Ed, Oxford, *Elsevier publishing*, ISBN 13: 978-0-7506-7972-5

Akbarabadi, M. and Piri, M., (2015) Co-sequestration of SO_2 with supercritical CO_2 in carbonates: an experimental study of capillary trapping, relative permeability, and capillary pressure. *Advances in Water Resources*, 77, pp.44-56.

Akhlaghinia, M., (2013) Experimental and Numerical Studies of Three-Phase Relative Permeability Isoperms for Heavy Oil Systems (Doctoral dissertation, Faculty of Graduate Studies and Research, University of Regina).

Al-Abri, A., Sidiq, H. and Amin, R., (2012) Mobility ratio, relative permeability and sweep efficiency of supercritical CO 2 and methane injection to enhance natural gas and condensate recovery: core flooding experimentation. *Journal of Natural Gas Science and Engineering*, 9, pp.166-171.

Al-Adasani, A. and Bai, B., (2010) Recent developments and updated screening criteria of enhanced oil recovery techniques*. International Oil and Gas Conference and Exhibition in China.* Society of Petroleum Engineers.

Al-Ghanim, W., Gharbi, R. and Algharaib, M.K., (2009) Designing a simultaneous water alternating gas process for optimizing oil recovery. EUROPEC/EAGE Conference and Exhibition. Society of Petroleum Engineers.

Al-Mamari, F., Al-shuraiqi, H., and Al-wahaibi, Y., (2007) Numerical simulation and experimental studies of oil recovery via First- contact miscible water-alternating- gas injection within shaley porous media, *Society of Petroleum Engineers Journal*, pp1-16.

Al-Menhali, A., Niu, B. and Krevor, S., (2015) Capillarity and wetting of carbon dioxide and brine during drainage in Berea sandstone at reservoir conditions. *Water Resources Research*, 51(10), pp.7895-7914.

Al-Mossawy, M., Demiral, B., and Anwar Raja, D., (2011) Foam dynamics in porous media and its applications in enhanced oil recovery: review*. International journal of recent research and applied studies,* pp 351-357.

Alzayer, H. A., Jahanbakhsh, A., Sohrabi,M., (2017) New Methodology for Numerical Simulation of Water-Alternating-Gas (WAG) Injection, *EAGE national improved oil recovery conference,* pp. 1-13.

Anderson, W.G., (1987) Wettability literature survey-part 6: the effects of wettability on waterflooding. *Journal of Petroleum Technology*, 39(12), pp.1-605.

Arogundade, O.A., Shahverdi, H.R. and Sohrabi, M., (2013) July. A study of three phase relative permeability and hysteresis in water alternating gas (WAG) injection. In SPE Enhanced Oil Recovery Conference. Society of Petroleum Engineers.

Azam, M.R., Tan, I.M., Ismail, L., Mushtaq, M., Nadeem, M. and Sagir, M., (2013) Static adsorption of anionic surfactant onto crushed Berea sandstone*. Journal of Petroleum Exploration and Production Technology*, 3(3), pp.195-201.

Baker, L.E., (1988) Three-phase relative permeability correlations. *SPE Enhanced Oil Recovery Symposium*. Society of Petroleum Engineers.

Baker, R., (1997) Reservoir management for waterfloods. *Journal of Canadian Petroleum Technology*, 36(04).

Barnes, J.R., Dirkzwager, H., Smit, J., Smit, J., On, A., Navarrete, R.C., Ellison, B. and Buijse, M.A., (2010) Application of internal olefin sulfonates and other surfactants

to EOR. Part 1: Structure-Performance relationships for selection at different reservoir conditions. *SPE Improved Oil Recovery Symposium*. Society of Petroleum Engineers.

Ahmadi, M.A. and Shadizadeh, S.R., (2013) Implementation of a high-performance surfactant for enhanced oil recovery from carbonate reservoirs. *Journal of Petroleum Science and Engineering*, 110, pp.66-73.

Basburg, B. and Z.T. Karpyn, (2008) “Determination of relative permeability and capillary pressure curves using an automated history-matching approach. *SPE Eastern Regional/AAPG Eastern section.*

Bennion, D.B. and Bachu, S., (2006) The impact of interfacial tension and pore size distribution/capillary pressure character on CO2 relative permeability at reservoir conditions in CO2-brine systems. *SPE/DOE Symposium on Improved Oil Recovery.* Society of Petroleum Engineers.

Bennion, D.B., Thomas, F.B., Bietz, R.F. and Bennion, D.W., (1996) Water and hydrocarbon phase trapping in porous media-diagnosis, prevention and treatment. *Journal of Canadian Petroleum Technology*, 35(10).

Bera, A., Kumar, T., Ojha, K. and Mandal, A., (2013) Adsorption of surfactants on sand surface in enhanced oil recovery: isotherms, kinetics and thermodynamic studies. *Applied Surface Science*, 284, pp.87-99.

Blom, S.M.P., Hagoort, J. and Soetekouw, D.P.N., (1997) January. Relative permeability at near-critical conditions. *SPE Annual Technical Conference and Exhibition.* Society of Petroleum Engineers.

Blunt, M.J., (2000) An empirical model for three-phase relative permeability*. SPE Journal,* 5(04), pp.435-445.

Buijse, M.A., Prelicz, R.M., Barnes, J.R. and Cosmo, C., (2010) Application of internal olefin sulfonates and other surfactants to EOR. Part 2: the design and execution of an ASP field test. *SPE Improved Oil Recovery Symposium*. Society of Petroleum Engineers.

Cao, P. and Siddiqui, S., (2011) Three-phase unsteady-state relative permeability measurements in consolidated cores using three immiscible liquids. *SPE Annual Technical Conference and Exhibition.* Society of Petroleum Engineers.

Christensen, J.R., Stenby, E.H., and Skauge, A., (1998) Review of WAG Field Experience, paper SPE 39883, presented at the International Petroleum Conference and Exhibition of Mexico, Villahermosa, Mexico.

Christensen, J.R., Stenby, E.H., and Skauge, A., (2001) Review of WAG Field Experience, paper SPE 39883. *International Petroleum Conference and Exhibition of Mexico, Villahermosa, Mexico.*

Christiansen, R.L. and Howarth, S.M., (1995) literature review and recommendations of methods for measuring relative permeability of anhydrite from the Salado formation at the waste isolation pilot plant. *Sandia National Laboratories*.

Cinar, Y. and Orr, F.M., (2005) Measurement of three-phase relative permeability with IFT variation. *SPE Reservoir Evaluation & Engineering*, 8(01), pp.33-43.

Dake, L.P., (2001) The practice of reservoir engineering (revised edition) (Vol. 36). Elsevier.

Dalen, V., Instefjord, R., and Cristensen, R., (1993) AWAG formation Pilot in the Lower Brent Formation at the Gullfaks Field*. European IOR Symposium, Moscow*.

Dandekar, A.Y., (2013) Petroleum reservoir rock and fluid properties. CRC press.

Dehghanpour, H., DiCarlo, D.A., Aminzadeh, B. and Mirzaei Galeh-Kalaei, M., (2010) January. Two-phase and three-phase saturation routes and relative permeability during fast drainage. *SPE Improved Oil Recovery Symposium*. Society of Petroleum Engineers.

Delshad, M. and Pope, G.A., (1989) Comparison of the three-phase oil relative permeability models. *Transport in Porous Media*, 4(1), pp.59-83.

Delshad, M., Pope, G.A. and Sepehrnoori, K., (1996) A compositional simulator for modelling surfactant enhanced aquifer remediation, 1 formulation. *Journal of Contaminant Hydrology*, 23(4), pp.303-327.

Donaldson, E.C., Chilingarian, G.V. and Yen, T.F. eds., (1989*) Enhanced oil recovery, II: Processes and operations* (Vol. 17). Elsevier.

Doghaish, N. M. (2008) *Analysis of Enhanced Oil Recovery-A Literature Review.* Dalhousie University. Halifax: unpublish work.

Drelich, J., Fang, C .and White, L. (2002) Measurement of interfacial tension in fluid-fluid systems, *Michigan Technological University, Houghton, Michigan.* pp3152- 3165

Dria, D.E., Pope, G.A. and Sepehrnoori, K., (1993) Three-phase gas/oil/brine relative permeabilities measured under CO2 flooding conditions. *SPE reservoir engineering*, 8(02), pp.143-150.

Du Yuqi, O.B. and Dacun, L., (2004) Literature review on methods to obtain relative permeability data. *5th Conference & Exposition on Petroleum Geophysics, Hyderabad-2004,* India, pp. 597-604

Eleri, O.O., Graue, A. and Skauge, A., (1995) Steady-state and unsteady-state two-phase relative permeability hysteresis and measurements of three-phase relative permeabilities using imaging techniques. *SPE Annual Technical Conference and Exhibition*. Society of Petroleum Engineers.

Elmofty, O. (2012) Surfactant Enhanced Oil Recovery by Wettability Alteration of Sandstone Reservoirs, Master's Thesis Paper 6928, Department of Geoscience, Geological and Petroleum Engineering, University of Missouri.

El Sharawy, M.S., (2016) Modelling of Two-Phase Relative Permeability in Cambrian and Early Miocene Sandstone Reservoirs: A Case Study, Egypt. *Arabian Journal for Science and Engineering*, 41(7), pp.2751-2770.

Elraies, K.A., (2014) Mechanism of Surfactant in Microemulsion Phase Behaviour. *Journal of Applied Sciences*, 14, pp.1049-1054.

Falode, O. and Manuel, E., (2014) Wettability effects on capillary pressure, relative permeability, and irreducible saturation using porous plate. *Journal of Petroleum Engineering*.

Farajzadeh, R., Lotfollahi, M., Eftekhari, A.A., Rossen, W.R. and Hirasaki, G.J.H., (2015) Effect of permeability on implicit-texture foam model parameters and the limiting capillary pressure. *Energy & fuels*, 29(5), pp.3011-3018.

Farn, R.J. ed., (2008) Chemistry and technology of surfactants. John Wiley & Sons.

Farokhpoor, R., Lindeberg, E.G.B., Torsæter, O., Mørk, M.B. and Mørk, A., (2014) Permeability and relative permeability measurements for CO2-brine system at reservoir conditions in low permeable sandstones in Svalbard*. Greenhouse Gases: Science and Technology*, 4(1), pp.36-52.

Flaaten, A., Nguyen, Q.P., Pope, G.A. and Zhang, J., (2009) A systematic laboratory approach to low-cost, high-performance chemical flooding. *SPE Reservoir Evaluation & Engineering*, 12(05), pp.713-723.

Foroozanfar, M. and Aminshahidy, B., (2013) Efficiency evaluation of immiscible water alternating gas (IWAG) process in one of Iranian oil reservoirs. *Global Journal of Science (GJSET) publishing*, Engineering and Technology, 14, pp.76-81.

Green, D., and Willhite, G. (1998) Enhanced oil recovery, SPE text book, Vol. 6, ISBN 1-55563-077-4, pp15.

Fuseni, A., Han, M. and Al-Mobith, A., (2013) Phase Behavior and Interfacial Tension Properties of an Amphoteric Surfactant for EOR Application. *SPE Saudi Arabia section technical symposium and exhibition*. Society of Petroleum Engineers.

Grader, A.S. and O'Meara Jr, D.J., (1988) Dynamic displacement measurements of three-phase relative permeabilities using three immiscible liquids. *SPE Annual Technical Conference and Exhibition*. Society of Petroleum Engineers.

Gupta, R. and Maloney, D., (2015) Applications of the intercept method to correct steady-state relative permeability for capillary end-effects. *International Symposium of the Society of Core Analysts,* St. John's Newfoundland and Labrador, Canada.

Hamouda, A.A., Karoussi, O. and Chukwudeme, E.A., (2008) Relative permeability as a function of temperature, initial water saturation and flooding fluid compositions for modified oil-wet chalk. *Journal of Petroleum Science and Engineering*, 63(1), pp.61-72.

Hirasaki, G.J., Miller, C.A. and Puerto, M., (2008) Recent advances in surfactant EOR. *SPE Annual Technical Conference and Exhibition*. Society of Petroleum Engineers.

Honarpour, M., Koederitz, L. and Harvey, A. H., (1986) Relative Permeability of Petroleum Reservoirs, CRC Press, Boca Raton, Florida.

Hustad, O.S. and Holt, T., (1992) Gravity stable displacement of oil by hydrocarbon gas after waterflooding. *SPE/DOE Enhanced Oil Recovery Symposium*. Society of Petroleum Engineers.

Ibrahim, M.N. and Koederitz, L.F., (2001) January. Two-phase steady-state and unsteady-state relative permeability prediction models. *SPE Middle East Oil Show*. Society of Petroleum Engineers.

Iglauer, S., Wu, Y., Shuler, P., Tang, Y. and Goddard, W.A., (2010) New surfactant classes for enhanced oil recovery and their tertiary oil recovery potential. *Journal of Petroleum Science and Engineering*, 71(1), pp.23-29.

Jamaloei, B.Y. and Kharrat, R., (2010) Analysis of microscopic displacement mechanisms of dilute surfactant flooding in oil-wet and water-wet porous media. *Transport in porous media*, *81*(1), p.1.

Jelmert, T.A., Chang, N., Høier, L., Pwaga, S., Iluore, C., Hundseth, Ø., Perales, F.J. and Idrees, M.U., 2010. Comparative Study of Different EOR Methods. *Norwegian University of Science & Technology, Trondheim, Norway*.

Jensen, J.A., and Friedmann, F., (1987) Physical and chemical effects of an oil phase on the propagation of foam in the porous media, *Society of Petroleum Engineers conference paper*, SPE 16375, pp 476-485.

Jiang, F. and Tsuji, T., (2017) Estimation of three-phase relative permeability by simulating fluid dynamics directly on rock-microstructure images. *Water Resources Research*, *53*(1), pp.11-32.

Juanes, R. and Spiteri, E., (2004) Impact of Relative Permeability Hysteresis on WAG Injection. J*ournal of Petroleum Science and Engineering*, *50*(2), pp.115-139.

Kianinejad, A., Chen, X. and DiCarlo, D.A., (2015) The effect of saturation path on three-phase relative permeability. *Water Resources Research*, 51(11), pp.9141-9164.

Kikuchi, M.M., Branco, C.C., Bonet, E.J., Zanoni, R.M. and Paiva, C.M., (2005) Water/oil relative permeability comparative study: steady versus unsteady state. *International Symposium of the Society of Core Analysts*.

Kim, S. and Santamarina, J.C., (2014) Engineered CO 2 injection: The use of surfactants for enhanced sweep efficiency. *International Journal of Greenhouse Gas Control,* 20, pp.324-332.

Knappskog, O.A., (2012) Evaluation of WAG injection at Ekofisk (Master's thesis, University of Stavanger, Norway).

Krevor, S., Pini, R., Zuo, L. and Benson, S.M., (2012) Relative permeability and trapping of CO2 and water in sandstone rocks at reservoir conditions. *Water Resources Research,* 48(2).

Kulkarni, K.N. and Datta-Gupta, A., (2000) Estimating relative permeability from production data: A streamline approach. *SPE Journal* 5(4), 402–411.

Kulkarni, R.N.; Watson, A.T.; and Nordtvedt, J.E., (1998) Estimation of porous media flow functions using NMR imaging data. *Magnetic Resonance Imaging* 16(5–6), 707–709.

Kulkarni, M. and Rao, D., (2005) Experimental investigation of miscible and immiscible water-alternating–gas (WAG) process, *Journal of Petroleum Science and Engineering*, pp1-20

Kuhlman, M. I., Falls, A. M., Hara, S. K., Monger-McClure, T. G., and Borchardt, J.K., (1992) "CO2 Foam with surfactants used below their critical micelle concentrations," *SPE Reservoir Engineering* (7), 445-452.

Lerch, D., (2010) Making Sense of Peak Oil and Energy Uncertainty. The Post Carbon Reader Series - Energy. Santa Rosa, California. *http://www.postcarbon.org/Reader /PCReaderLerch-Energy.pdf*

Levitt, D., Jackson, A., Heinson, C., Britton, L.N., Malik, T., Dwarakanath, V. and Pope, G.A., (2006) January. Identification and evaluation of high-performance EOR surfactants. *SPE/DOE Symposium on Improved Oil Recovery*. Society of Petroleum Engineers.

Li, H., D. Yang and M. Arhuoma, (2010) “Relative permeability estimation from displacement experiments using EnKF method”, *Paper SPE 131633 presented at the CPS/SPE International Oil & Gas Conference.*

Lin, E.C. and Poole, E.S., (1991) Numerical evaluation of single-slug, WAG, and hybrid CO2 injection processes, Dollarhide Devonian Unit, Andrews County, Texas. *SPE Reservoir Engineering*, 6(04), pp.415-420.

Lobo, L., Nikolov, A and Wasan, D. (1989) Foam stability in the presence of oil: on the importance of the second viral coefficient, *Journal of dispersion, science and technology*, pp143-161.

Loeve, D., Wilschut, F., Hanea, R.H., Maas, J.G., Van Hooff, P.M.E. , van den Hoek, P.J. , Douma, S.G. , Van Doren , J.F.M., (2011) Simultaneous determination of relative permeability and capillary pressure curves by assisted history matching several scal experiments. *Society of Core Analysts.* PP.1-13.

Lohne, A. and Virnovsky, G., (2006) Three-phase upscaling in Capillary and Viscous Limit. *SPE/DOE Symposium on improved oil recovery, Tulsa*.

Lomeland, F., Ebeltoft, E. and Thomas, W.H., (2005) A new versatile relative permeability correlation. *International Symposium of the Society of Core Analysts, Toronto, Canada*. pp 1-12.

Manceau, J.C., Ma, J., Li, R., Audigane, P., Jiang, P.X., Xu, R.N., Tremosa, J. and Lerouge, C., (2015) Two- phase flow properties of a sandstone rock for the CO2/water system: Core-flooding experiments, and focus on impacts of mineralogical changes. *Water Resources Research*, 51(4), pp.2885-2900.

Mandal, A., (2015) Chemical flood enhanced oil recovery: a review. *International Journal of Oil, Gas and Coal Technology,* 9(3), pp.241-264.

Modaresghazani, J., (2015) Experimental and simulation study of relative permeabilities in heavy oil/water/gas systems (Doctoral dissertation, University of Calgary).

Nguyen, Q. P., (2011) Gas Trapping During Foamed Flow in Porous Media, Computed Tomography - Special Applications, *Dr. Luca Saba (Ed*.), ISBN: 978-953-307-723-9, InTech.

Oak, M.J., Baker, L.E. and Thomas, D.C., (1990) Three-phase relative permeability of Berea sandstone. *Journal of Petroleum Technology*, 42(08), pp.1-054.

Osei-Bonsou, K., Shokri, N., and Grassia. P., (2015) Foam stability in the presence and absence of hydrocarbons; from bubble-to bulk scale, *Journal of Colloid and Surfaces: Physiochemical and Engineering aspects*, pp 514-526.

Osei-Bonsu, K, Grassia, P & Shokri, N., (2017) 'Relationship between bulk foam stability, surfactant formulation and oil displacement efficiency in porous media' *Fuel*, vol 203, pp. 403-410.

Paria, S. and Khilar, K.C., (2004) A review on experimental studies of surfactant adsorption at the hydrophilic solid–water interface. *Advances in colloid and interface science,* 110(3), pp.75-95.

Pejic, D. and Maini, B.B., (2003) Three-phase relative permeability of petroleum reservoirs. *SPE Latin American and Caribbean Petroleum Engineering Conference*. Society of Petroleum Engineers.

Pipes, L., and Lawrence, H., (2014) Applied Mathematics for Engineers and Physicists; 3rd ed., Dover Publications, USA.

Rafati, R., Haddad, A.S. and Hamidi, H., (2016) Experimental study on stability and rheological properties of aqueous foam in the presence of reservoir natural solid particles. *Colloids and Surfaces A: Physicochemical and Engineering Aspects*, 509, pp.19-31.

Reynolds, C.A. and Krevor, S., (2015) Characterizing flow behaviour for gas injection: Relative permeability of CO2-brine and N2-water in heterogeneous rocks. *Water Resources Research*, 51(12), pp.9464-9489.

Romero-Zerón, L., (2012) Advances in Enhanced Oil Recovery Processes. *INTECH Open Access Publisher*.

Sagir, M., Tan, I.M., Mushtaq, M., Pervaiz, M., Tahir, M.S. and Shahzad, K., (2016) CO2 mobility control using CO2 philic surfactant for enhanced oil recovery. *Journal of Petroleum Exploration and Production Technology*, 6(3), pp.401-407.

Sandersen, S.B., von Solms, N. and Stenby, E.H., (2011) Pressure Effect on Phase Behavior of Surfactant System. *25th European Symposium on Applied Thermodynamics.*

Saeedi, M. and Pooladi-Darvish, M., (2011) Revisiting the drainage relative permeability measurement by centrifuge method using a forward–backward modelling scheme. *Transport in porous media*, 86(1), pp.49-71.

Salehi, M., Safarzadeh, M., Sahraei, E. and Alireza., (2013) Experimental study of surfactant alternating gas injection versus water alternating gas and waterflooding enhanced oil recovery methods. *Society of Petroleum Engineers Journal*, pp1-13.

Saliu, O.W., Sohrabi, M. and Shahverdi, H., (2014) Are Existing Three Phase Relative Permeability Models Adequate in Modelling Heavy Oil WAG Processes? *SPE Heavy Oil Conference-Canada*. Society of Petroleum Engineers.

Sandersen, S.B., Stenby, E.H. and von Solms, N., (2012) Enhanced oil recovery with surfactant flooding (Doctoral dissertation, Technical University of Denmark Tekniske

University, Centre for Energy Resources Engineering. Centre for Energy Resources Engineering).

Sarem, A.M., (1966) Three-phase relative permeability measurements by unsteady-state method. *Society of Petroleum Engineers Journal*, 6(03), pp.199-205.

Satter, A., Iqbal, G.M. and Buchwalter, J.L., (2008) Practical enhanced reservoir engineering: assisted with simulation software. Pennwell Books.

Saraf, D.N., Batycky, J.P., Jackson, C.H. and Fisher, D.B., (1982) January. An experimental investigation of three-phase flow of water-oil-gas mixtures through water-wet sandstones. *SPE California Regional Meeting*. Society of Petroleum Engineers.

Schneider, F.N. and Owens, W.W., (1970) Sandstone and carbonate two-and three-phase relative permeability characteristics. *Society of Petroleum Engineers Journal,* 10(01), pp.75-84.

Sendra user guide. (2011). Retrieved from http: www.sendra.no.

Shahverdi, H., (2012) Characterization of three-phase flow and WAG injection in oil reservoirs (Doctoral dissertation, Heriot-Watt University).

Shahverdi, H., Sohrabi, M., Fatemi, M. and Jamiohlamady, M., (2011a) Evaluation of three phase relative permeability models for WAG injection using water–wet core flood experiments, *SPE Journal*, pp 1-15.

Shahverdi,H. and Sohrabi,M.(2012b) Three phase relative permeability and hysteresis model for simulation of water alternating gas(WAG) injection, *Society of Petroleum Engineers Journal*, pp 1-11.

Shen, P., Zhu, B., Li, X.B. and Wu, Y.S., (2010) An experimental study of the influence of interfacial tension on water–oil two-phase relative permeability. *Transport in porous media*, 85(2), pp.505-520.

Sheng, J., (2011) Modern Chemical Enhanced oil recovery. Oxford, Gulf publishing, ISBN 978-1-85617-745-0, pp 20.

Schramm, L.L., (2000) Surfactants: fundamentals and applications in the petroleum industry. Cambridge University Press.

Siddiqui, S., Hicks, P.J. and Grader, A.S., (1996) Verification of Buckley-Leverett three-phase theory using computerized tomography. *Journal of Petroleum Science and Engineering*, 15(1), pp.1-21.

Skauge, A., and Berg, E., (1997) Immiscible WAG injection in the Fensfjord formation of the Brage oil field. *European Symposium on Improved Oil Recovery*, Hague.

Skauge, A., and Dale, E., (2007) Progress in immiscible WAG injection*, Society of Petroleum Engineers Journal*, pp1-6.

Skauge, A., Veland, I. and Larsen, J.A., (1999) Factors influencing three-phase flow parameters in WAG experiments. *Society of Core Analysts Symposium, Golden Colorado*, Volume: paper SCA 9932 paper SCA, 9932, pp.1-4.

Skauge, A. and Fotland, P., (1990) Effect of pressure and temperature on the phase behaviour of micro emulsions. *SPE Reservoir Engineering*, 5(04), pp.601-608.

Solairaj, S., Britton, C., Kim, D.H., Weerasooriya, U. and Pope, G.A., (2012) Measurement and analysis of surfactant retention. *SPE Improved Oil Recovery Symposium.* Society of Petroleum Engineers.

Somasundaran, P. and Zhang, L., (2006) Adsorption of surfactants on minerals for wettability control in improved oil recovery processes. *Journal of Petroleum Science and Engineering*, 52(1), pp.198-212.

Soroush, M., Wessel-Berg, D., Torsaeter, O. and Kleppe, J., (2013) Investigating impact of flow rate and wettability on residual trapping in CO2 storage in saline aquifers through relative permeability experiments. *Energy and Environment Research,* 3(2), p.53.

Spildo, K., Johannessen, A.M. and Skauge, A., (2012) Low salinity waterflood at reduced capillarity. *SPE Improved Oil Recovery Symposium*. Society of Petroleum Engineers.

Spiteri, E., and Juanes, R. (2004) Impact of relative permeability hysteresis on the numerical simulation of WAG injection. *Journal of Petroleum Science and Engineering*, pp115-135.

Stone, H.L., (1970) Probability model for estimating three-phase relative permeability. *Journal of Petroleum Technology*, 22(02), pp.214-218.

Suramairy, R.A., and Abdulrahman, R.K., (2015) "Uncertainty in WAG Injection Modelling using Empirical methods and Three-Phase Pore-Network Modeling with Rock Heterogeneity Effect", *International Journal of Engineering Trends and Technology* (IJETT), V19(1),12-18. ISSN: 2231-5381.

Thakur, G.C., and Satter, A., (1998) Integrated waterflood asset management. Tulsa: PennWell.

Tiab, D. and Donaldson, E.C., (2015) Petrophysics: theory and practice of measuring reservoir rock and fluid transport properties. Gulf professional publishing.

Toth, J., Bodi, T., Szucs, P. and Civan, F., (2002) Convenient formulae for determination of relative permeability from unsteady-state fluid displacements in core plugs. *Journal of Petroleum Science and Engineering*, 36(1), pp.33-44.

Touray, S., (2013) Effect of water alternating gas injection on ultimate oil recovery. Master's thesis, Dalhousie University, Halifax.

Watson, A.T.; Kulkarni, R.; Nordtvedt, J.E.; Sylte, A.; and Urkedal, H., (1998) Estimation of Porous Media Flow Functions. *Measurement Science and Technology*, 9(6), 898–905.

Weifeng, L., Qingjie, L., Zhang, Z., Desheng, M.A., Kangyun, W.U. and Zhenpeng, L.E.N.G., (2012) Measurement of three-phase relative permeabilities. *Petroleum Exploration and Development*, 39(6), pp.758-763.

www.dataphysics.de [Accessed 16 December 2016].

Yuqi, O.B. and Dacun, L., (2004) Literature review on methods to obtain relative permeability data*. 5th Conference & Exposition on Petroleum Geophysics, Hyderabad.*

Zahoo, M., Derahman, M., and Yunan, H., (2011) Wag process design, *Brazilian journal of petroleum and gas*, pp109 -121.

Zekri, A.Y., Nasr, M.S. and AlShobakyh, A., (2011) January. Evaluation of oil recovery by water alternating gas (WAG) injection-oil-wet & water-wet systems. *SPE enhanced oil recovery conference*. Society of Petroleum Engineers.

Zuo, L., Chen, Y., Dengen, Z. and Kamath, J., (2014) Three-phase relative permeability modelling in the simulation of WAG Injection. *SPE Reservoir Evaluation & Engineering*, 17(03), pp.326-339.

Appendices

Publications

Conference

Perekaboere Ivy Sagbana[1], Pedro Diaz[2], Maria Astrid Centeno[3] (2016), "Evaluation of ultra-low surfactant concentration system for chemical flooding", 15th European mathematics of oil recovery conference.

Perekaboere Ivy Sagbana[1], Pedro Diaz[2], Maclean Eneotu[3], Maria Centeno[4], Farzin Vajihi[5], Arash Farhadi[6] (2017), "Application of low concentration surfactant enhanced water-alternating-gas flooding", 19th European Symposium on Improved Oil Recovery in Stavanger, Norway.

Perekaboere Ivy Sagbana[1], Pedro Diaz[2] (2016), "Impact of low concentration surfactant on interfacial tension and water/oil relative permeability", 2nd International conference and expo on oil and gas. Rome, Italy.

Perekaboere Ivy Sagbana[1], Pedro Diaz[2], Sarkodie Kwame[3] (2017), "Numerical simulation of surfactant enhanced water-alternating-gas flooding", the 31st International Symposium of the Society of Core Analysts**.** The Hofburg Palace, Vienna, Austria.

Farzin Vajihi[1], Pedro Diaz[2]**, Perekaboere Ivy Sagbana[3]**, Hassan Zabihi[4], Arash Farhadi[5] (2017), "Effect of low salinity water injection on wettability and capillary pressure in carbonates", The 31st International Symposium of the Society of Core Analysts**.** The Hofburg Palace, Vienna, Austria.

Journals

Perekaboere Ivy Sagbana[1], Pedro Diaz[2], Maria Astrid Centeno[3] (2016), "Experimental investigation of surfactant effects on two-phase gas/oil relative permeability, Journal of Petroleum Science and Engineering" (Submitted).

Maclean Eneotu[1], **Perekaboere Ivy Sagbana[2]**, Pedro Diaz[3], Maria Centeno[4] (2017), "A comparison of numerical simulators in the prediction of water flood performance in stratified reservoirs", Journal of Petroleum Science and Engineering (Submitted).

Award and Prizes:

Winner – 3 minutes' thesis presentation competition. London South Bank University.

Experimental equipment

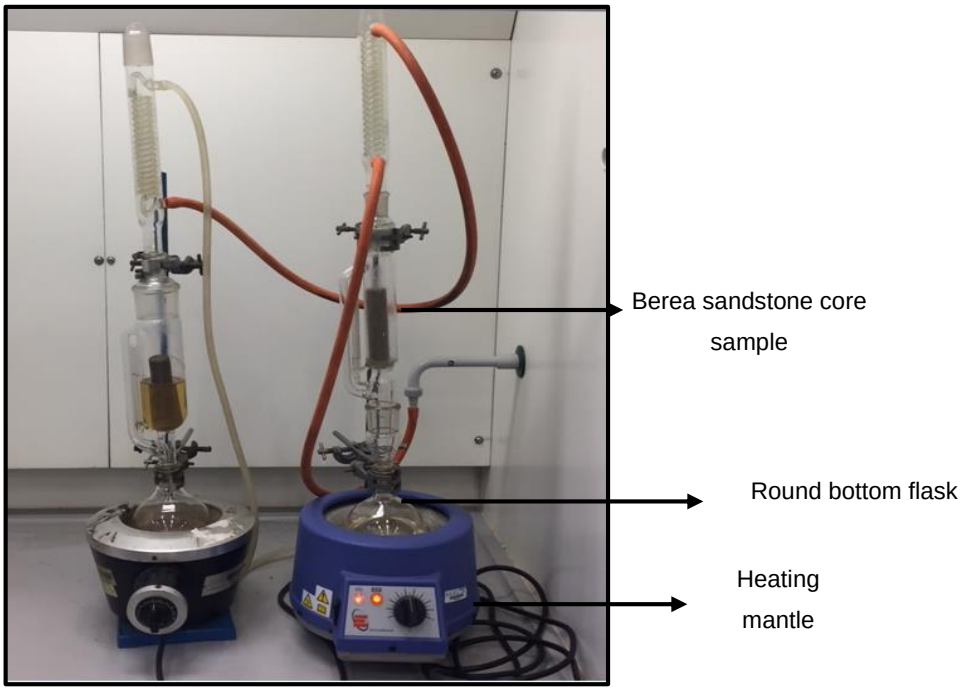

A1: Soxhlet extractor used for core sample cleaning.

A2: Displacement Pumps

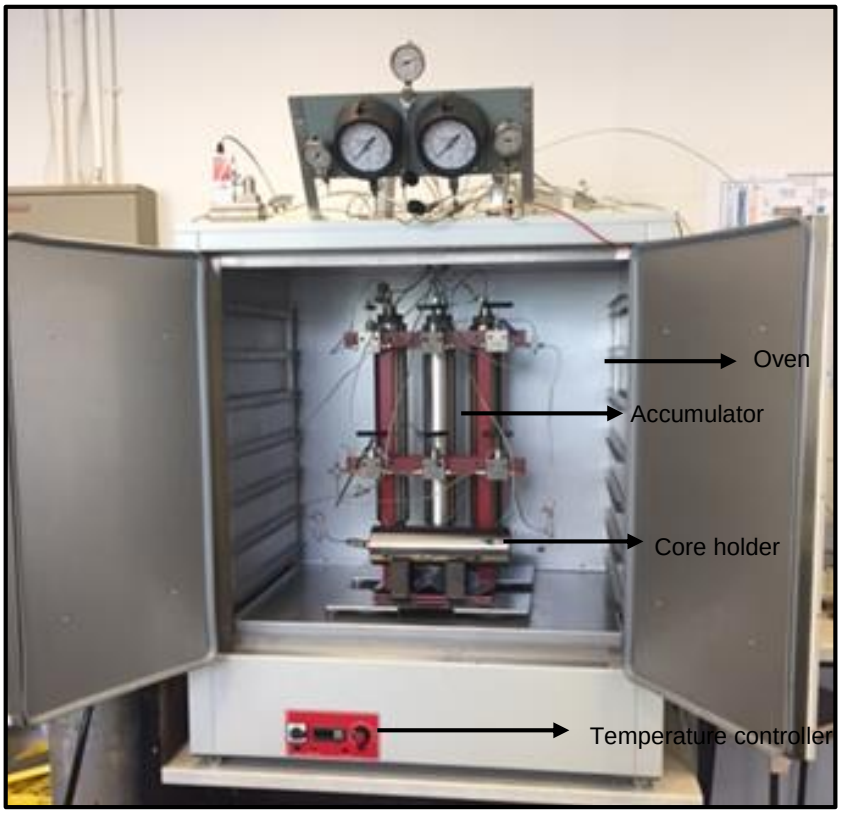

A3: Core flood apparatus.

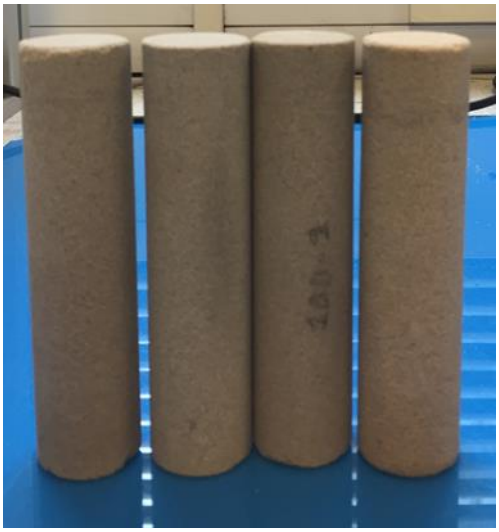

A4: Berea sandstone core samples.

A5: Rubber sleeve holding core sample in core holder.

A6: Bronkhorst gas meter.

A7: Bronkhorst gas flow controller.

A8: Bronkhorst pressure transducer.

A9: Back pressure regulator.

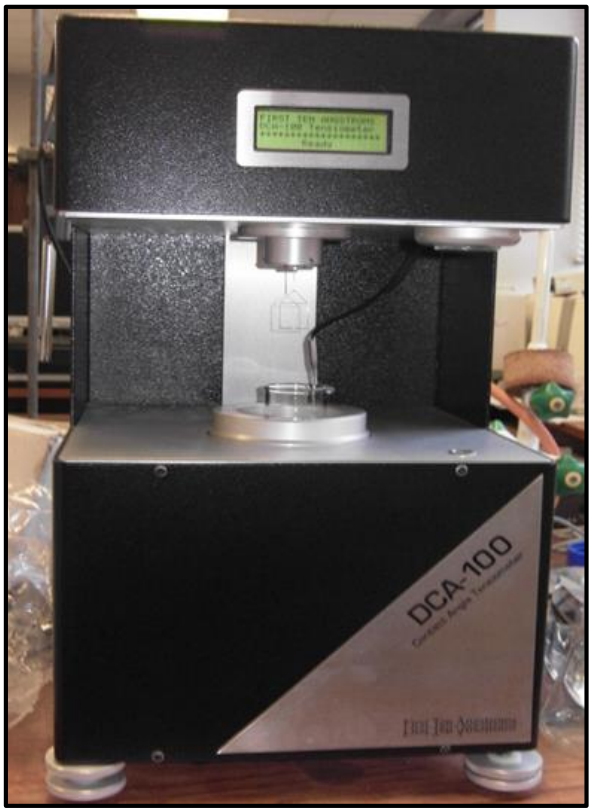

A10: DCA contact angle tensiometer.

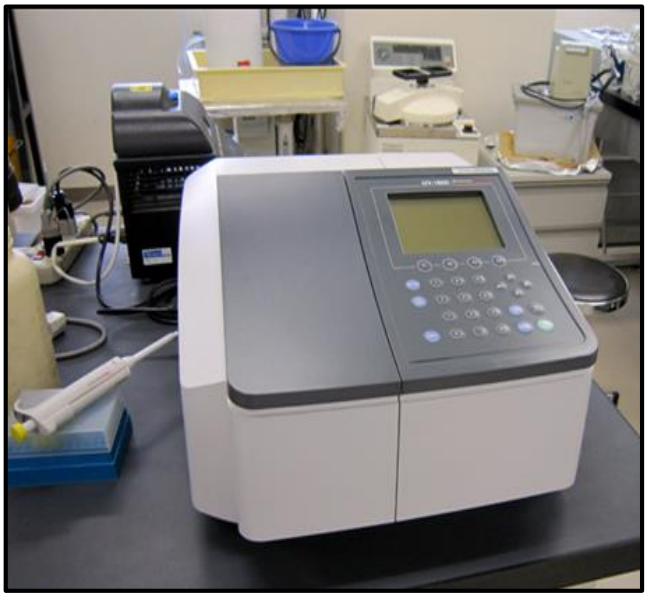

A11: UV spectrometer.

Error analysis

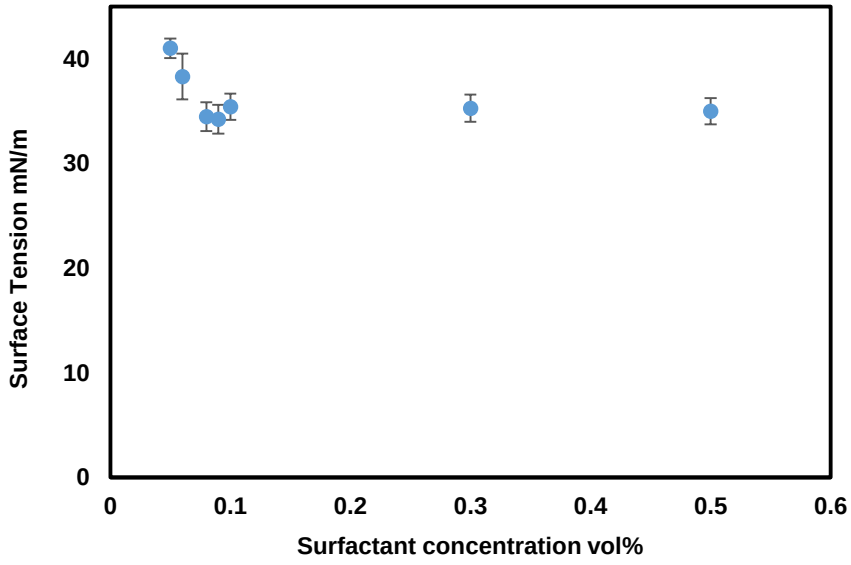

A12: Alcohol alkoxy sulphate CMC measurement.

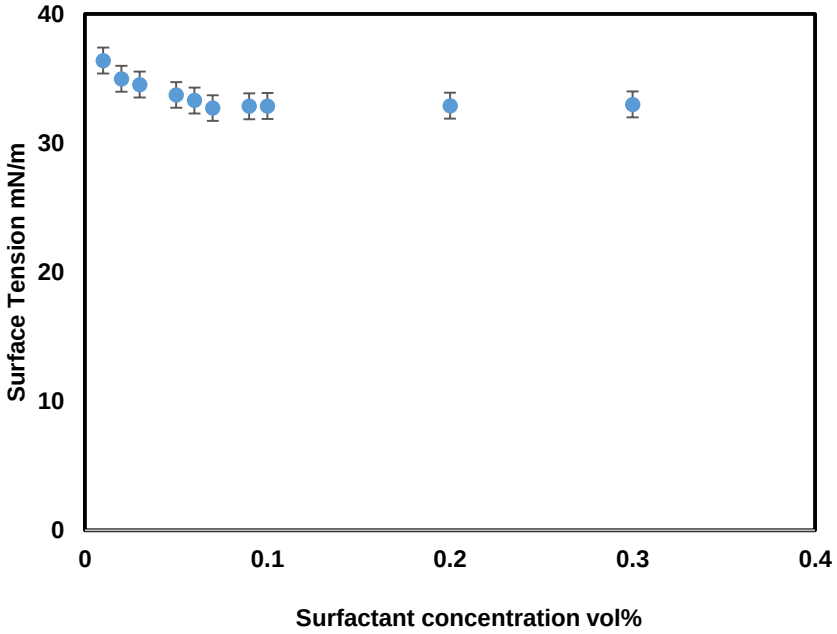

A13: Alcohol propoxy sulphate CMC measurement.

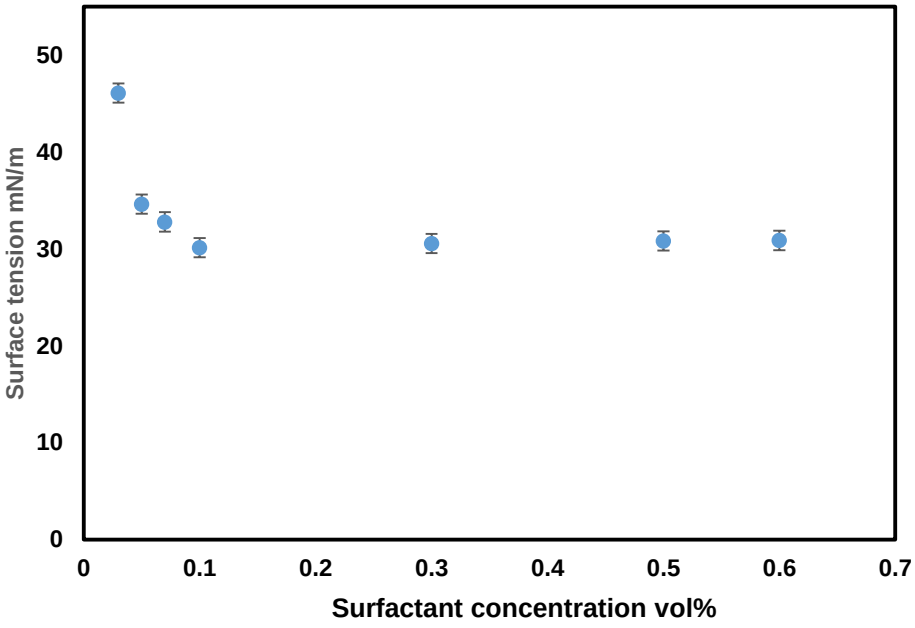

A14: Methyl ester sulfonate CMC measurement.

DATA-file Structure for Eclipse

An Eclipse DATA-file is a text file used as an input file to the simulator. The DAT file comprises of eight different sections started by a section header, which must be shown in a prescribed order. A few thousand keywords are available to best describe the reservoir conditions (Eclipse 100 manual, 2013).

The required order of the DATA-file is as follows:

RUNSPEC [Required] - This contains run specifications like the grid size, table size, number of wells, phases present in the simulation. For this research, the phases present are water, oil, gas and surfactant.

GRID [Required]. - This defines the shape and dimensions of the grid, and petrophysical data like porosity, permeability and net-to-gross.

EDIT [Optional] - Edit changes defined by user can be applied to grid data after Eclipse has processed them can be defined in this section.

PROPS [Required] – This includes the fluid and rock properties like relative permeabilities, PVT tables, three phase relative permeability correlation and for

surfactant alternating gas flooding properties such as capillary desaturation curve, surfactant interfacial tension, adsorption.

REGIONS [Optional] - Is used to define different regions which have different properties, e.g. initial conditions.

SOLUTION [Required] – Describes how the model is to be initialized.

SUMMARY [Optional] - This section is used to specify which data items to write to report file.

SCHEDULE [Required] – This section presents well definitions, description of operating schedule, convergence control is defined in this section. Production specifications, such as production rates, bottom-hole pressure etc. are defined in this section.